Teleportacja
i kryptografia kwantowa

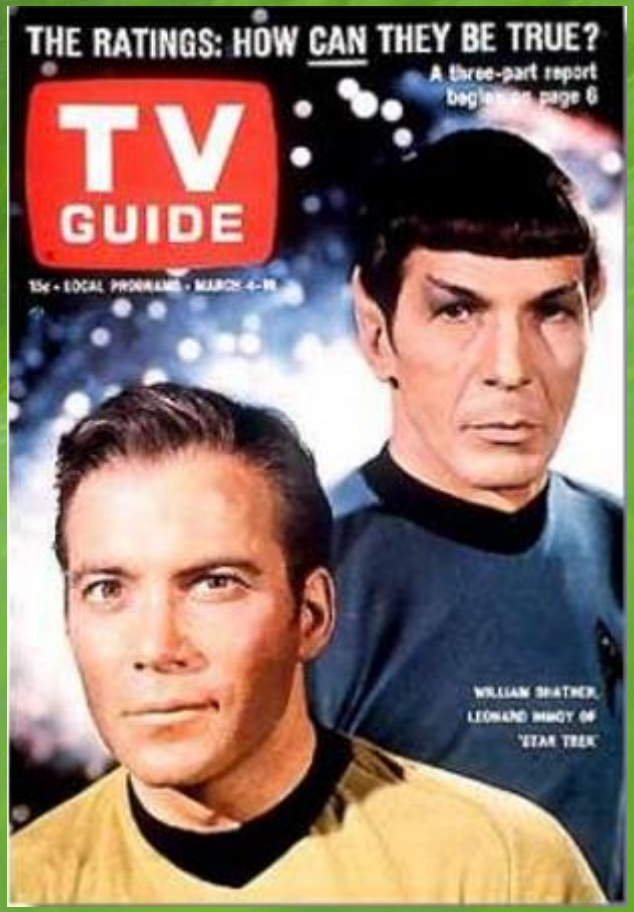

Jacek.Szczytko@fuw.edu.pl Wydział Fizyki UW

Sprawy bieżące

Ankiety

http://usosweb.**fuw.edu.pl**

"Dla studentów">"Ankiety".

Opis wielu cząstek kwantowych

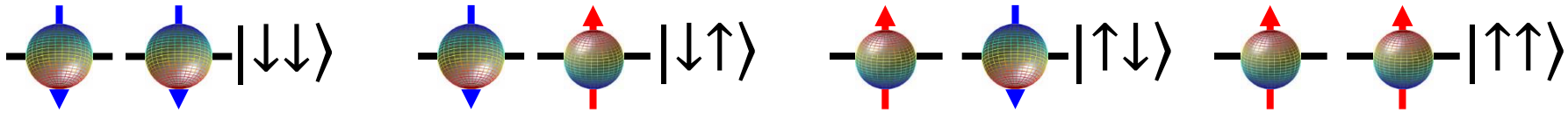

Stany Bella

$$\left|\Phi^{+}\right\rangle = \frac{1}{\sqrt{2}}\left(\left|\downarrow\downarrow\right\rangle + \left|\uparrow\uparrow\right\rangle\right) \qquad \left|\Psi^{+}\right\rangle = \frac{1}{\sqrt{2}}\left(\left|\downarrow\uparrow\right\rangle + \left|\uparrow\downarrow\right\rangle\right)$$

$$\left|\Phi^{-}\right\rangle = \frac{1}{\sqrt{2}}\left(\left|\downarrow\downarrow\right\rangle - \left|\uparrow\uparrow\right\rangle\right) \qquad \left|\Psi^{-}\right\rangle = \frac{1}{\sqrt{2}}\left(\left|\downarrow\uparrow\right\rangle - \left|\uparrow\downarrow\right\rangle\right)$$

Ale stanów Bella nie da się przedstawić w postaci iloczynu dwóch funkcji

jednocząstkowych typu: $\left|\Phi\right\rangle = \left|\varphi_1\right\rangle\left|\varphi_2\right\rangle$ gdzie $\left|\varphi_i\right\rangle = a_{i1}\left|\uparrow\right\rangle + a_{i2}\left|\downarrow\right\rangle$

Stany Bella są **SPLĄTANE**

spiny, polaryzacja fotonów, atom + foton, dwa atomy, atom w różnych stanach...

Splątane stany - EPR

Uwaga 3: liniowa kombinacja funkcji falowych też jest funkcja falową (zasada superpozycji)

$$\Psi = A\Psi_A + B\Psi_B$$

Nie dodajemy prawdopodobieństw!

$$|\Psi|^2 = (A\Psi_A + B\Psi_B)^2 \neq A^2|\Psi_A|^2 + B^2|\Psi_B|^2$$

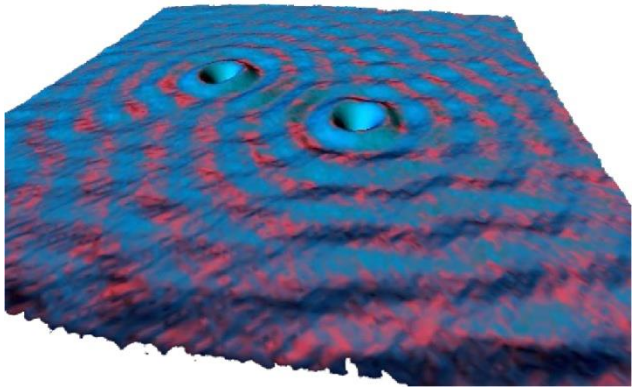

$$|\Psi|^2 = A^2|\Psi_A|^2 + B^2|\Psi_B|^2 + 2AB\Psi_A\Psi_B$$

Człon interferencyjny

por. WYKŁAD nr 3

Uwaga 4: ewolucja funkcji falowej jest DETERMINISTYCZNA. Jednak w momencie pomiaru „dowiadujemy" się w jakim stanie jest funkcja (tzw. *redukcja f. falowej*)

$$\Psi = A\Psi_A + B\Psi_B$$

pomiar ***A*** lub ***B***

prawdopodobieństwo A^2 lub B^2

$$\Psi = \Psi_A \longrightarrow \Psi = \Psi_A$$

$$\Psi = \Psi_B \longrightarrow \Psi = \Psi_B$$

Splątane stany - EPR

LETTERS
PUBLISHED ONLINE: 21 DECEMBER 2015 | DOI: 10.1038/NPHYS3605
nature physics

Generation of heralded entanglement between distant hole spins

Aymeric Delteil[1†], Zhe Sun[1†], Wei-bo Gao[1,2†], Emre Togan[1], Stefan Faelt[1] and Ataç Imamoğlu[1*]

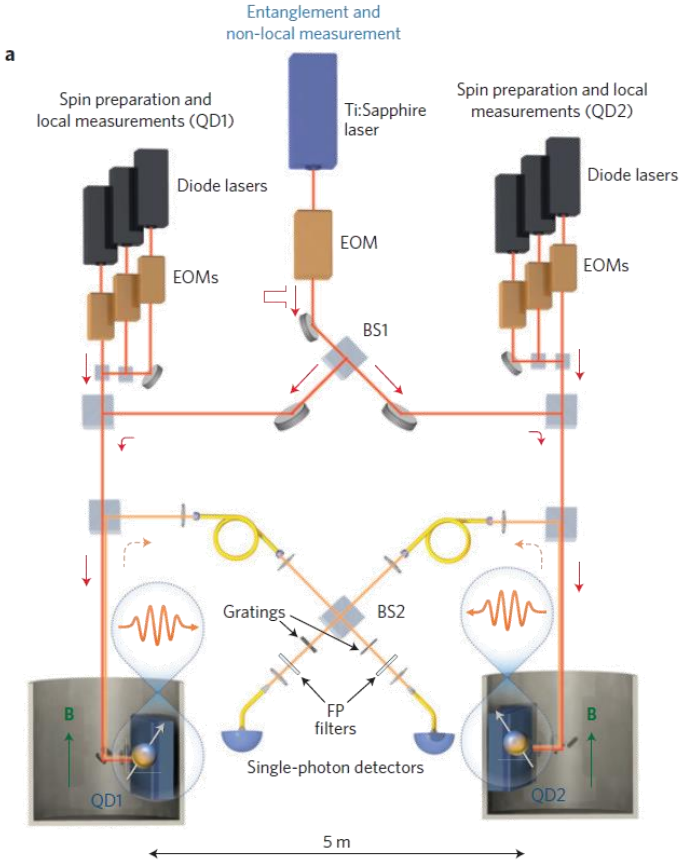

Splątane stany - EPR

RESEARCH ARTICLE

QUANTUM OPTICS

Satellite-based entanglement distribution over 1200 kilometers

Juan Yin,[1,2] Yuan Cao,[1,2] Yu-Huai Li,[1,2] Sheng-Kai Liao,[1,2] Liang Zhang,[2,3] Ji-Gang Ren,[1,2] Wen-Qi Cai,[1,2] Wei-Yue Liu,[1,2] Bo Li,[1,2] Hui Dai,[1,2] Guang-Bing Li,[1,2] Qi-Ming Lu,[1,2] Yun-Hong Gong,[1,2] Yu Xu,[1,2] Shuang-Lin Li,[1,2] Feng-Zhi Li,[1,2] Ya-Yun Yin,[1,2] Zi-Qing Jiang,[3] Ming Li,[3] Jian-Jun Jia,[3] Ge Ren,[4] Dong He,[4] Yi-Lin Zhou,[5] Xiao-Xiang Zhang,[6] Na Wang,[7] Xiang Chang,[8] Zhen-Cai Zhu,[5] Nai-Le Liu,[1,2] Yu-Ao Chen,[1,2] Chao-Yang Lu,[1,2] Rong Shu,[2,3] Cheng-Zhi Peng,[1,2]* Jian-Yu Wang,[2,3]* Jian-Wei Pan[1,2]*

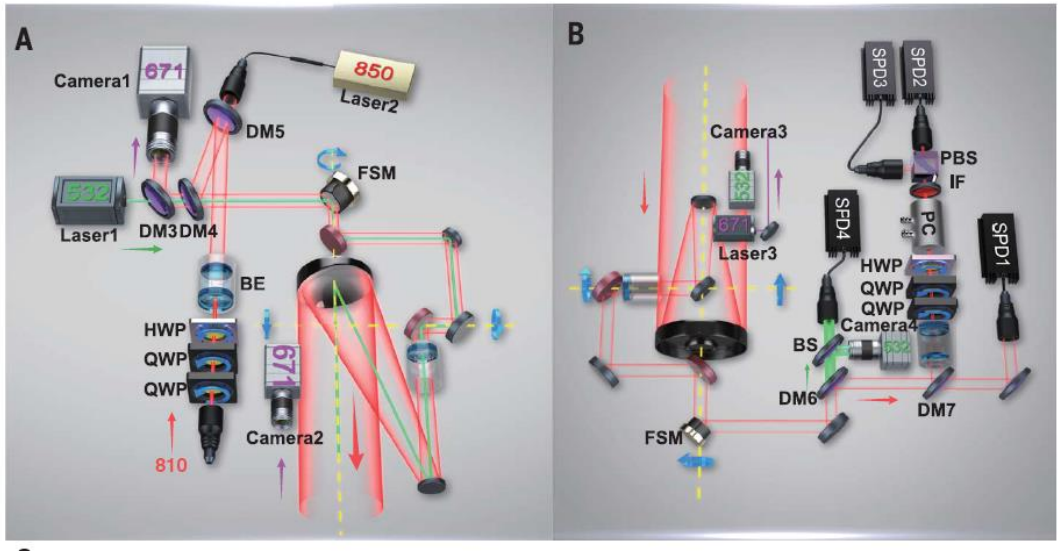

LETTER

doi:10.1038/nature23675

Ground-to-satellite quantum teleportation

Ji-Gang Ren[1,2], Ping Xu[1,2], Hai-Lin Yong[1,2], Liang Zhang[2,3], Sheng-Kai Liao[1,2], Juan Yin[1,2], Wei-Yue Liu[1,2], Wen-Qi Cai[1,2], Meng Yang[1,2], Li Li[1,2], Kui-Xing Yang[1,2], Xuan Han[1,2], Yong-Qiang Yao[4], Ji Li[5], Hai-Yan Wu[5], Song Wan[6], Lei Liu[6], Ding-Quan Liu[3], Yao-Wu Kuang[3], Zhi-Ping He[3], Peng Shang[1,2], Cheng Guo[1,2], Ru-Hua Zheng[7], Kai Tian[8], Zhen-Cai Zhu[6], Nai-Le Liu[1,2], Chao-Yang Lu[1,2], Rong Shu[2,3], Yu-Ao Chen[1,2], Cheng-Zhi Peng[1,2], Jian-Yu Wang[2,3] & Jian-Wei Pan[1,2]

Splątane stany - EPR

ARTICLE

doi:10.1038/nature23655

Satellite-to-ground quantum key distribution

Sheng-Kai Liao[1,2], Wen-Qi Cai[1,2], Wei-Yue Liu[1,2], Liang Zhang[2,3], Yang Li[1,2], Ji-Gang Ren[1,2], Juan Yin[1,2], Qi Shen[1,2], Yuan Cao[1,2], Zheng-Ping Li[1,2], Feng-Zhi Li[1,2], Xia-Wei Chen[1,2], Li-Hua Sun[1,2], Jian-Jun Jia[3], Jin-Cai Wu[3], Xiao-Jun Jiang[4], Jian-Feng Wang[4], Yong-Mei Huang[5], Qiang Wang[5], Yi-Lin Zhou[6], Lei Deng[6], Tao Xi[7], Lu Ma[8], Tai Hu[9], Qiang Zhang[1,2], Yu-Ao Chen[1,2], Nai-Le Liu[1,2], Xiang-Bin Wang[2], Zhen-Cai Zhu[6], Chao-Yang Lu[1,2], Rong Shu[2,3], Cheng-Zhi Peng[1,2], Jian-Yu Wang[2,3] & Jian-Wei Pan[1,2]

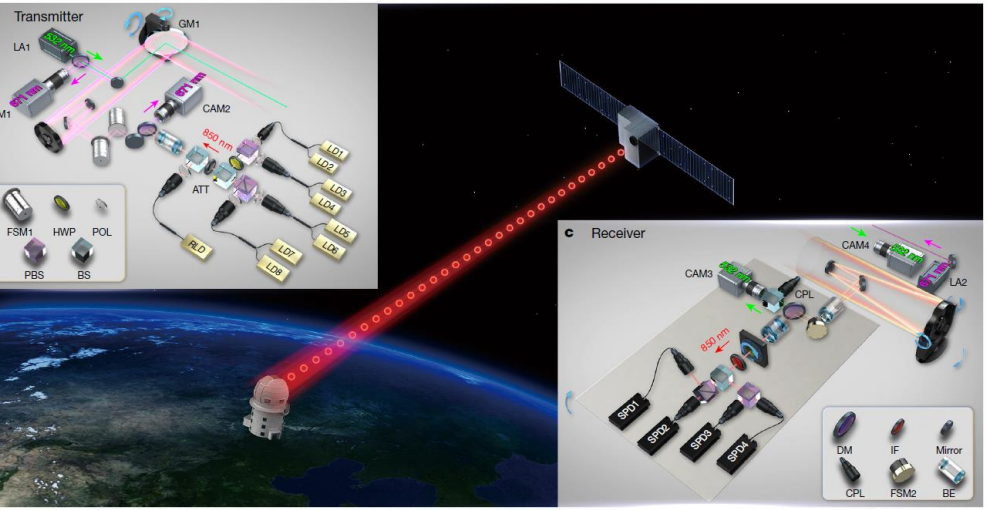

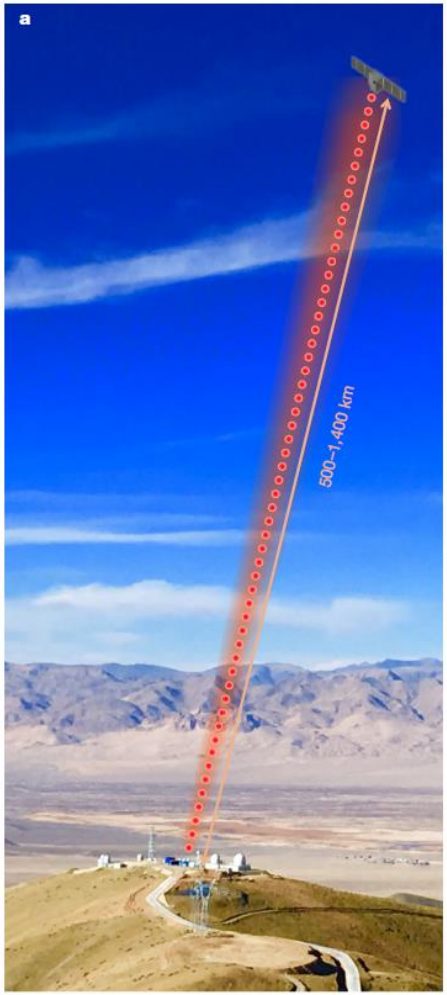

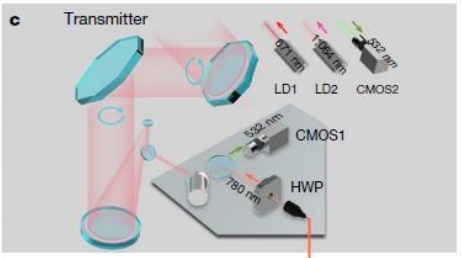

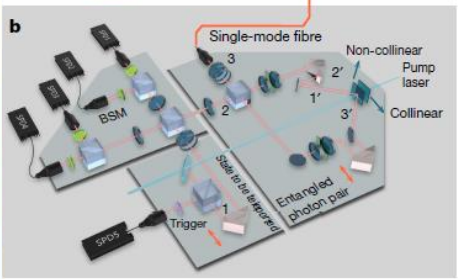

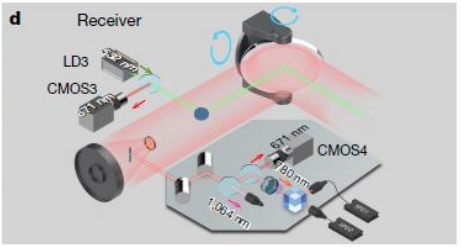

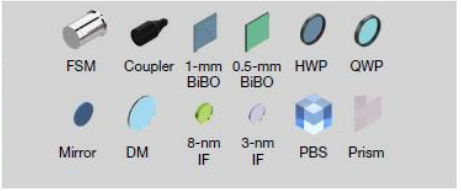

Splątane stany - EPR

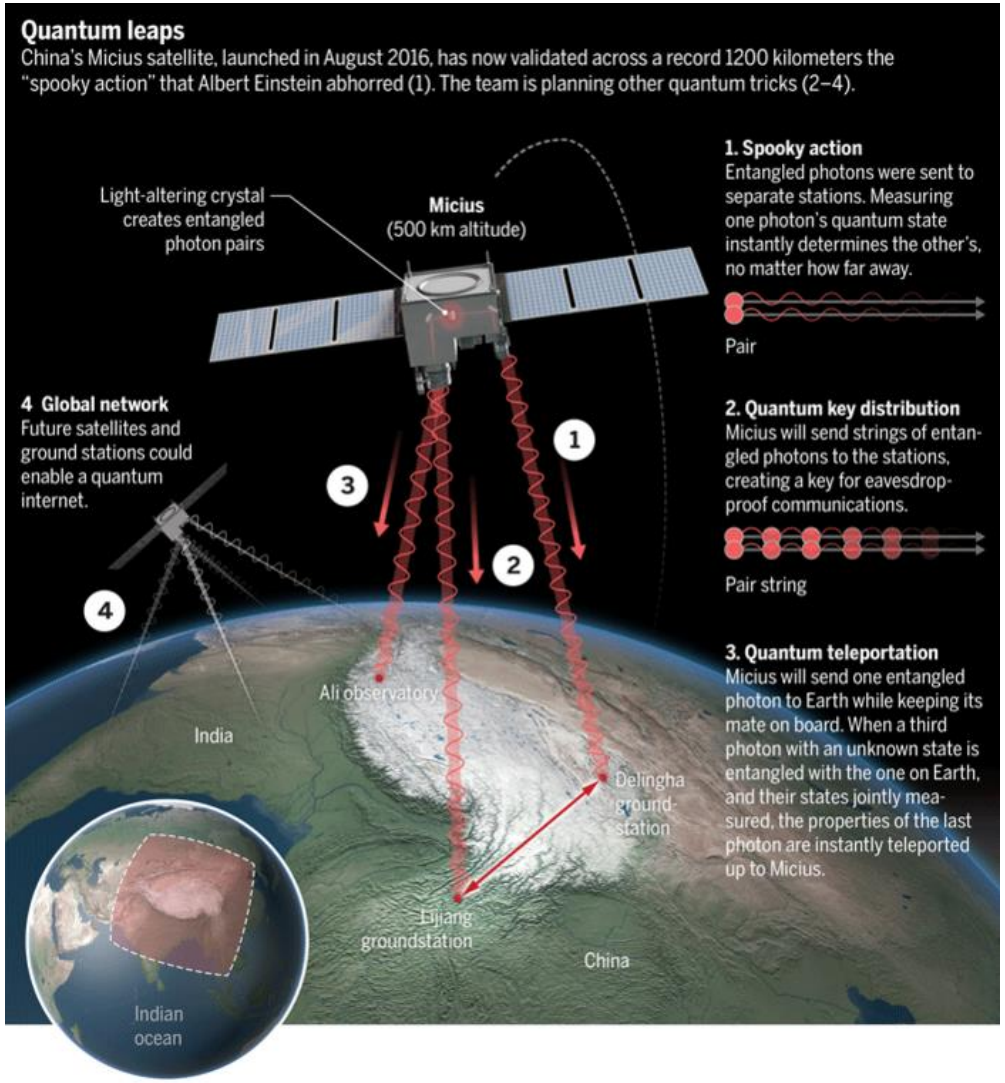

Splątane stany - EPR

FORSAL.PL

szukaj

Notowania | Biznes | Gospodarka | Świat | Finanse | Praca | Nieruchomości | Transport | Lifestyle | Motoforsal

LIFESTYLE › TECHNOLOGIE

RAPORTY SPECJALNE: Szczepionka przeciw Covid-19 | Tarcza antykryzysowa | Prognozy gospodarcze | Koronakryzys | Ceny mieszkań

W Chinach powstała największa kwantowa sieć komunikacyjna. Informacji biegnących przez te łącza nie da się przechwycić

dzisiaj, 09:02

Ten tekst przeczytasz w mniej niż minutę

Pekin, Chiny / ShutterStock

Aż 4600 km mierzy kwantowa chińska sieć komunikacyjna. Obejmuje ona zarówno łącza światłowodowe, jak i satelitarne. Informacje biegnące przez kwantowe łącza uznaje się za niemożliwe do przechwycenia.

Naukowcy z Uniwersytetu Nauki i Technologii Chin, na łamach pisma Nature opisali rekordowo rozległą sieć, opartą na technologii kwantowej dystrybucji klucza (QDT - Quantum Key Distribution). To technologia, która umożliwia całkowitą ochronę przed przechwytywaniem informacji.

Obie komunikujące się z sobą strony przekazują w niej sobie klucz służący do szyfrowania i odczytu wiadomości, który zapisany jest w stanach kwantowych cząstek, np. fotonów. Stany kwantowe mają to do siebie, że próba ich odczytania zawsze je zmienia. Jeśli więc ktoś przechwyci klucz, komunikujące się strony natychmiast się o tym dowiedzą.

Chiny stworzyły właśnie sieć tego typu, która łączy ponad 700 punktów. Wykorzystuje do tego celu dwa łącza satelitarne i ponad 2 tys. km światłowodów.

Sieć, w której każdy użytkownik może komunikować się z dowolnym innym użytkownikiem, obejmuje w sumie dystans 4,600 km.

Więcej informacji na stronie Nature (https://www.nature.com/articles/s41586-020-03093-8) (PAP)

NIE PRZEGAP


Polski paszport jak polisa. Brazylijczycy i Argentyńczycy starają się o obywatelstwo starej ojczyzny


Domy modułowe powstają jak grzyby po deszczu. "Przynajmniej kilkanaście tys. rocznie"


Lepsza Europa, gorsza Europa. Trudno skleić to, co zostało niesprawiedliwie rozcięte


Sojka: Żyć niespiesznie. Wyścig szczurów trochę zelżał [WYWIAD]

POLECAMY


Wojska Polskiego droga donikąd. Rząd nie wspiera ani przemysłu, ani armii


Applebaum: Orbán jest sprytniejszy niż Kaczyński i lepiej rozumie świat Zachodu [WYWIAD]


Euroobligacje związą ze sobą państwa UE silniej niż traktaty akcesyjne


Marzenia o wielkim strzyżeniu. Czy anulowanie długów to dobry pomysł? [OPINIA]


Egzorcyzmowanie niemieckiego ducha na Ziemiach Odzyskanych [WYWIAD]


Pomiędzy cenzurą a mową nienawiści. Rzetelne media odtrutką na fake newsy [OPINIA]

Article

An integrated space-to-ground quantum communication network over 4,600 kilometres

https://doi.org/10.1038/s41586-020-03093-8

Received: 1 March 2019

Accepted: 2 November 2020

Published online: 06 January 2021

Yu-Ao Chen[1,2]✉, Qiang Zhang[1,2], Teng-Yun Chen[1,2], Wen-Qi Cai[1,2], Sheng-Kai Liao[1,2], Jun Zhang[1,2], Kai Chen[1,2], Juan Yin[1,2], Ji-Gang Ren[1,2], Zhu Chen[1,2], Sheng-Long Han[1,2], Qing Yu[3], Ken Liang[3], Fei Zhou[4], Xiao Yuan[1,2], Mei-Sheng Zhao[1,2], Tian-Yin Wang[1,2], Xiao Jiang[1,2], Liang Zhang[2,5], Wei-Yue Liu[1,2], Yang Li[1,2], Qi Shen[1,2], Yuan Cao[1,2], Chao-Yang Lu[1,2], Rong Shu[2,5], Jian-Yu Wang[2,5], Li Li[1,2], Nai-Le Liu[1,2], Feihu Xu[1,2], Xiang-Bin Wang[4], Cheng-Zhi Peng[1,2]✉ & Jian-Wei Pan[1,2]✉

Fig. 1 | Illustration of the integrated space-to-ground quantum network.

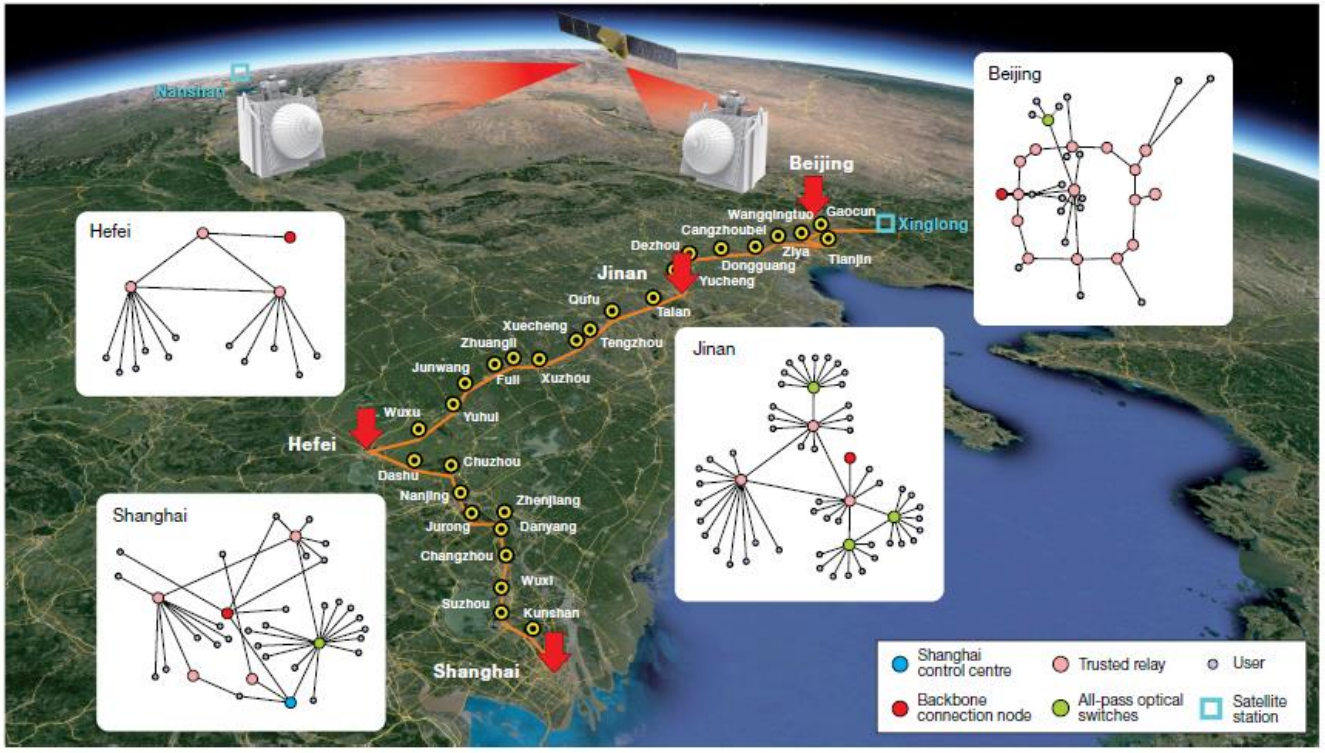

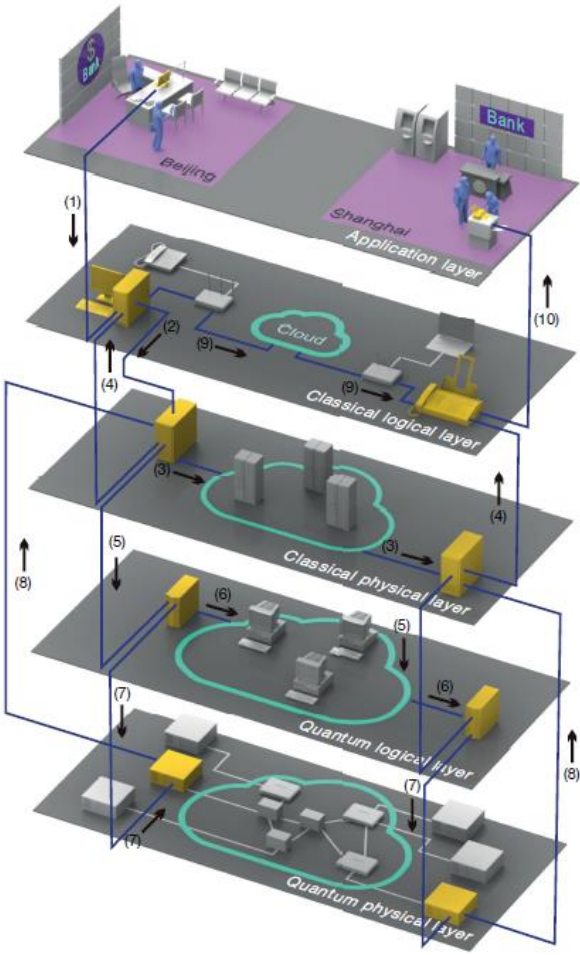

Fig. 2 | Network architecture and administration.

Kwantowa teleportacja

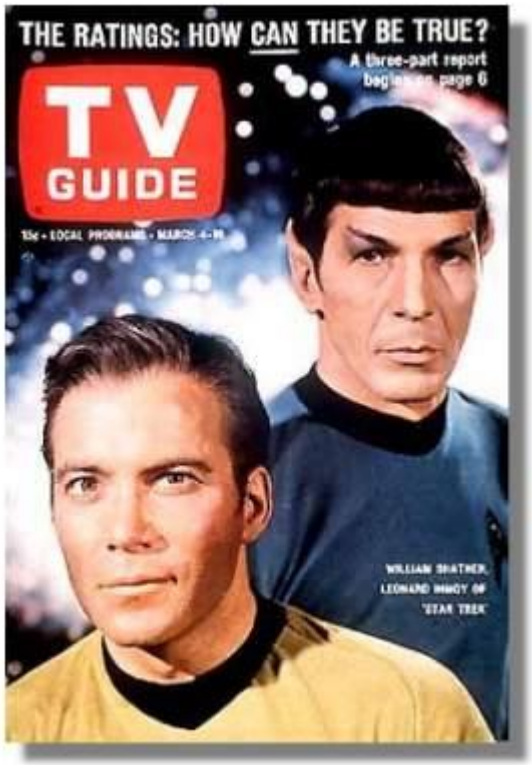

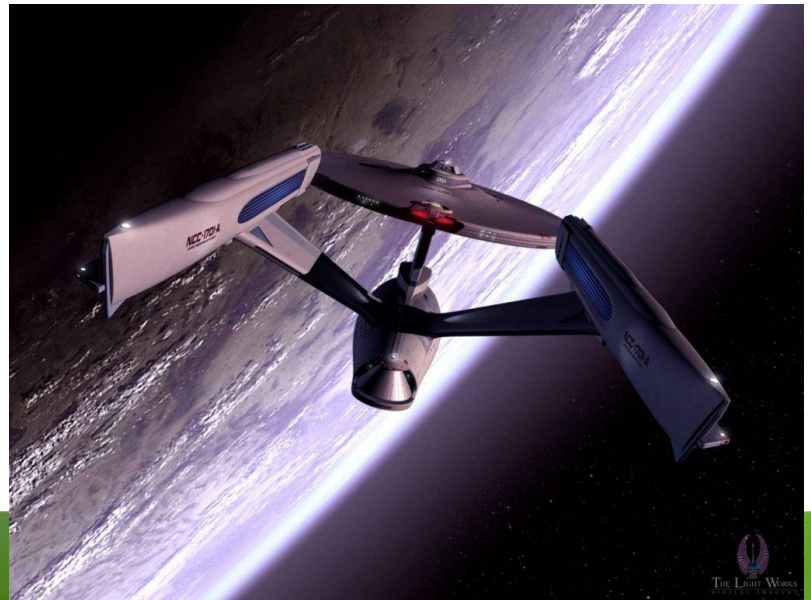

Kwantowa teleportacja

IBM CREW Six researchers--Richard Jozsa, William K. Woolters, Charles H. Bennett *(back row, left to right)* Gilles Brassard, Claude Crepeau and Asher Peres *(front row)*--proposed quantum teleportation in 1993.

Kwantowa teleportacja

PHYSICAL REVIEW
LETTERS

VOLUME 70 | 29 MARCH 1993 | NUMBER 13

Teleporting an Unknown Quantum State via Dual Classical and Einstein-Podolsky-Rosen Channels

Charles H. Bennett,[1] Gilles Brassard,[2] Claude Crépeau,[2,3]
Richard Jozsa,[2] Asher Peres,[4] and William K. Wootters[5]
[1] *IBM Research Division, T.J. Watson Research Center, Yorktown Heights, New York 10598*
[2] *Département IRO, Université de Montréal, C.P. 6128, Succursale "A", Montréal, Québec, Canada H3C 3J7*
[3] *Laboratoire d'Informatique de l'École Normale Supérieure, 45 rue d'Ulm, 75230 Paris CEDEX 05, France*[a]
[4] *Department of Physics, Technion–Israel Institute of Technology, 32000 Haifa, Israel*
[5] *Department of Physics, Williams College, Williamstown, Massachusetts 01267*
(Received 2 December 1992)

An unknown quantum state $|\phi\rangle$ can be disassembled into, then later reconstructed from, purely classical information and purely nonclassical Einstein-Podolsky-Rosen (EPR) correlations. To do so the sender, "Alice," and the receiver, "Bob," must prearrange the sharing of an EPR-correlated pair of particles. Alice makes a joint measurement on her EPR particle and the unknown quantum system, and sends Bob the classical result of this measurement. Knowing this, Bob can convert the state of his EPR particle into an exact replica of the unknown state $|\phi\rangle$ which Alice destroyed.

Kwantowa teleportacja

Dwucząstkowe stany splątane, baza Bella

$$\left|\Phi^{+}\right\rangle = \frac{1}{\sqrt{2}}\left(\left|\downarrow\downarrow\right\rangle + \left|\uparrow\uparrow\right\rangle\right) \qquad \left|\Psi^{+}\right\rangle = \frac{1}{\sqrt{2}}\left(\left|\downarrow\uparrow\right\rangle + \left|\uparrow\downarrow\right\rangle\right)$$

$$\left|\Phi^{-}\right\rangle = \frac{1}{\sqrt{2}}\left(\left|\downarrow\downarrow\right\rangle - \left|\uparrow\uparrow\right\rangle\right) \qquad \left|\Psi^{-}\right\rangle = \frac{1}{\sqrt{2}}\left(\left|\downarrow\uparrow\right\rangle - \left|\uparrow\downarrow\right\rangle\right)$$

Alice

Bob

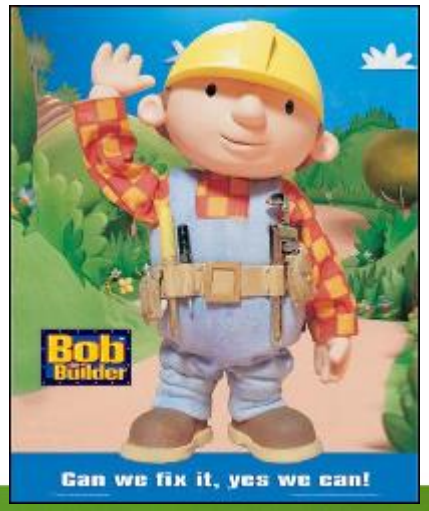

Kwantowa teleportacja

$$|\phi\rangle = a|\uparrow_1\rangle + b|\downarrow_1\rangle$$

$$|\Psi^-_{2,3}\rangle = \frac{1}{\sqrt{2}}\left(|\downarrow_2\uparrow_3\rangle - |\uparrow_2\downarrow_3\rangle\right)$$

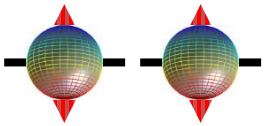

Alice

Bob

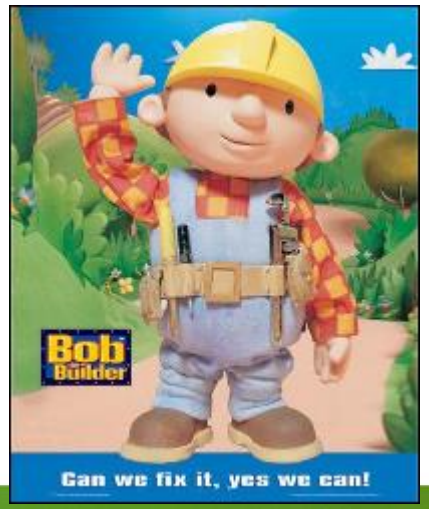

Kwantowa teleportacja

$$|\phi\rangle = a|\uparrow_1\rangle + b|\downarrow_1\rangle$$

$$|\Psi^-_{2,3}\rangle = \frac{1}{\sqrt{2}}\left(|\downarrow_2\uparrow_3\rangle - |\uparrow_2\downarrow_3\rangle\right)$$

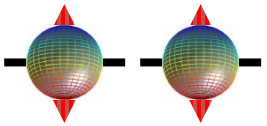

Alice

Bob

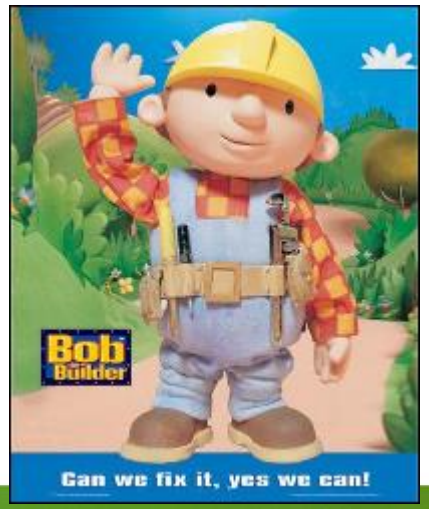

Kwantowa teleportacja

$$|\phi\rangle = a|\uparrow_1\rangle + b|\downarrow_1\rangle$$

$$|\Psi^-_{2,3}\rangle = \frac{1}{\sqrt{2}}\left(|\downarrow_2 \blacksquare\rangle - |\uparrow_2 \blacksquare\rangle\right)$$

$$|\Psi^-_{2,3}\rangle = \frac{1}{\sqrt{2}}\left(|\blacksquare\uparrow_3\rangle - |\blacksquare\downarrow_3\rangle\right)$$

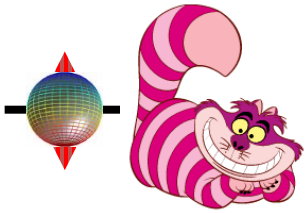

Alice

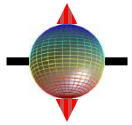

Bob

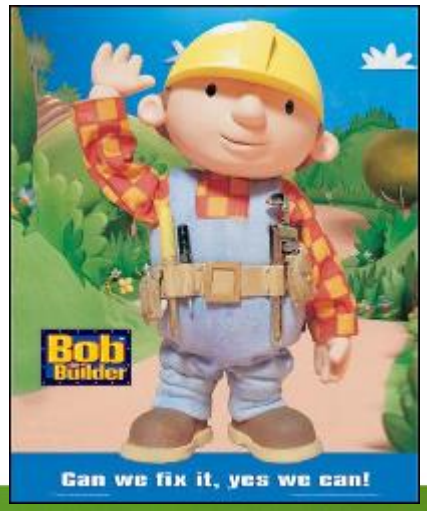

Kwantowa teleportacja

$$|\phi\rangle = a|\uparrow_1\rangle + b|\downarrow_1\rangle$$

$$|\Psi^-_{2,3}\rangle = \frac{1}{\sqrt{2}}\left(|\downarrow_2 \blacksquare\rangle - |\uparrow_2 \blacksquare\rangle\right)$$

$$|\Psi^-_{2,3}\rangle = \frac{1}{\sqrt{2}}\left(|\blacksquare\uparrow_3\rangle - |\blacksquare\downarrow_3\rangle\right)$$

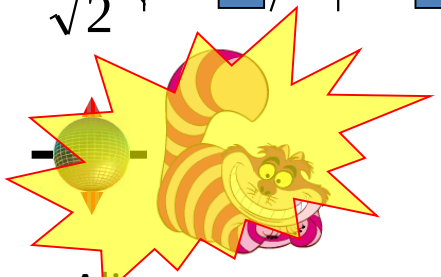

Alice

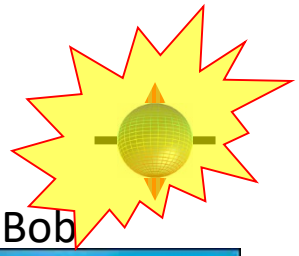

Bob

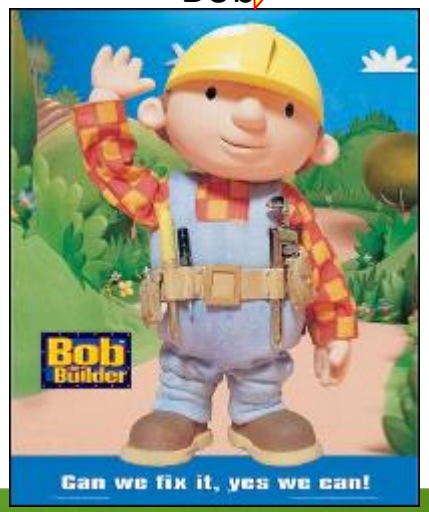

Kwantowa teleportacja

pufff...

$$\left|\Psi_{2,1}^{-}\right\rangle = \frac{1}{\sqrt{2}}\left(\left|\downarrow_2\uparrow_1\right\rangle - \left|\uparrow_2\downarrow_1\right\rangle\right)$$

$$\left|\phi\right\rangle = \begin{bmatrix} 0 & 1 \\ 1 & 0 \end{bmatrix}\left(a\left|\uparrow_3\right\rangle + b\left|\downarrow_3\right\rangle\right)$$

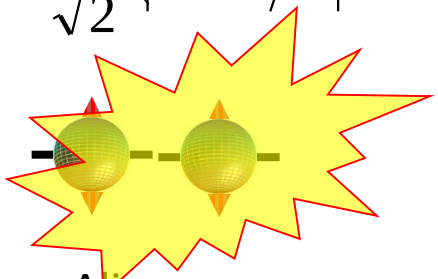

Alice

Bob

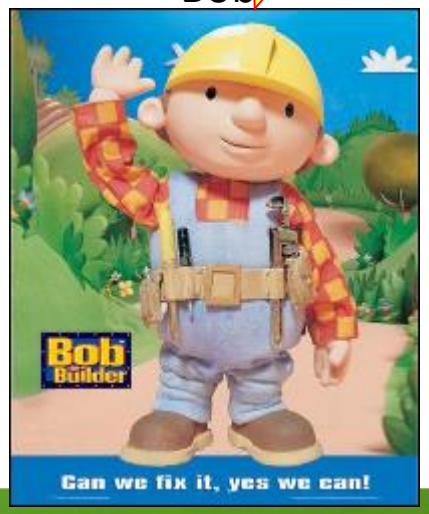

Kwantowa teleportacja

$$\left|\Psi_{2,1}^{-}\right\rangle = \frac{1}{\sqrt{2}}\left(\left|\downarrow_2\uparrow_1\right\rangle - \left|\uparrow_2\downarrow_1\right\rangle\right)$$

$$\left|\phi\right\rangle = \begin{bmatrix} 0 & 1 \\ 1 & 0 \end{bmatrix}\left(a\left|\uparrow_3\right\rangle + b\left|\downarrow_3\right\rangle\right)$$

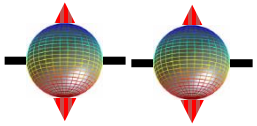

Alice

Bob

Kwantowa teleportacja

$$\left|\Psi_{2,1}^{-}\right\rangle = \frac{1}{\sqrt{2}}\left(\left|\downarrow_2\uparrow_1\right\rangle - \left|\uparrow_2\downarrow_1\right\rangle\right)$$

$$\left|\phi\right\rangle = a\left|\uparrow_3\right\rangle + b\left|\downarrow_3\right\rangle$$

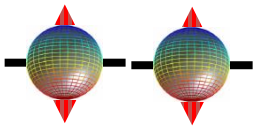

Alice

Bob

Kwantowa teleportacja

1. Przekazywana jest stan obiektu, a nie sam obiekt fizyczny.
2. Obiekt nie jest skopiowany (por. zasada Heisenberga, *zakaz klonowania*)
3. Informacja nie porusza się szybciej niż światło.
4. Trudności w pomiarze wszystkich czterech stanów Bella (wydajność).

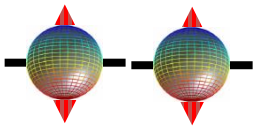

Alice

Bob

Kwantowa teleportacja

Anton Zeilinger

Institute of Experimental Physics, University of Vienna,

Teleportacja stanów fotonowych

Nature, **390**, 575 (1997)

Experimental quantum teleportation

Dik Bouwmeester, Jian-Wei Pan, Klaus Mattle, Manfred Eibl, Harald Weinfurter & Anton Zeilinger

Institut für Experimentalphysik, Universität Innsbruck, Technikerstr. 25, A-6020 Innsbruck, Austria

Quantum teleportation—the transmission and reconstruction over arbitrary distances of the state of a quantum system—is demonstrated experimentally. During teleportation, an initial photon which carries the polarization that is to be transferred and one of a pair of entangled photons are subjected to a measurement such that the second photon of the entangled pair acquires the polarization of the initial photon. This latter photon can be arbitrarily far away from the initial one. Quantum teleportation will be a critical ingredient for quantum computation networks.

Kwantowa teleportacja

Anton Zeilinger

Institute of Experimental Physics, University of Vienna,

Teleportacja stanów fotonowych

Nature, **390**, 575 (1997)

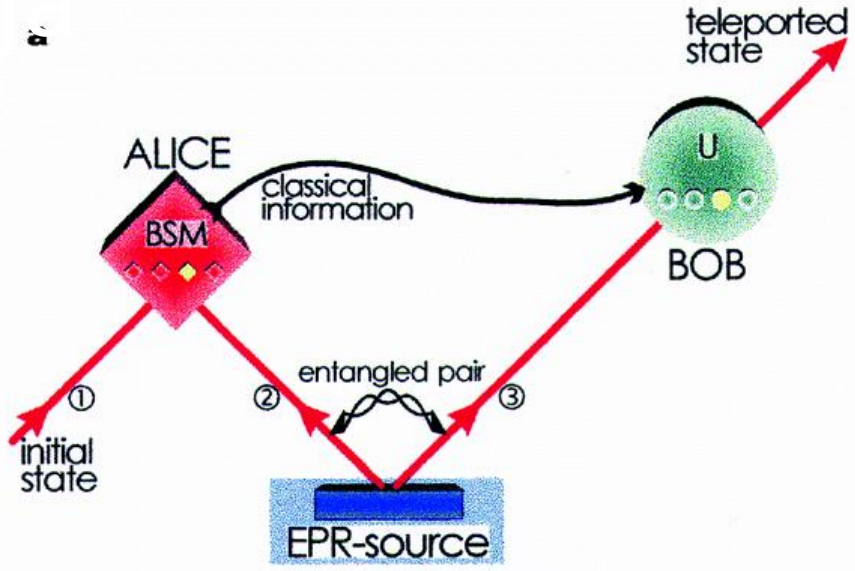

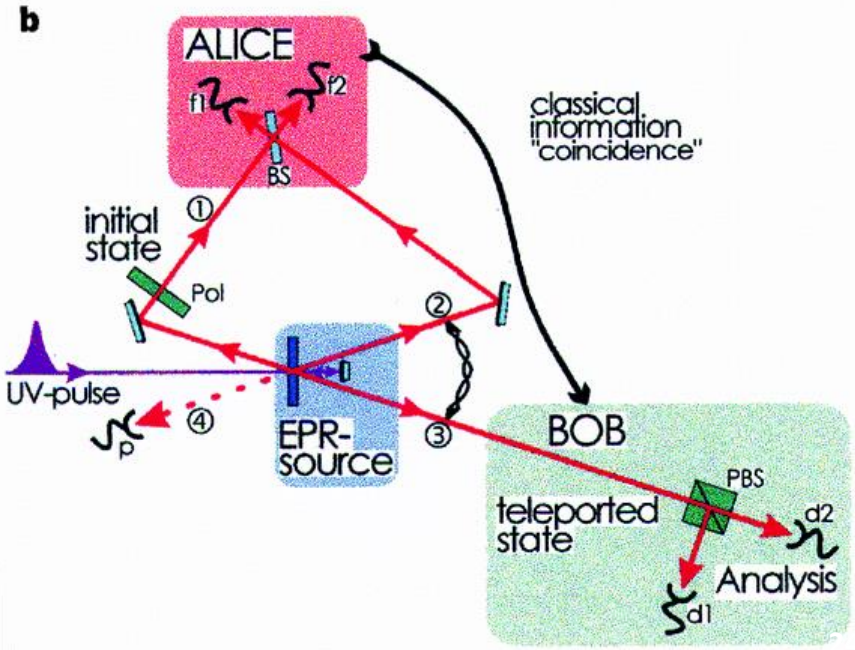

Kwantowa teleportacja

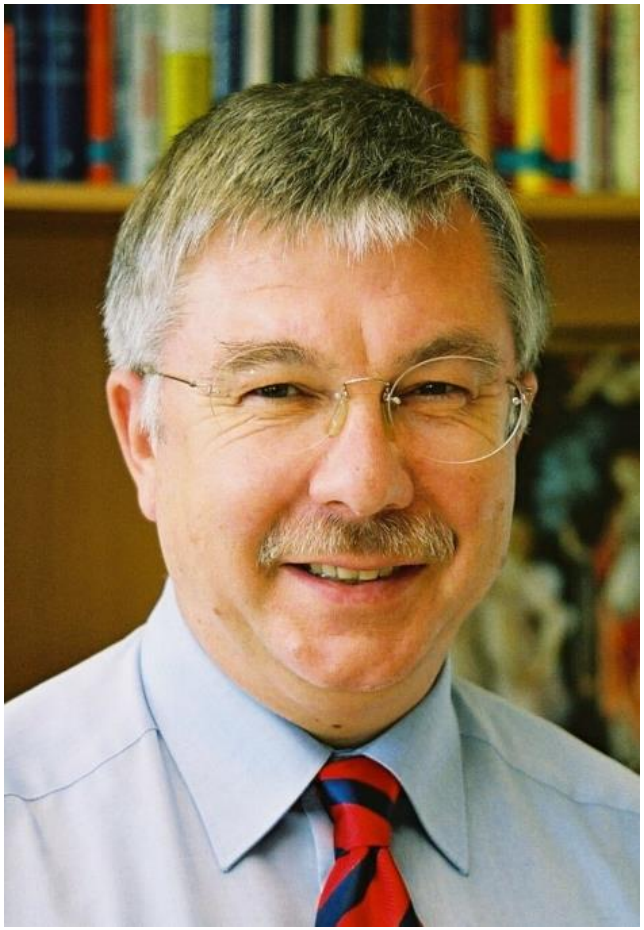

Reiner Blatt

Institute of Experimental Physics, University of Insbruck,

Deterministic quantum teleportation with atoms

M. Riebe[1], H. Häffner[1], C. F. Roos[1], W. Hänsel[1], J. Benhelm[1], G. P. T. Lancaster[1], T. W. Körber[1], C. Becher[1], F. Schmidt-Kaler[1], D. F. V. James[2] & R. Blatt[1,3]

[1]*Institut für Experimentalphysik, Universität Innsbruck, Technikerstraße 25, A-6020 Innsbruck, Austria*
[2]*Theoretical Division T-4, Los Alamos National Laboratory, Los Alamos NM 87545, USA*
[3]*Institut für Quantenoptik und Quanteninformation, Österreichische Akademie der Wissenschaften, Technikerstraße 25, A-6020 Innsbruck, Austria*

Teleportacja stanów kwantowych jonów $^{40}Ca^{+}$ w pułapce jonowej

Nature, **429**, 734 (2004)

Kwantowa teleportacja

Table 1 **Pulse sequence of the teleportation protocol.**

	Action	Comment
1	Light at 397 nm	Doppler preparation
2	Light at 729 nm	Sideband cooling
3	Light at 397 nm	Optical pumping
Entangle		
4	$R_3^+(\pi/2,3\pi/2)$	Entangle ion 3 with motional qubit
5	$R_2^C(\pi,3\pi/2)$	Prepare ion 2 for entanglement
6	$R_2^+(\pi,\pi/2)$	Entangle ion 2 with ion 3
7	Wait for 1 μs – 10,000 μs	Standby for teleportation
8	$R_3^H(\pi,0)$	Hide target ion
9	$R_1^C(\vartheta_\chi,\varphi_\chi)$	Prepare source ion 1 in state χ
Rotate into Bell basis		
10	$R_2^+(\pi,3\pi/2)$	Get motional qubit from ion 2
11	$R_1^+(\pi/\sqrt{2},\pi/2)$	Composite pulse for phasegate
12	$R_1^+(\pi,0)$	Composite pulse for phasegate
13	$R_1^+(\pi/\sqrt{2},\pi/2)$	Composite pulse for phasegate
14	$R_1^+(\pi,0)$	Composite pulse for phasegate
15	$R_1^C(\pi,\pi/2)$	Spin echo on ion 1
16	$R_3^H(\pi,\pi)$	Unhide ion 3 for spin echo
17	$R_3^C(\pi,\pi/2)$	Spin echo on ion 3
18	$R_3^H(\pi,0)$	Hide ion 3 again
19	$R_2^+(\pi,\pi/2)$	Write motional qubit back to ion 2
20	$R_1^C(\pi/2,3\pi/2)$	Part of rotation into Bell basis
21	$R_2^C(\pi/2,\pi/2)$	Finalize rotation into Bell basis
Read out		
22	$R_2^H(\pi,0)$	Hide ion 2
23	PMDetection for 250 μs	Read out of ion 1 with photomultiplier
24	$R_1^H(\pi,0)$	Hide ion 1
25	$R_2^H(\pi,\pi)$	Unhide ion 2
26	PMDetection for 250 μs	Read out of ion 2 with photomultiplier
27	$R_2^H(\pi,0)$	Hide ion 2
28	Wait 300 μs	Let system rephase; part of spin echo
29	$R_3^H(\pi,\pi)$	Unhide ion 3
30	$R_3^C(\pi/2,3\pi/2+\phi)$	Change basis
Reconstruction		
31	$R_3^C(\pi,\phi)$	$\left.\begin{matrix} i\sigma_x \\ -i\sigma_y \end{matrix}\right\} = -i\sigma_z$ conditioned on PM detection 1
32	$R_3^C(\pi,\pi/2+\phi)$	
33	$R_3^C(\pi,\phi)$	$i\sigma_x$ conditioned on PM detection 2
34	$R_3^C(\vartheta_\chi,\varphi_\chi+\pi+\phi)$	Inverse of preparation of χ with offset ϕ
35	Light at 397 nm	Read out of ion 3 with camera

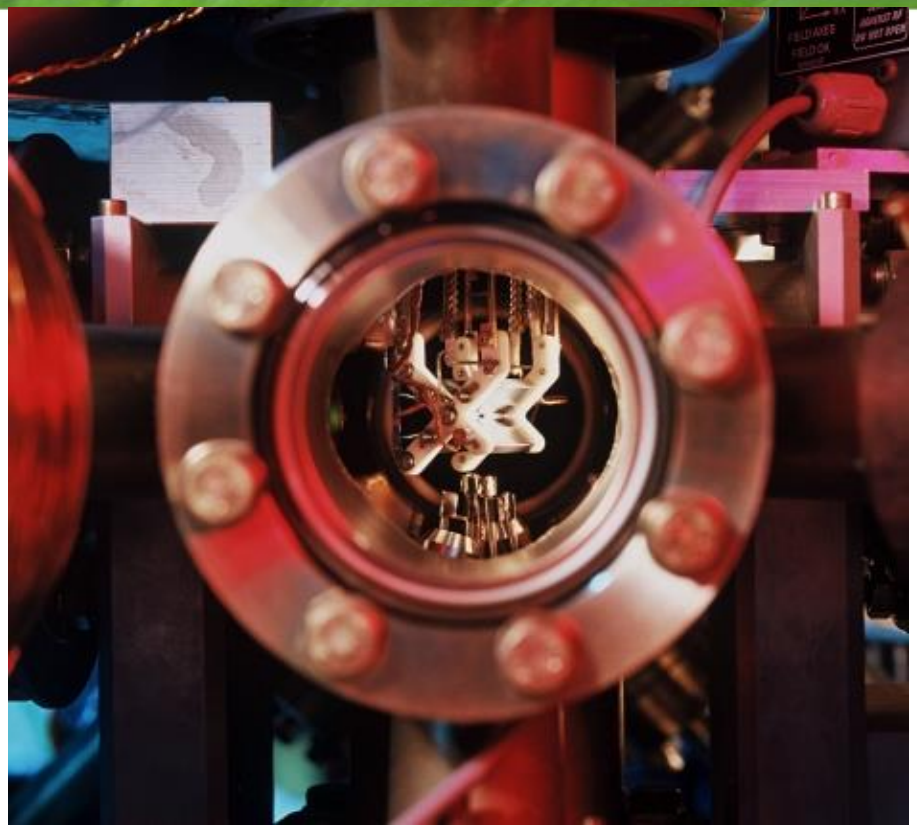

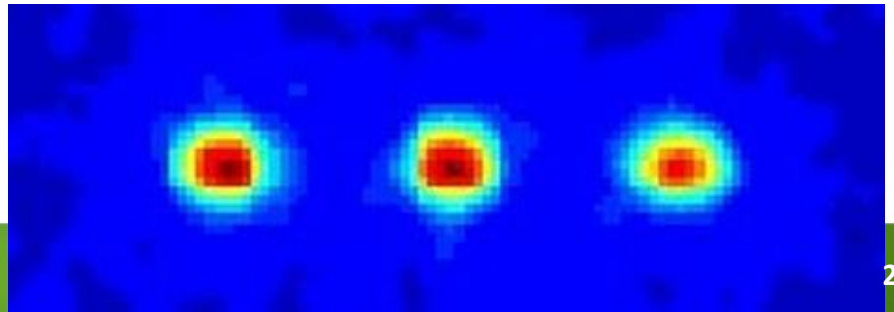

Maszyna do teleportacji

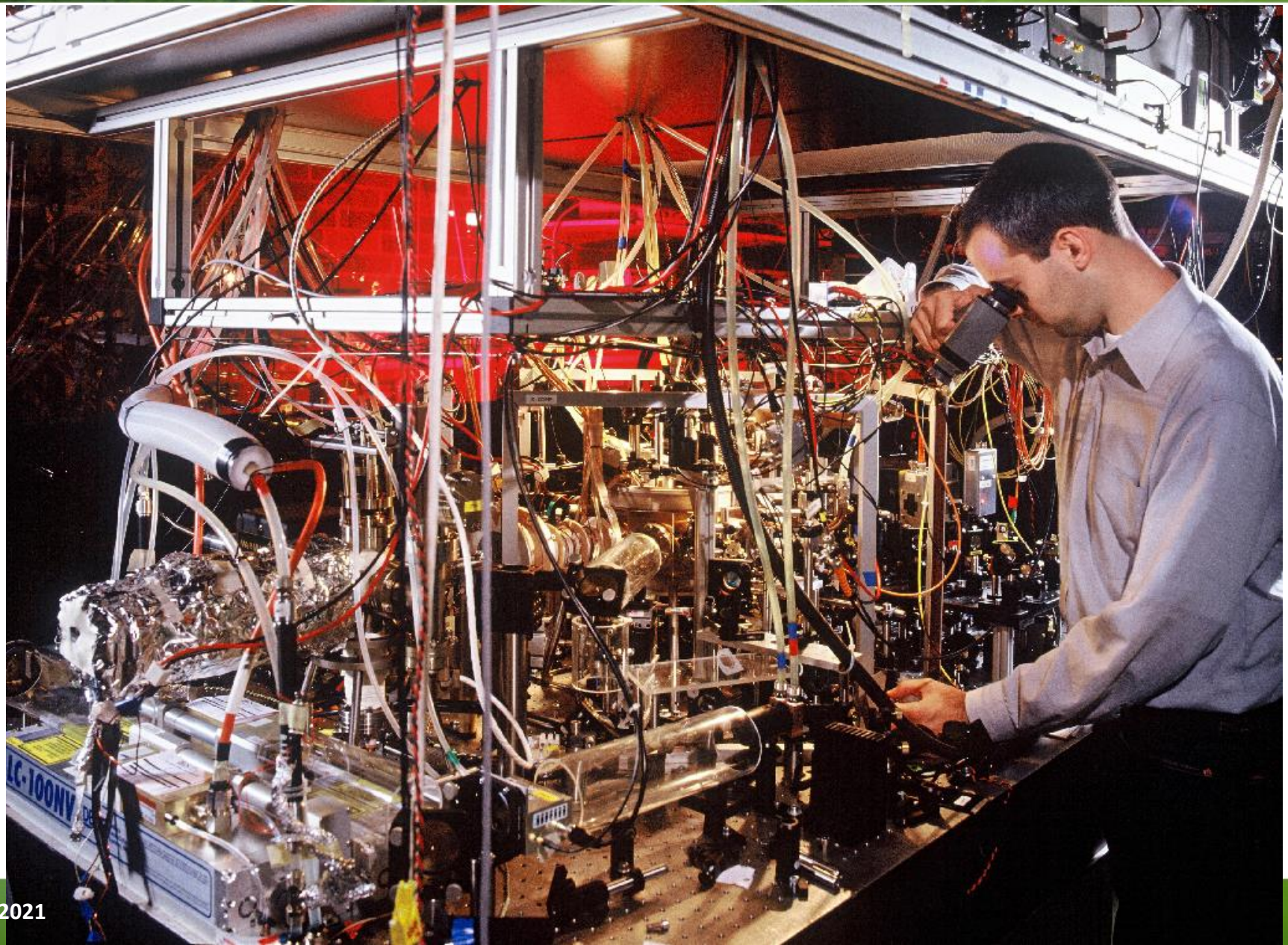

Quantum Teleporation: The Math

Three qubit joint state of Alice, Bob, and "Victor" who prepared $|\psi\rangle$:

$$|\chi\rangle = |\psi\rangle_V \otimes |\Phi^{(+)}\rangle_{AB} = (\alpha|0\rangle_V + \beta|1\rangle_V) \otimes (|0\rangle_A \otimes |0\rangle_B + |1\rangle_A \otimes |1\rangle_B)$$

$$= \frac{1}{2}\Big[(|0\rangle_V \otimes |0\rangle_A + |1\rangle_V \otimes |1\rangle_A) \otimes (\alpha|0\rangle_B + \beta|1\rangle_B) + (|0\rangle_V \otimes |0\rangle_A - |1\rangle_V \otimes |1\rangle_A) \otimes (\alpha|0\rangle_B - \beta|1\rangle_B)$$

$$+ (|0\rangle_V \otimes |1\rangle_A + |1\rangle_V \otimes |0\rangle_A) \otimes (\alpha|1\rangle_B + \beta|0\rangle_B) + (|0\rangle_V \otimes |1\rangle_A - |1\rangle_V \otimes |0\rangle_A) \otimes (\alpha|1\rangle_B - \beta|0\rangle_B)\Big]$$

$$|\chi\rangle = \frac{1}{2}\left(|\Phi^{(+)}\rangle_{VA} \otimes |\psi\rangle_B + |\Phi^{(-)}\rangle_{VA} \otimes Z|\psi\rangle_B + |\Psi^{(+)}\rangle_{VA} \otimes X|\psi\rangle_B - i|\Psi^{(-)}\rangle_{VA} \otimes Y|\psi\rangle_B\right)$$

A measurement by Alice in Bell-basis leaves Bob's qubit in one of four states:

$$\left\{|\psi\rangle_B,\ Z|\psi\rangle_B,\ X|\psi\rangle_B,\ Y|\psi\rangle_B\right\}$$

Alice uses the classical channel to tell Bob which Bell state she found.
Bob can then put his qubit in the unknown state, through application of a Pauli.

sciencealert

Trending

(aleksandarnakovski/iStock)

PHYSICS

Quantum Teleportation Reported in a Qutrit For The First Time

DAVID NIELD 26 DEC 2019

PHYSICAL REVIEW LETTERS **123,** 070505 (2019)

Editors' Suggestion | Featured in Physics

Quantum Teleportation in High Dimensions

Yi-Han Luo,[1,2] Han-Sen Zhong,[1,2] Manuel Erhard,[3,4] Xi-Lin Wang,[1,2] Li-Chao Peng,[1,2] Mario Krenn,[3,4] Xiao Jiang,[1,2] Li Li,[1,2] Nai-Le Liu,[1,2] Chao-Yang Lu,[1,2,*] Anton Zeilinger,[3,4,†] and Jian-Wei Pan[1,2,‡]

[1]*Hefei National Laboratory for Physical Sciences at Microscale and Department of Modern Physics, University of Science and Technology of China, Hefei, 230026, China*

[2]*CAS Centre for Excellence in Quantum Information and Quantum Physics, Hefei, 230026, China*

[3]*Austrian Academy of Sciences, Institute for Quantum Optics and Quantum Information (IQOQI), Boltzmanngasse 3, A-1090 Vienna, Austria*

[4]*Vienna Center for Quantum Science and Technology (VCQ), Faculty of Physics, University of Vienna, A-1090 Vienna, Austria*

(Received 20 June 2019; published 15 August 2019)

https://www.sciencealert.com/quantum-teleportation-reported-in-a-qutrit-for-the-first-time

Kryptografia kwantowa

Jacek.Szczytko@fuw.edu.pl Wydział Fizyki UW

Zakaz klonowania

Źródło: Lucas Film

Zakaz klonowania

Źródło: internet

Klonowanie stanów kwantowych

$$|\Psi\rangle \rightarrow |\Psi\rangle, |\Psi\rangle, |\Psi\rangle, |\Psi\rangle, |\Psi\rangle, |\Psi\rangle, |\Psi\rangle \ldots$$

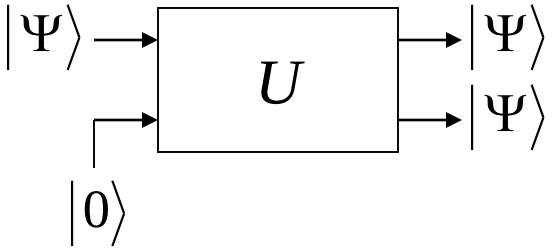

„czysta kartka”

Wtedy $U|\Psi\rangle|0\rangle = |\Psi\rangle|\Psi\rangle$

$U|0\rangle|0\rangle = |0\rangle|0\rangle$

$U|1\rangle|0\rangle = |1\rangle|1\rangle$

Ale dla $|\Psi\rangle = \alpha|0\rangle + \beta|1\rangle$ Dostajemy sprzeczność bo:

$$U|\Psi\rangle|0\rangle = U(\alpha|0\rangle + \beta|1\rangle)|0\rangle = \alpha U|0\rangle|0\rangle + \beta U|1\rangle|0\rangle = \alpha|0\rangle|0\rangle + \beta|1\rangle|1\rangle \neq |\Psi\rangle|\Psi\rangle$$

!

bo $|\Psi\rangle|\Psi\rangle = \alpha^2|0\rangle|0\rangle + \alpha\beta|0\rangle|1\rangle + \beta\alpha|1\rangle|0\rangle + \beta^2|1\rangle|1\rangle$

Kryptografia Kwantowa

- http://zon8.physd.amu.edu.pl/~tanas/

1.4 Proste szyfry

Szyfr Cezara

szyfr podstawieniowy monoalfabetyczny

A B C D E F G H I J K L M N O P R S T U V W X Y Z
D E F G H I J K L M N O P R S T U V W X Y Z A B C

tekst jawny $\longrightarrow$ K R Y P T O G R A F I A
kryptogram $\longrightarrow$ N U B T W S J U D I L D

- http://zon8.physd.amu.edu.pl/~tanas/

Kryptografia Kwantowa

- http://zon8.physd.amu.edu.pl/~tanas/

Szyfr Vigenère'a

	A	B	C	D	E	F	G	H	I	J	K	L	M	N	O	P	R	S	T	U	V	W	X	Y	Z
B	B	C	D	E	F	G	H	I	J	K	L	M	N	O	P	R	S	T	U	V	W	X	Y	Z	A
C	C	D	E	F	G	H	I	J	K	L	M	N	O	P	R	S	T	U	V	W	X	Y	Z	A	B
D	D	E	F	G	H	I	J	K	L	M	N	O	P	R	S	T	U	V	W	X	Y	Z	A	B	C
E	E	F	G	H	I	J	K	L	M	N	O	P	R	S	T	U	V	W	X	Y	Z	A	B	C	D
F	F	G	H	I	J	K	L	M	N	O	P	R	S	T	U	V	W	X	Y	Z	A	B	C	D	E
G	G	H	I	J	K	L	M	N	O	P	R	S	T	U	V	W	X	Y	Z	A	B	C	D	E	F
H	H	I	J	K	L	M	N	O	P	R	S	T	U	V	W	X	Y	Z	A	B	C	D	E	F	G
I	I	J	K	L	M	N	O	P	R	S	T	U	V	W	X	Y	Z	A	B	C	D	E	F	G	H
J	J	K	L	M	N	O	P	R	S	T	U	V	W	X	Y	Z	A	B	C	D	E	F	G	H	I
K	K	L	M	N	O	P	R	S	T	U	V	W	X	Y	Z	A	B	C	D	E	F	G	H	I	J
L	L	M	N	O	P	R	S	T	U	V	W	X	Y	Z	A	B	C	D	E	F	G	H	I	J	K
M	M	N	O	P	R	S	T	U	V	W	X	Y	Z	A	B	C	D	E	F	G	H	I	J	K	L
N	N	O	P	R	S	T	U	V	W	X	Y	Z	A	B	C	D	E	F	G	H	I	J	K	L	M
O	O	P	R	S	T	U	V	W	X	Y	Z	A	B	C	D	E	F	G	H	I	J	K	L	M	N
P	P	R	S	T	U	V	W	X	Y	Z	A	B	C	D	E	F	G	H	I	J	K	L	M	N	O
R	R	S	T	U	V	W	X	Y	Z	A	B	C	D	E	F	G	H	I	J	K	L	M	N	O	P
S	S	T	U	V	W	X	Y	Z	A	B	C	D	E	F	G	H	I	J	K	L	M	N	O	P	R
T	T	U	V	W	X	Y	Z	A	B	C	D	E	F	G	H	I	J	K	L	M	N	O	P	R	S
U	U	V	W	X	Y	Z	A	B	C	D	E	F	G	H	I	J	K	L	M	N	O	P	R	S	T
V	V	W	X	Y	Z	A	B	C	D	E	F	G	H	I	J	K	L	M	N	O	P	R	S	T	U
W	W	X	Y	Z	A	B	C	D	E	F	G	H	I	J	K	L	M	N	O	P	R	S	T	U	V
X	X	Y	Z	A	B	C	D	E	F	G	H	I	J	K	L	M	N	O	P	R	S	T	U	V	W
Y	Y	Z	A	B	C	D	E	F	G	H	I	J	K	L	M	N	O	P	R	S	T	U	V	W	X
Z	Z	A	B	C	D	E	F	G	H	I	J	K	L	M	N	O	P	R	S	T	U	V	W	X	Y

klucz ⟶ S Z Y M P A N S S Z Y M

tekst ⟶ K R Y P T O G R A F I A

krypt. ⟶ C P W C I O U I S E G M

Kryptografia Kwantowa

Szyfr Vernama (one-time pad)

tekst jawny	⟶	S	Z	Y	F	R
binarnie	⟶	01010011	01011010	01011001	01000110	01010010
klucz	⟶	01110010	01010101	11011100	10110011	00101011
kryptogram	⟶	00100001	00001111	10000101	11110101	01111001

- Klucz jest losowym ciągiem bitów.
- Kryptogram jest także losowym ciągiem bitów i jeśli nie znamy klucza to nie dowiemy się niczego o tekście jawnym.
- Jeśli klucz jest tak długi jak wiadomość i użyty tylko raz, to szyfr ten gwarantuje bezpieczeństwo absolutne.
- Współczesne metody kryptograficzne sprowadzają się do obliczeń w systemie binarnym, czyli operacji na bitach.

•http://zon8.physd.amu.edu.pl/~tanas/

Kryptologia

Marian Rejewski

Jerzy Różycki

Henryk Zygalski

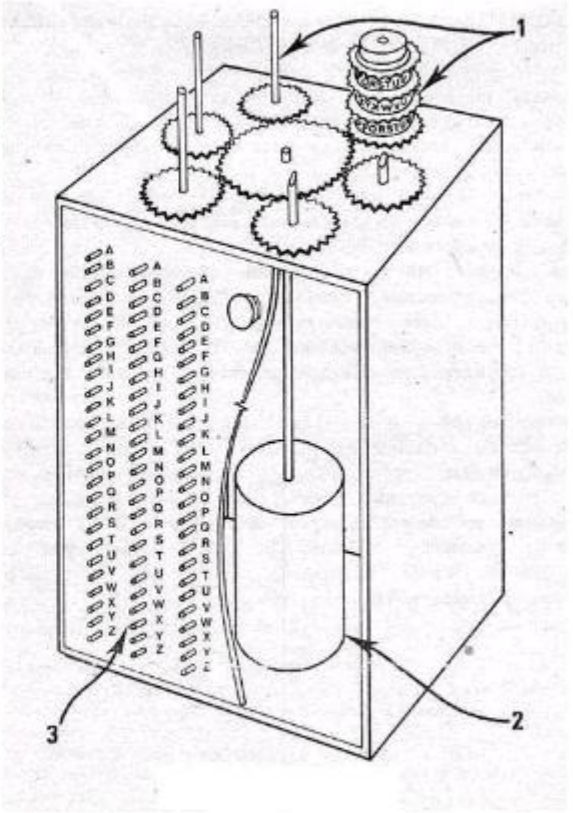

Enigma 1918/1923

images from http://www.armyradio.com/publish/Articles/The_Enigma_Code_Breach/

Szyfry nie do złamania

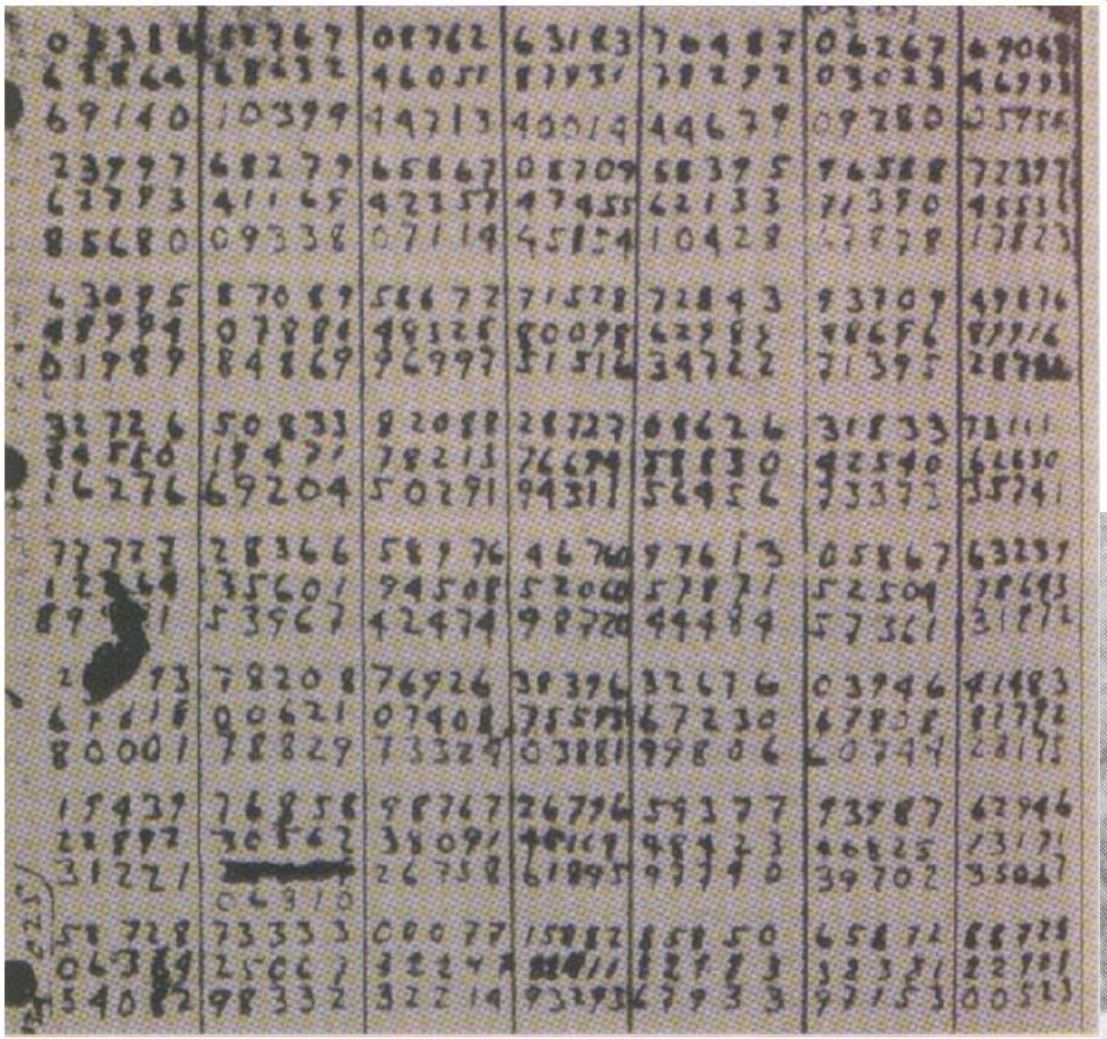

Klucze jednorazowe – nie do złamania!

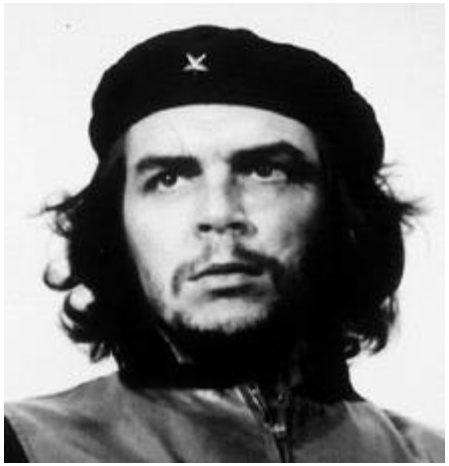

Kryptografia

Alice

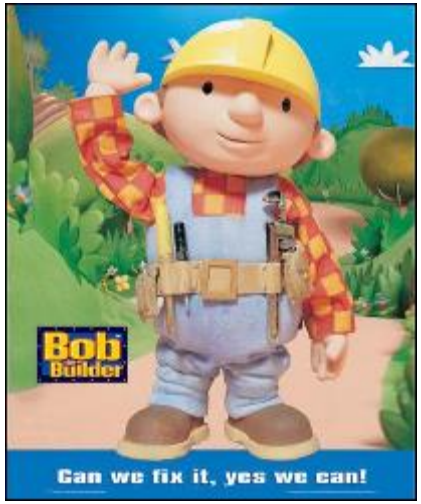

Bob

Kryptografia

Alice

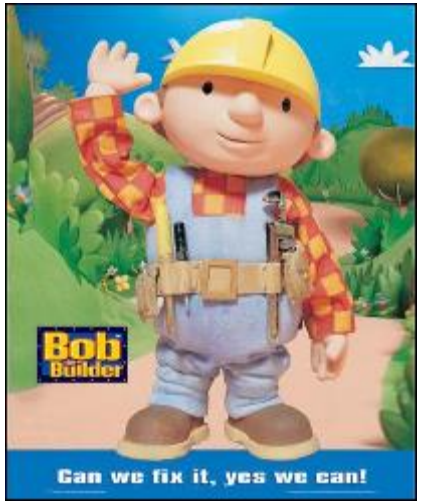

Bob

Eve (eavesdropper)

Kryptografia

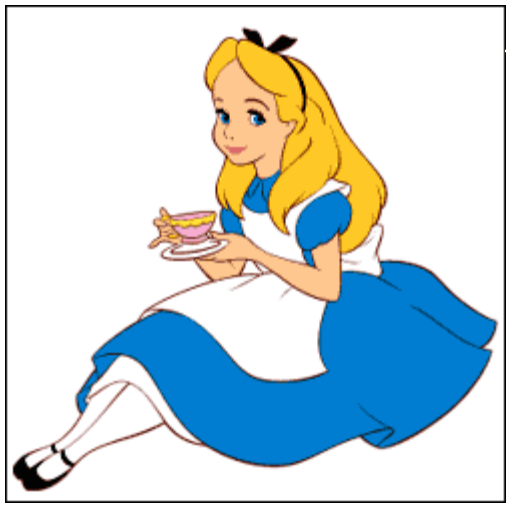

Alice

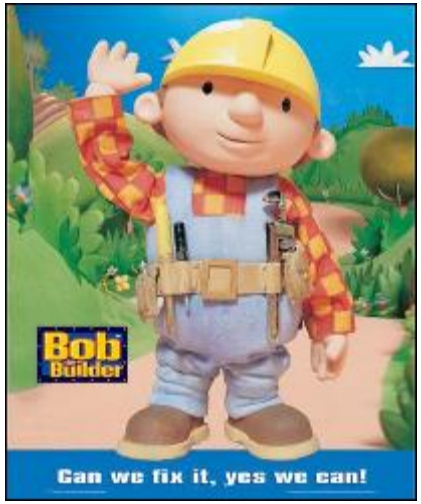

Bob

Eve

Kryptografia

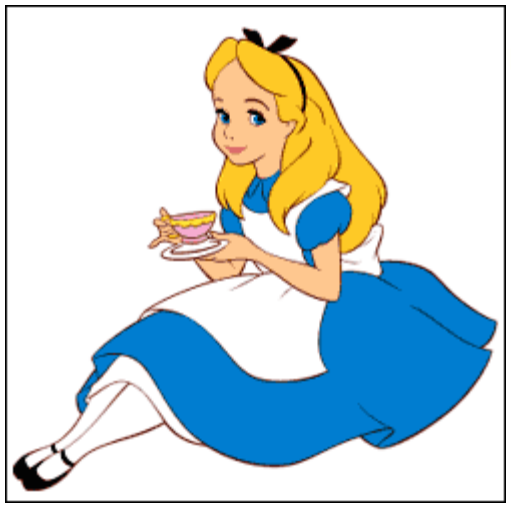

Alice

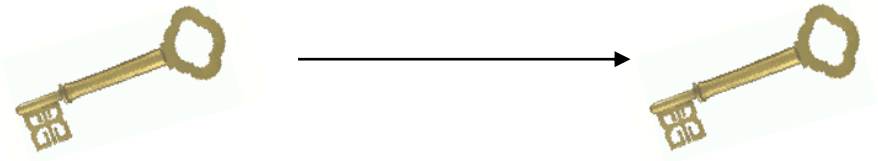

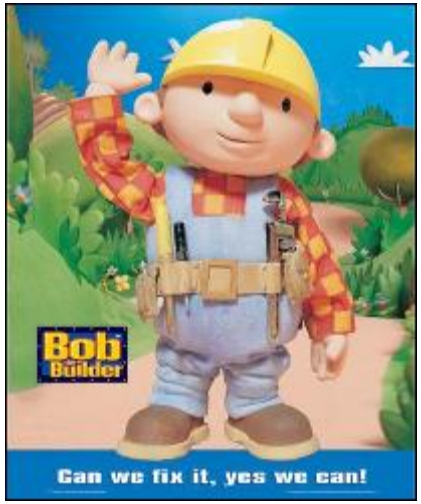

Bob

Eve

Kryptografia

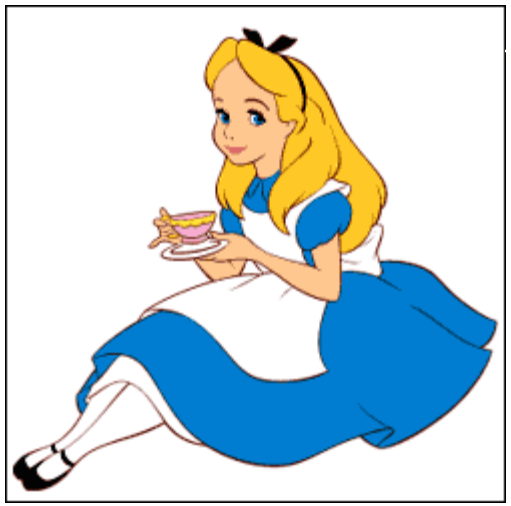

Alice

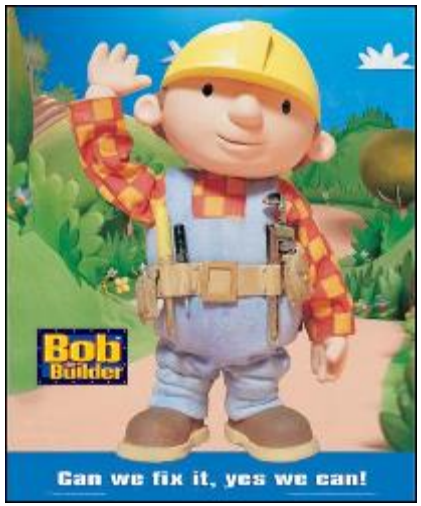

Bob

Eve

Kryptografia

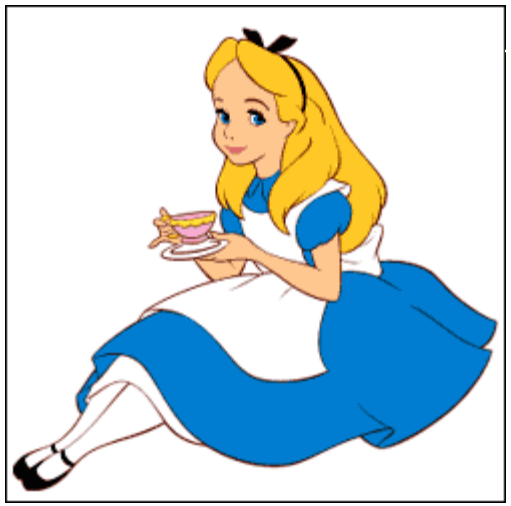

Alice

Aby mieć bezpieczny kanał łączności trzeba mieć bezpieczny kanał łączności...

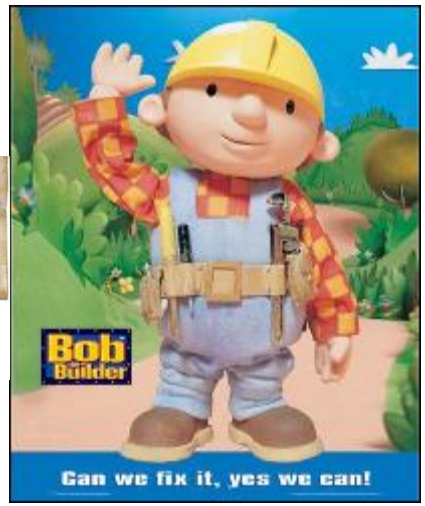

Bob

Eve

Kryptografia klucza publicznego

Alice

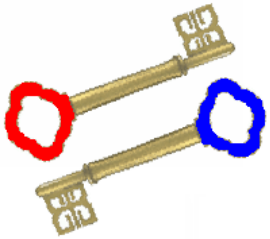

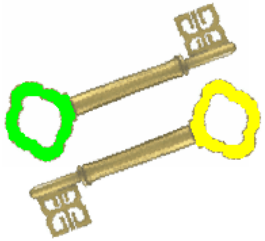

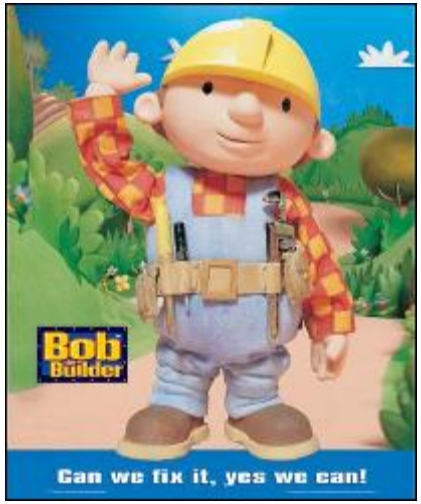

Bob

Kryptografia klucza publicznego

Alice

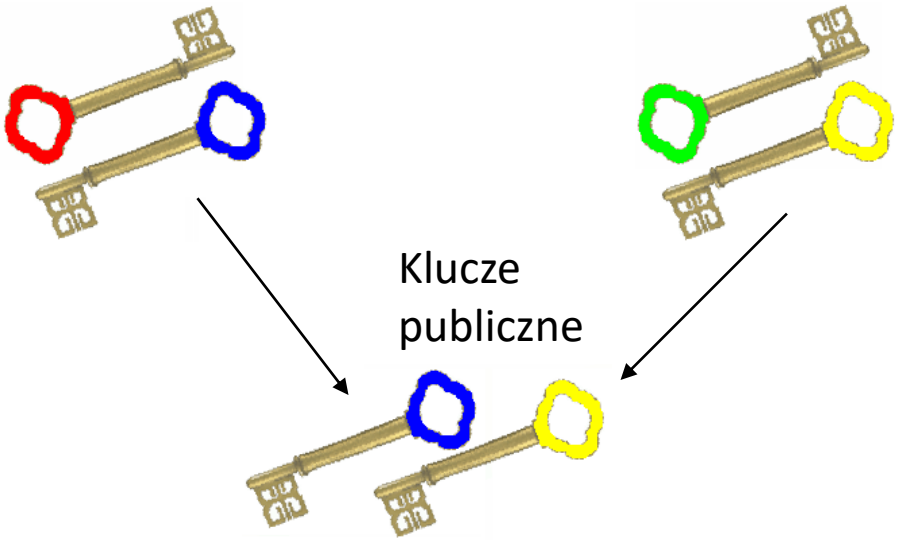

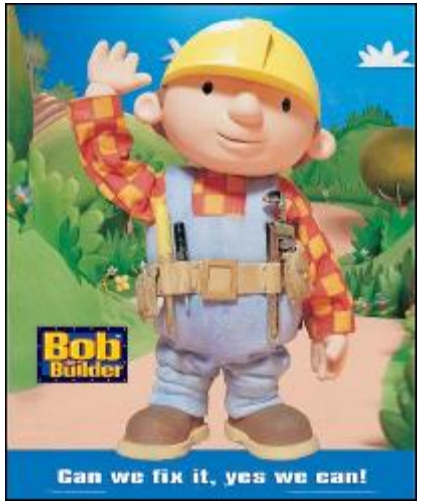

Bob

Kryptografia klucza publicznego

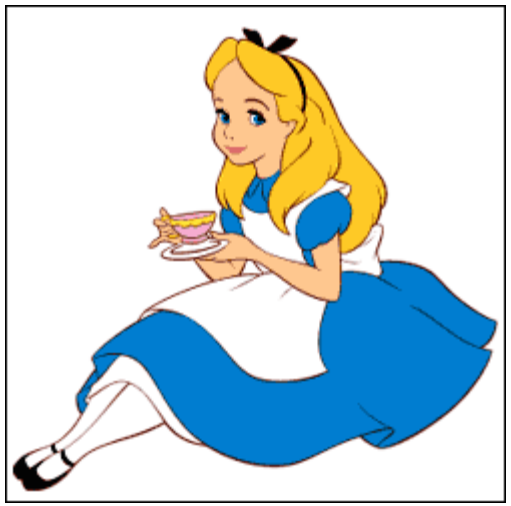

Alice

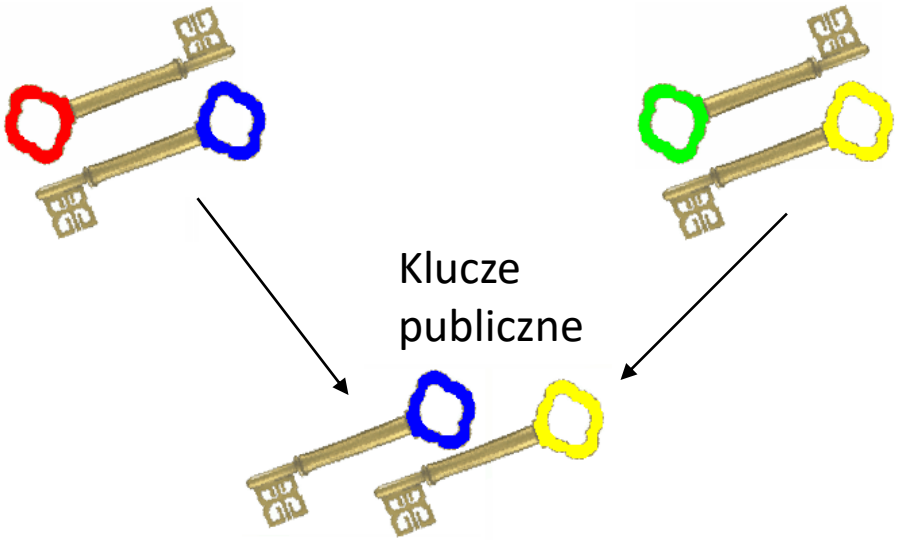

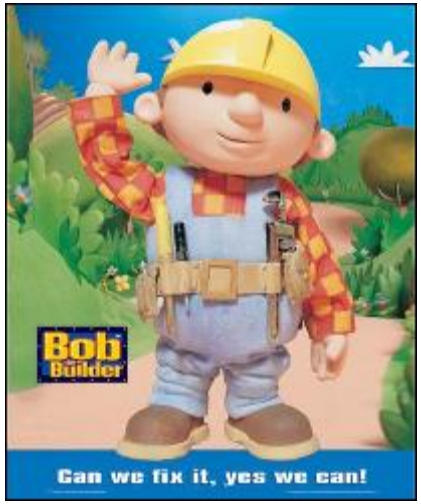

Bob

Kryptografia klucza publicznego

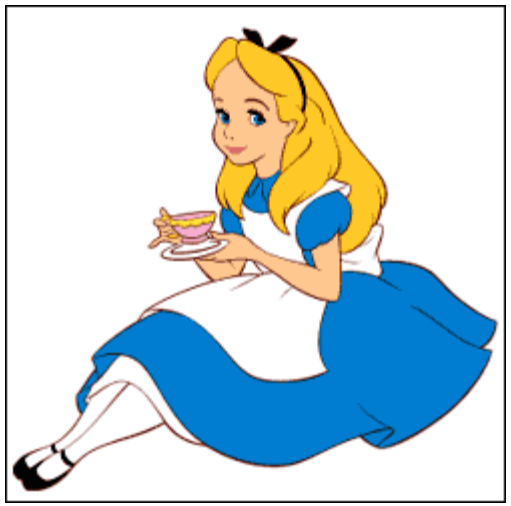

Alice

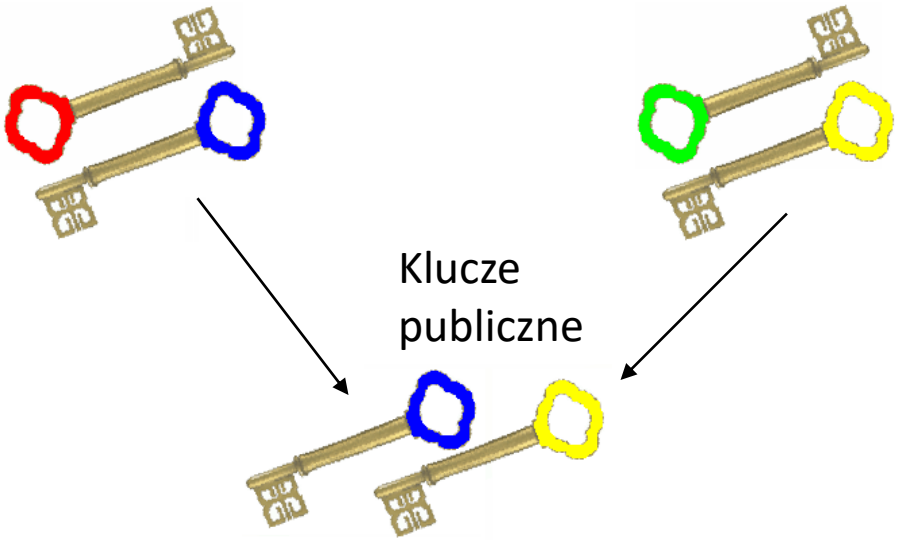

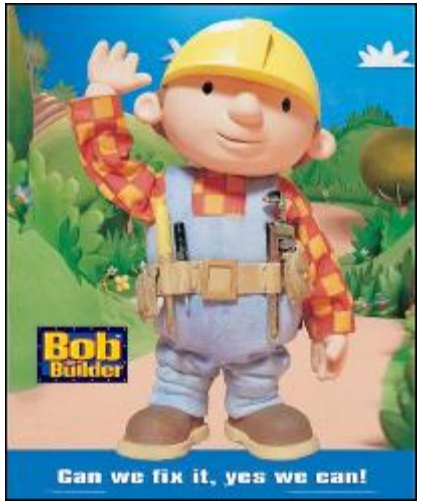

Bob

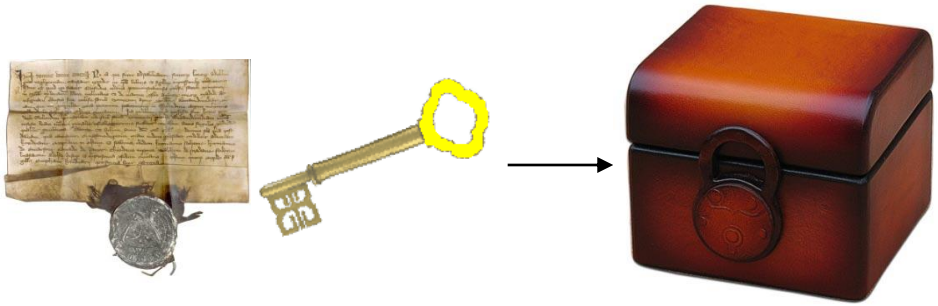

Kryptografia klucza publicznego

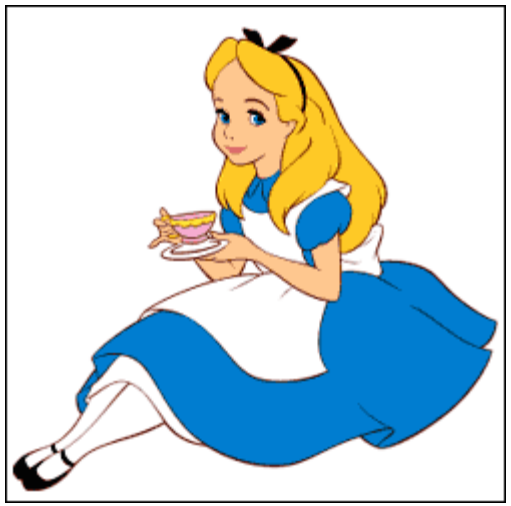

Alice

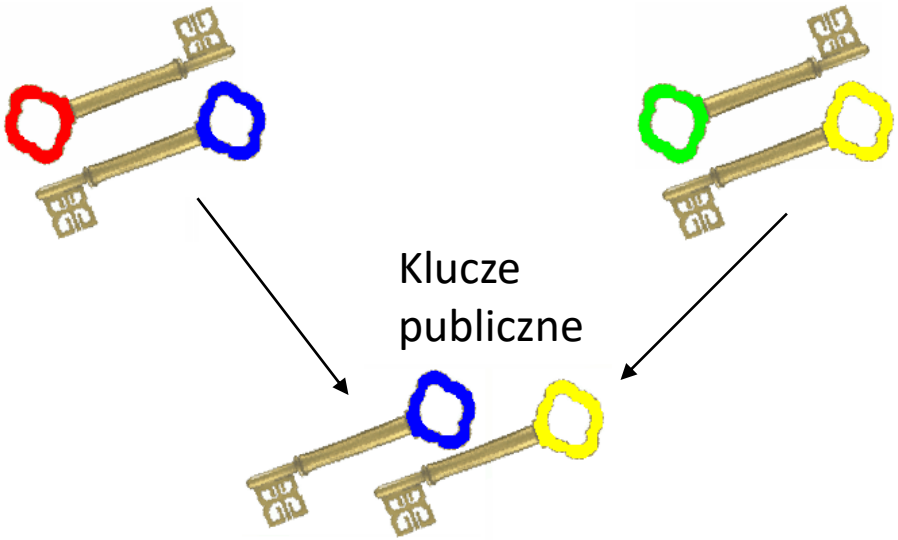

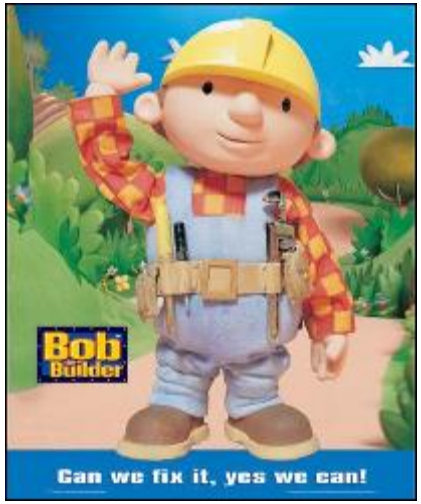

Bob

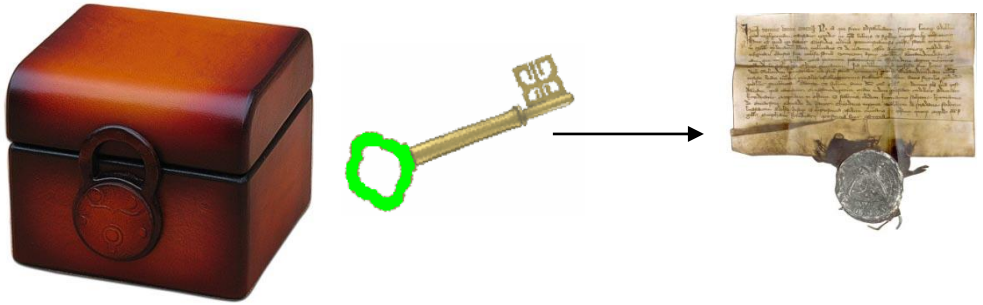

Kryptografia klucza publicznego

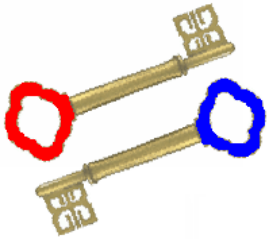
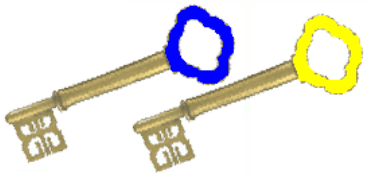

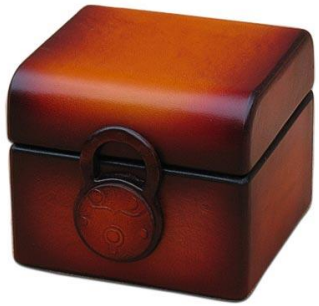
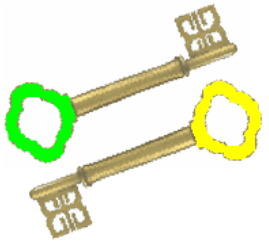

•Bezpieczenstwo systemu kryptograficznego z kluczem publicznym jest oparte na istnieniu funkcji jednostronnych, dla których znalezienie wartosci samej funkcji jest łatwe zas znalezienie argumentu funkcji kiedy znamy jej wartosc jest obliczeniowo trudne (jak trudne to zalezy od aktualnego stanu wiedzy i rozwoju techniki)

•Najbardziej znany kryptosystem z kluczem publicznym, RSA, opiera sie na trudnosci z rozkładem liczby na czynniki (faktoryzacja)

•Systemy takie nie gwarantuja pełnego bezpieczenstwa. Nie mozna wykluczyc, ze ktoś znajdzie efektywny algorytm faktoryzacji liczb.
W istocie taki algorytm juz istnieje. Jest to algorytm Shora! Wymaga on jednak komputera kwantowego!.

Kryptografia klucza publicznego

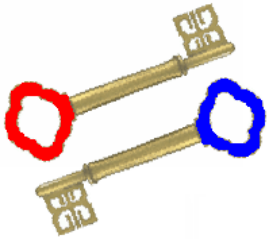
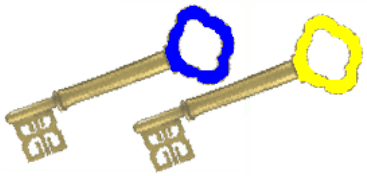

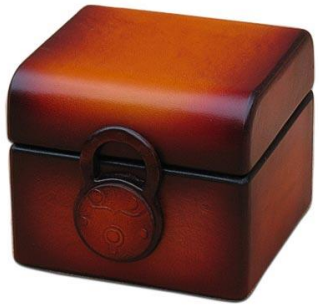
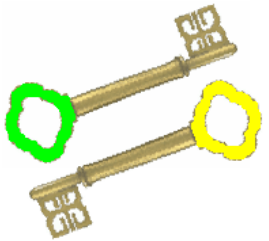

W 1994 r. RSA 129 został złamany na 1600 stacjach roboczych w ciagu 8 miesiecy

Eve

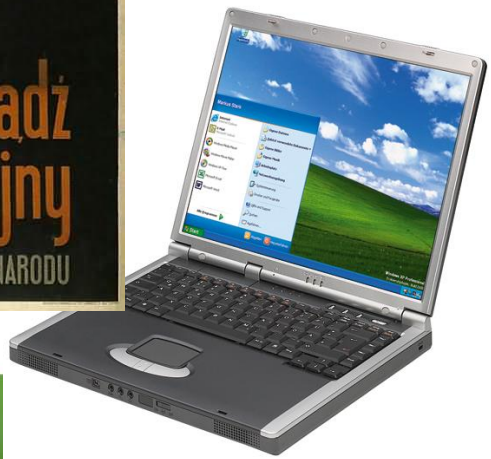

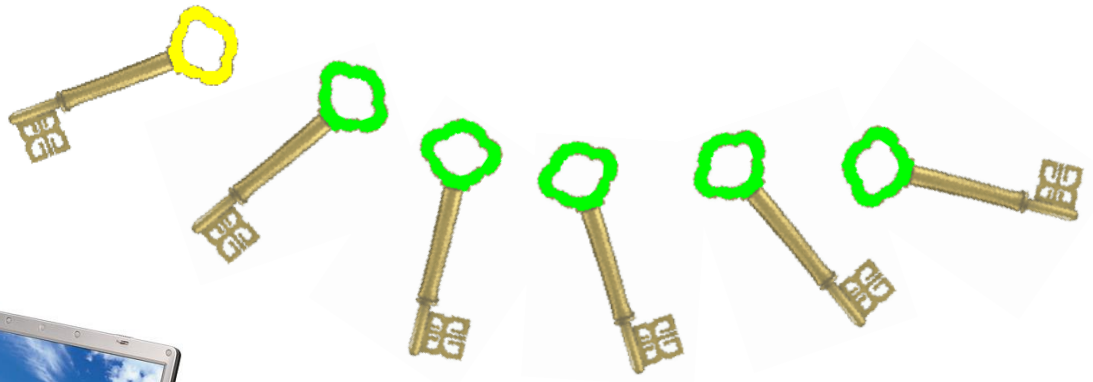

Kryptografia kwantowa

Wielokrotna i bezpieczna procedura uzgadniania klucza jednorazowego

http://wug.physics.uiuc.edu/courses/phys214/fall04/

Kryptografia kwantowa

Charles Bennett

Gilles Brassard

Wielokrotna i bezpieczna procedura uzgadniania klucza jednorazowego

QUANTUM CRYPTOGRAPHY: PUBLIC KEY DISTRIBUTION AND COIN TOSSING

Charles H. Bennett (IBM Research, Yorktown Heights NY 10598 USA)
Gilles Brassard (dept. IRO, Univ. de Montreal, H3C 3J7 Canada)

International Conference on Computers, Systems & Signal Processing Bangalore, India December 10-12, 1984

When elementary quantum systems, such as polarized photons, are used to transmit digital information, the uncertainty principle gives rise to novel cryptographic phenomena unachieveable with traditional transmission media, e.g. a communications channel on which it is impossible in principle to eavesdrop without a high probability of disturbing the transmission in such a way as to be detected. Such a quantum channel can be used in conjunction with ordinary insecure classical channels to distribute random key information between two users with the assurance that it remains unknown to anyone else, even when the users share no secret information initially. We also present a protocol for coin-tossing by exchange of quantum messages, which is secure against traditional kinds of cheating, even by an opponent with unlimited computing power, but ironically can be subverted by use of a still subtler quantum phenomemon, the Einstein-Podolsky-Rosen paradox.

... principle impossible to counterfeit, and multiplexing two or three messages in such a way that reading one destroys the others. More recently [BBBW], quantum coding has been used in conjunction with public key cryptographic techniques to yield several schemes for unforgeable subway tokens. Here we show that quantum coding by itself achieves one of the main advantages of public key cryptography by permitting secure distribution of random key information between parties who share no secret information initially, provided the parties have access, besides the quantum channel, to an ordinary channel susceptible to passive but not active eavesdropping. Even in the presence of active eavesdropping, the two parties can still distribute key securely if they share some secret information initially, provided the eavesdropping is not so active as to suppress communications completely. We also present a protocol for coin tossing by exchange of quantum messages. Except where otherwise noted the protocols

Kryptografia kwantowa

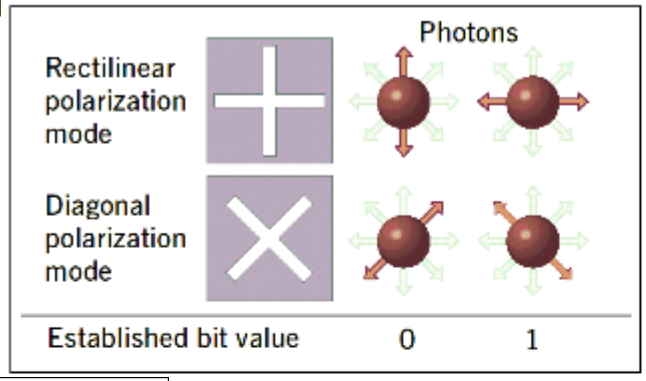

Protokół BB84 (Bennett, Brassard, 1984)

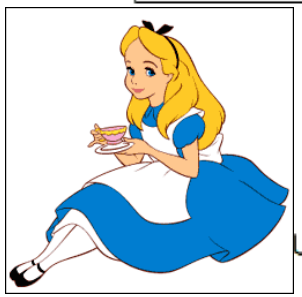

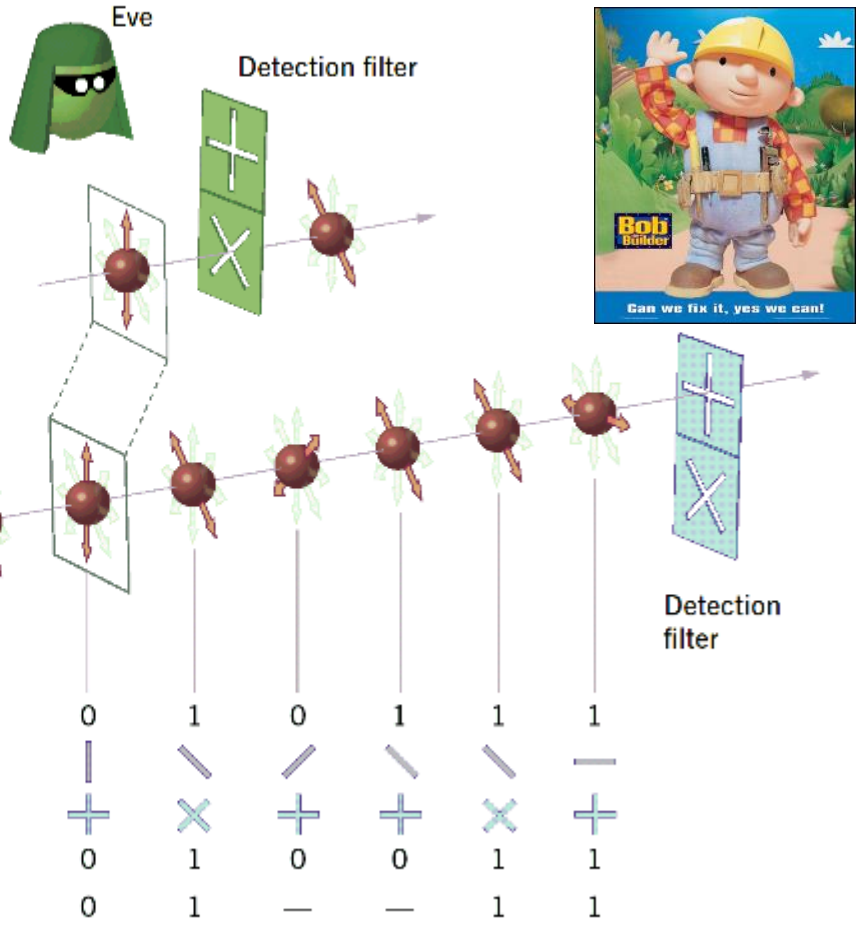

Bolek publicznie informuje Alicje jakiej bazy uzywał, zaś Alicja informuje go czy była to baza właściwa czy nie.

Kryptografia kwantowa

Uwagi:
Porównując bity wysłane przez Alicję z bitami zarejestrowanymi przez Bolka możemy podzielić bity zarejestrowane przez Bolka na trzy kategorie:
– bity pewne (średnio 50 %) — te dla których Bolek wybrał prawidłową bazę i które mogą być traktowane jako klucz kryptograficzny;
– bity prawidłowe pomimo złego wyboru bazy (średnio 25 %);
– bity nieprawidłowe (srednio 25 %).

Zatem prawdopodobieństwo tego, że zarejestrowany bit będzie prawidłowy (taki sam jak bit wysłany) jest równe 3/4
• Prawdopodobieństwo zarejestrowania bitu nieprawidłowego wynosi wiec 1/4

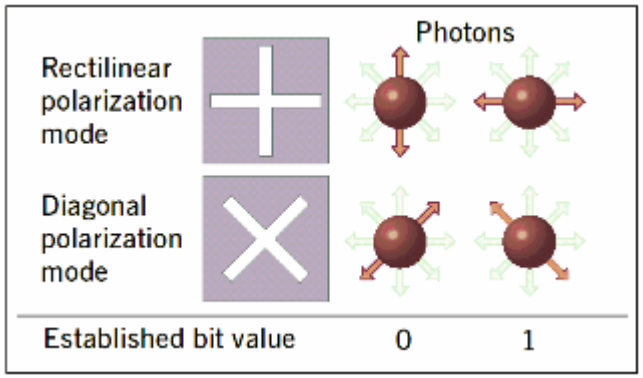

Kryptografia kwantowa

Uwagi:
Jeśli Ewa podsłuchuje stosując strategię tzw. *nieprzezroczystego podsłuchu*, to wybiera losowo bazę prostą lub ukośną, dokonuje pomiaru polaryzacji w tej bazie i następnie przesyła do Bolka foton o takiej polaryzacji jaką zmierzyła.

- Dokonywane przez Ewę pomiary muszą wprowadzić błędy, które Alicja i Bolek mogą wykryć przy uzgadnianiu klucza.

Takie błedy Alicja i Bolek mogą wykryć wybierając losowo pewną liczbę bitów klucza i porównując publicznym kanałem ich wartości. Te bity oczywiście następnie się wyrzuca.

- Jeśli liczba błędów przekracza założony poziom to uznaje się, że kanał był podsłuchiwany i procedurę uzgadniania klucza rozpoczyna się od nowa.

- **Mechanika kwantowa nie dopuszcza możliwości pasywnego podsłuchu. Bezpieczeństwo kwantowego systemu kryptograficznego gwarantowane jest przez prawa fizyki!**

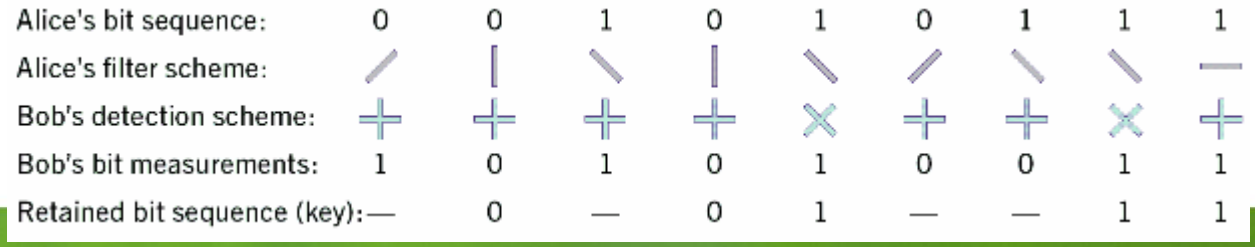

Produkty


ID QUANTIQUE - Mozilla Firefox
Plik Edycja Widok Przejdź Zakładki Narzędzia Pomoc
http://www.idquantique.com/
Idź
Getting Started Latest Headlines Gazeta.pl Murator :: Indeks Tabela NBP Slownik Ang. Slownik Fra. Google Desktop
id Quantique
Products Ordering Support Company News Contact Site Map
SWISS MADE
Are you protected against industrial espionage?
DO YOU TRUST THE SECURITY OF YOUR DATA NETWORK ?
Is your sensitive data as secure as you think?
Latest news
June 05:
A turnkey service to secure communications, based on QC, is now available in Switzerland. Strategic partnership between Fibrelac and idQ (pdf, English or French).
Network Security
Quantum Cryptography [QC] Systems
Vectis
[commercial applications]
Clavis
[research applications]
Overview of idQ's product offering in the field of QC.
Reasons why QC is the most secure technology.
Understanding QC: an introduction (pdf).
Securing networks with the Vectis Link Encryptor (pdf).
Future-proof data confidentiality with QC (pdf).
Random Number Generators [RNGs]
Quantis
Random numbers generation using Quantum Physics (pdf).
Algorithmic randomness, quantum physics and incompleteness (pdf).
Operating Systems supported by Quantis-PCI cards.
What makes Quantis a unique random number generator?
Optical Instrumentation
Photon counters - VIS
Counter arrays - VIS
Photon counters - NIR
Short pulse laser sources
Products overview
Besides its strong focus on Network Security applications, id Quantique is also a leading provider of Optical Instrumentation Products. The company's innovative photonic solutions are used in industrial, commercial and research applications.
© copyright 2005 id Quantique SA, All rights reserved
Zakończono
Disabled

Produkty

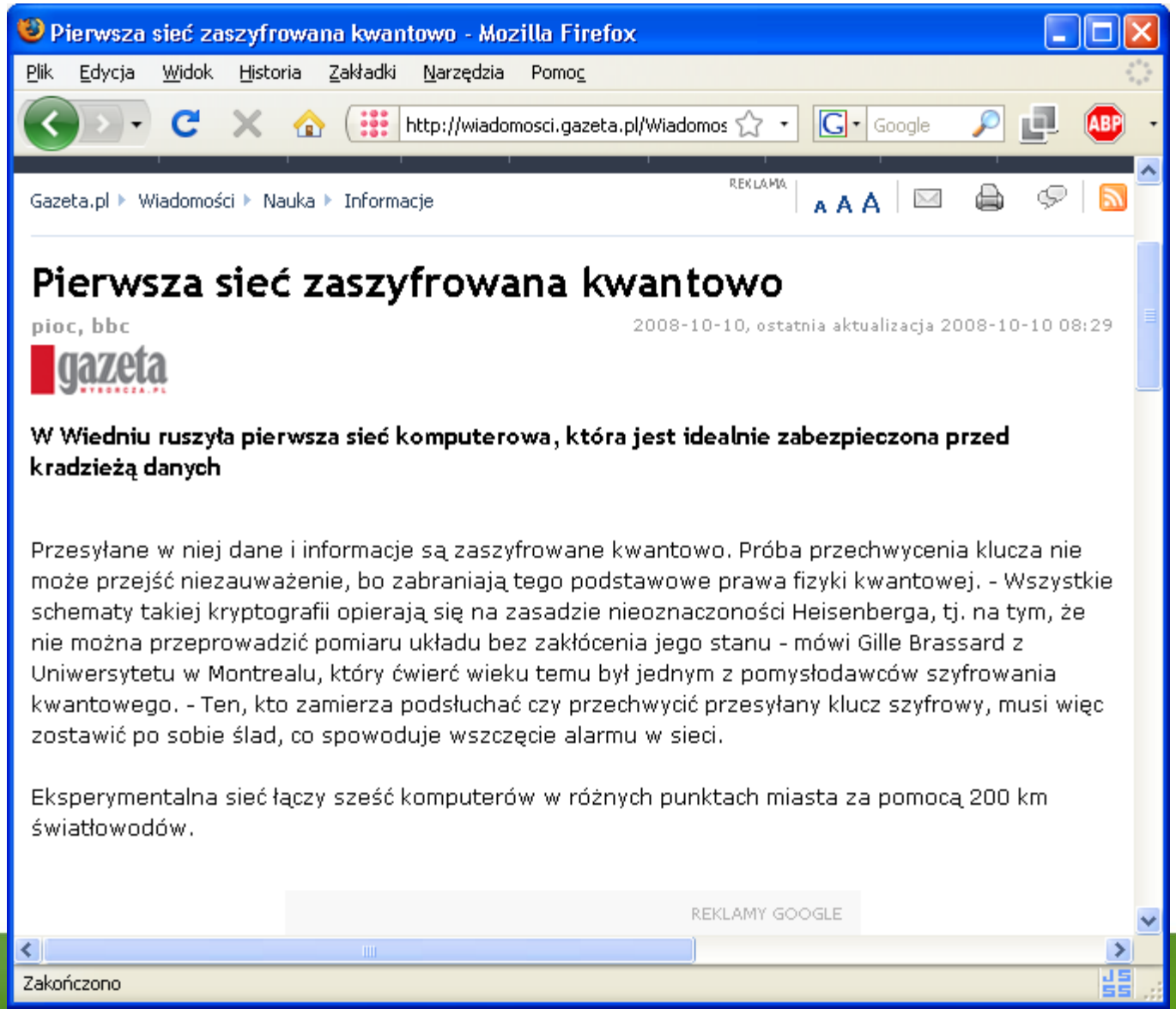
Pierwsza sieć zaszyfrowana kwantowo - Mozilla Firefox
Plik Edycja Widok Historia Zakładki Narzędzia Pomoc
http://wiadomosci.gazeta.pl/Wiadomos
Google
Gazeta.pl ▸ Wiadomości ▸ Nauka ▸ Informacje
REKLAMA
A A A
Pierwsza sieć zaszyfrowana kwantowo
pioc, bbc
2008-10-10, ostatnia aktualizacja 2008-10-10 08:29
gazeta
W Wiedniu ruszyła pierwsza sieć komputerowa, która jest idealnie zabezpieczona przed kradzieżą danych
Przesyłane w niej dane i informacje są zaszyfrowane kwantowo. Próba przechwycenia klucza nie może przejść niezauważenie, bo zabraniają tego podstawowe prawa fizyki kwantowej. - Wszystkie schematy takiej kryptografii opierają się na zasadzie nieoznaczoności Heisenberga, tj. na tym, że nie można przeprowadzić pomiaru układu bez zakłócenia jego stanu - mówi Gille Brassard z Uniwersytetu w Montrealu, który ćwierć wieku temu był jednym z pomysłodawców szyfrowania kwantowego. - Ten, kto zamierza podsłuchać czy przechwycić przesyłany klucz szyfrowy, musi więc zostawić po sobie ślad, co spowoduje wszczęcie alarmu w sieci.
Eksperymentalna sieć łączy sześć komputerów w różnych punktach miasta za pomocą 200 km światłowodów.
REKLAMY GOOGLE
Zakończono

Produkty


MagiQ Technologies - Mozilla Firefox
Plik Edycja Widok Przejdź Zakładki Narzędzia Pomoc
http://www.magiqtech.com/index.php
Idź
Getting Started Latest Headlines Gazeta.pl Murator :: Indeks Tabela NBP Slownik Ang. Slownik Fra. Google Desktop
MagiQ™
Products & Solutions | Research | About MagiQ | Press & Events | Partners
Search
Quantum Information Solutions for the Real World.
News
CSO
Quantum Physics to the Rescue
More...
The Register
Quantum crypto moves out of the lab
More...
Forbes.com
Next-Generation Networks: The Hacker-Proof Network
More...
CNET News.com
Quantum crypto firm charts way to mainstream
More...
Scientific American
Best-Kept Secrets: Quantum Cryptography from Theory to Laboratory
More...
The Industrial Physicist
Quantum Key Distribution
More...
MagiQ QPN
QPN datasheet
QPN™ Research
QPN datasheet
Presenting the first commercial quantum cryptography solutions.
Press Releases
MagiQ Solves Quantum Cryptography Geomagnetic Interference Problem
MagiQ Announces New, Next Generation Quantum Cryptography Solution
MagiQ and Cavium
Product Information
QPN Overview Presentation
New Weapon to Protect Online Privacy
QPN Executive Summary
QPN Data Sheet
Company Information
MagiQ at NITSL 2005
MagiQ Celebrates Five Years of Progress
Quantum Cryptography Gets Practical by Bob Gelfond
CIO Ask the Expert: Bob Gelfond

Produkty

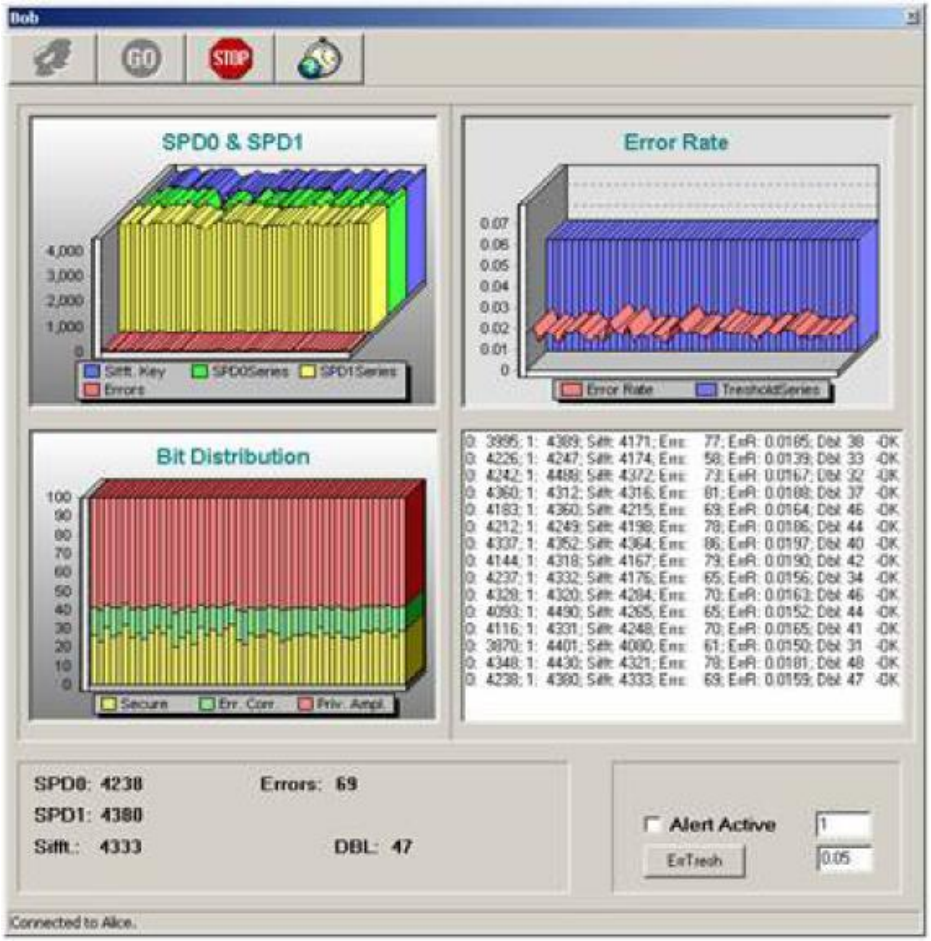
Bob
GO
STOP
SPD0 & SPD1
Error Rate
Bit Distribution
SPD0: 4238
Errors: 69
SPD1: 4380
Sift.: 4333
DBL: 47
Alert Active
ErrTresh
Connected to Alice.

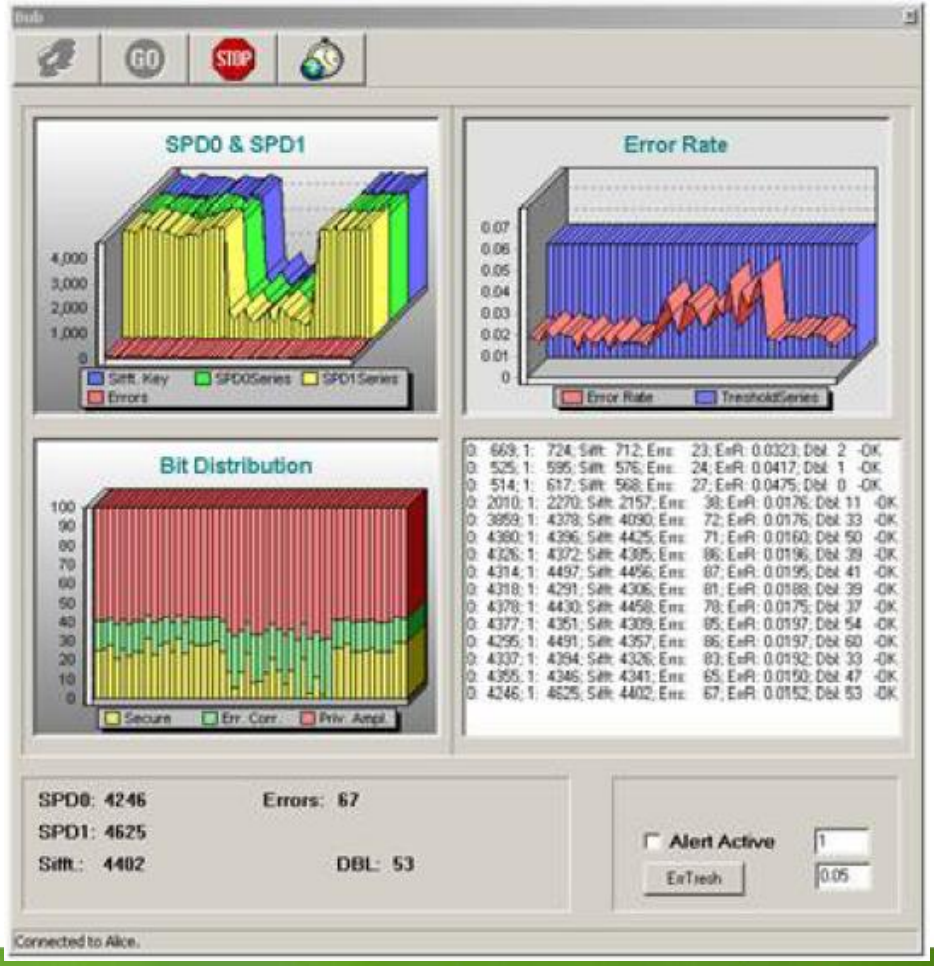
Bob
GO
STOP
SPD0 & SPD1
Error Rate
Bit Distribution
SPD0: 4246
Errors: 67
SPD1: 4625
Sift.: 4402
DBL: 53
Alert Active
ErrTresh
Connected to Alice.

PHYSICAL REVIEW
LETTERS

VOLUME 67 5 AUGUST 1991 NUMBER 6

Quantum Cryptography Based on Bell's Theorem

Artur K. Ekert

Merton College and Physics Department, Oxford University, Oxford OX1 3PU, United Kingdom

(Received 18 April 1991)

Practical application of the generalized Bell's theorem in the so-called key distribution process in cryptography is reported. The proposed scheme is based on the Bohm's version of the Einstein-Podolsky-Rosen *gedanken experiment* and Bell's theorem is used to test for eavesdropping.

VOLUME 67 NUMBER 6

Q

Merton College ar *ed Kingdom*

Practical applicatio process in cryp-
tography is reported. nstein-Podolsky-
Rosen *gedanken exper*

Artur Ekert

Kryptografia kwantowa

Artur Ekert

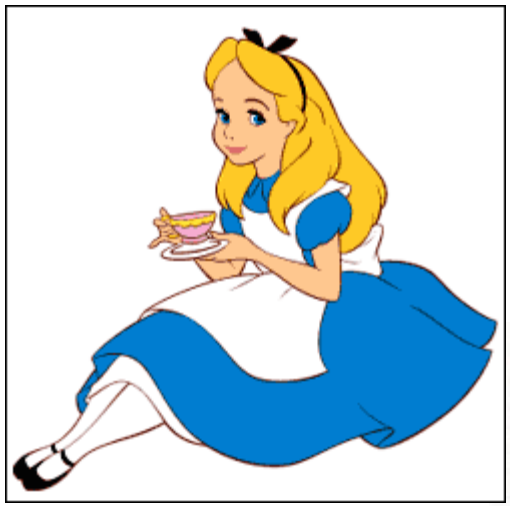

Alice

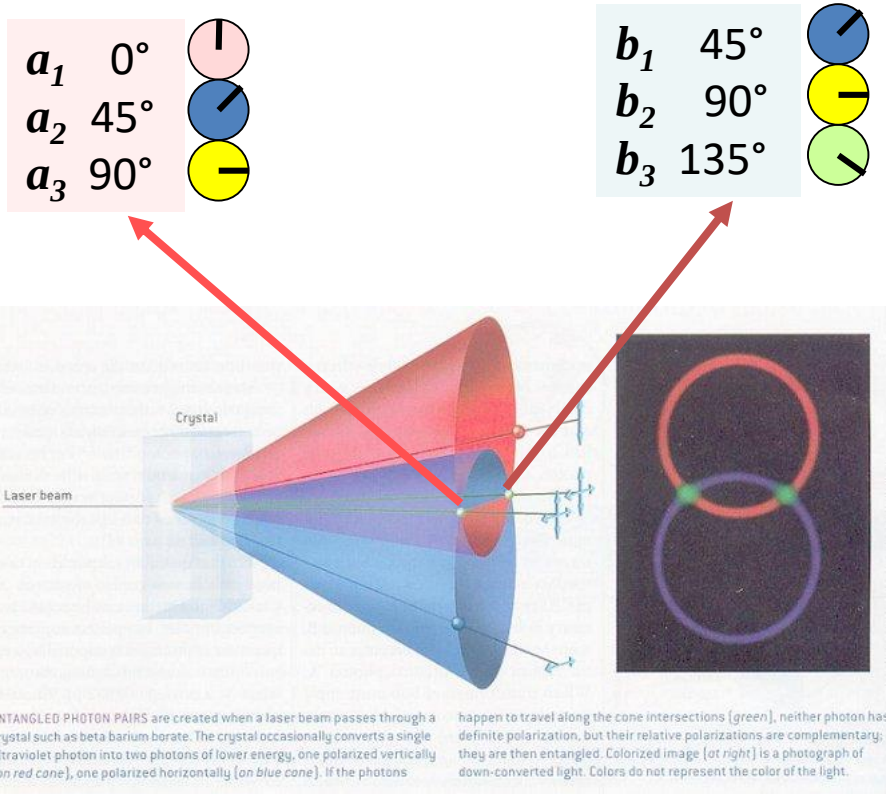

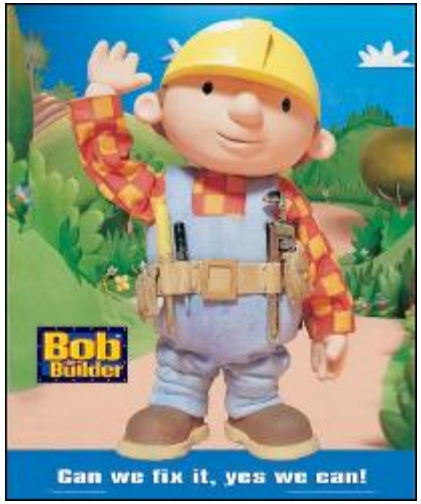

Bob

Kryptografia kwantowa

Artur Ekert

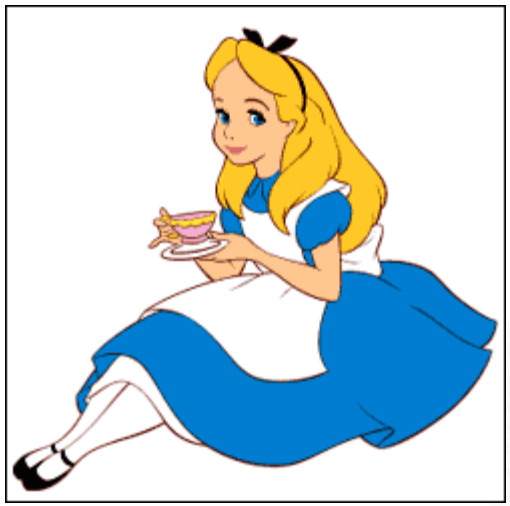

Alice

a_1 0°
a_2 45°
a_3 90°

b_1 45°
b_2 90°
b_3 135°

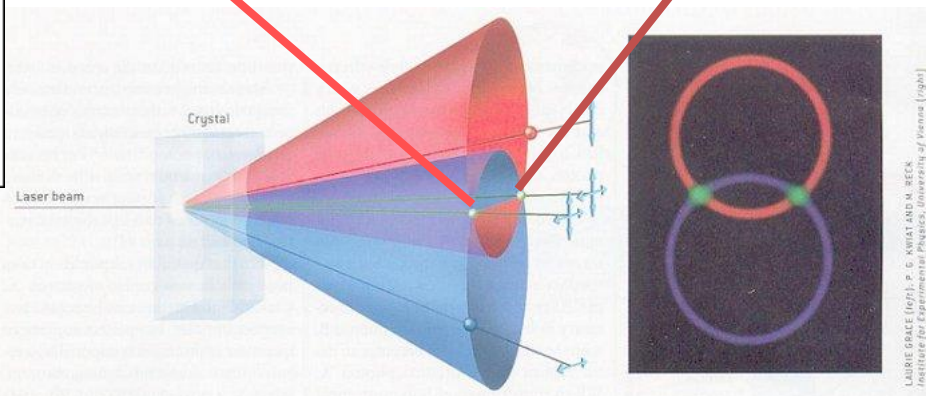

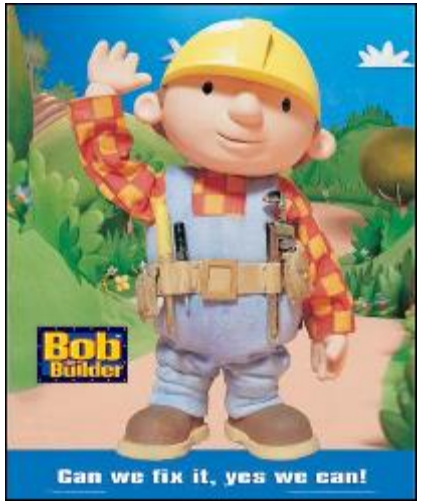

Bob

a																					
	1	0	1	1	0	0	0	1	0	1	x	1	0	1	1	0	0	1	1	1	0
b																					
	1	0	0	0	1	1	0	1	1	1	0	0	0	0	0	1	0	1	0	1	1
	t	0	1	t	0	0	t	1	0	1	x	t	0	1	t	t	t	1	t	t	t

jawne

jawne

test (jawny)

Klucz: 0100101011…

After the transmission has taken place, Alice and Bob can announce in public the orientations of the analyzers they have chosen for each particular measurement and divide the measurements into two separate groups: a first group for which they used different orientation of analyzers, and a second group for which they used the same orientation of their analyzers. They discard all measurements in which either or both of them failed to register a particle at all. Subsequently, Alice and Bob can reveal publicly the results they obtained but within the first group of measurements only. This allows them to establish the value of S, which, if the particles were not directly or indirectly "disturbed," should reproduce the result of Eq. (4). This assures the legitimate users that the results they obtained within the second group of measurements are anticorrelated and can be converted into a secret string of bits—the key. This secret key may be then used in a conventional cryptographic communication between Alice and Bob.

$$S=E(\mathbf{a}_1,\mathbf{b}_1)-E(\mathbf{a}_1,\mathbf{b}_3)+E(\mathbf{a}_3,\mathbf{b}_1)+E(\mathbf{a}_3,\mathbf{b}_3)\,. \tag{3}$$

Again, quantum mechanics requires

$$S=-2\sqrt{2}\,. \tag{4}$$

The eavesdropper cannot elicit any information from the particles while in transit from the source to the legitimate users, simply because there is no information encoded there. The information "comes into being" only after the legitimate users perform measurements and communicate in public afterwards. The eavesdropper may try to substitute his own prepared data for Alice and Bob to misguide them, but as he does not know which orientation of the analyzers will be chosen for a given pair of particles, there is no good strategy to escape from being detected.

$$S=\int \rho(\mathbf{n}_a,\mathbf{n}_b)\,d\mathbf{n}_a\,d\mathbf{n}_b[\sqrt{2}\mathbf{n}_a\cdot\mathbf{n}_b]\,, \tag{6}$$

which implies

$$-\sqrt{2}\le S\le\sqrt{2}\,, \tag{7}$$

Kryptografia kwantowa

PHYSICAL REVIEW A VOLUME 56, NUMBER 2 AUGUST 1997

Optimal eavesdropping in quantum cryptography. I. Information bound and optimal strategy

Christopher A. Fuchs,[1] Nicolas Gisin,[2] Robert B. Griffiths,[3] Chi-Sheng Niu,[3] and Asher Peres[4,*]
[1]*Norman Bridge Laboratory of Physics 12-33, California Institute of Technology, Pasadena, California 91125*
[2]*Group of Applied Physics, University of Geneva, CH 1211 Geneva 4, Switzerland*
[3]*Department of Physics, Carnegie-Mellon University, Pittsburgh, Pennsylvania 15213*
[4]*Institute for Theoretical Physics, University of California, Santa Barbara, California 93106*
(Received 31 January 1997)

We consider the Bennett-Brassard cryptographic scheme, which uses two conjugate quantum bases. An eavesdropper who attempts to obtain information on qubits sent in one of the bases causes a disturbance to qubits sent in the other basis. We derive an upper bound to the accessible information in one basis, for a given error rate in the conjugate basis. Independently fixing the error rates in the conjugate bases, we show that both bounds can be attained simultaneously by an optimal eavesdropping probe. The probe interaction and its subsequent measurement are described explicitly. These results are combined to give an expression for the optimal information an eavesdropper can obtain for a given average disturbance when her interaction and measurements are performed signal by signal. Finally, the relation between quantum cryptography and violations of Bell's inequalities is discussed. [S1050-2947(97)01708-3]

Kryptografia kwantowa

We take the framework for our problem directly from quantum cryptography. In order to take advantage of Alice's delayed information on the basis that was used, Eve's optimal strategy is the following: she lets a probe, initially in some standard state $|\psi_0\rangle$, interact unitarily with the qubit sent by Alice. (There is no loss of generality in this, because any physical nonunitary interaction is equivalent to a unitary one with a higher dimensional probe.) Eve's probe is then stored until Alice announces the basis that was used, and only after that is it measured by Eve.

In a convenient notation, if Alice sends state $|x\rangle$, the result may be written as

$$|x\rangle \otimes |\psi_0\rangle \rightarrow |X\rangle, \qquad (1)$$

where $|X\rangle$ is an entangled state of the probe and the photon that Alice sent to Bob. Likewise, for the other signals that Alice may send, the results of Eve's intervention are entangled states, $|Y\rangle$, $|U\rangle$, and $|V\rangle$. Since the interaction is unitary, it follows from

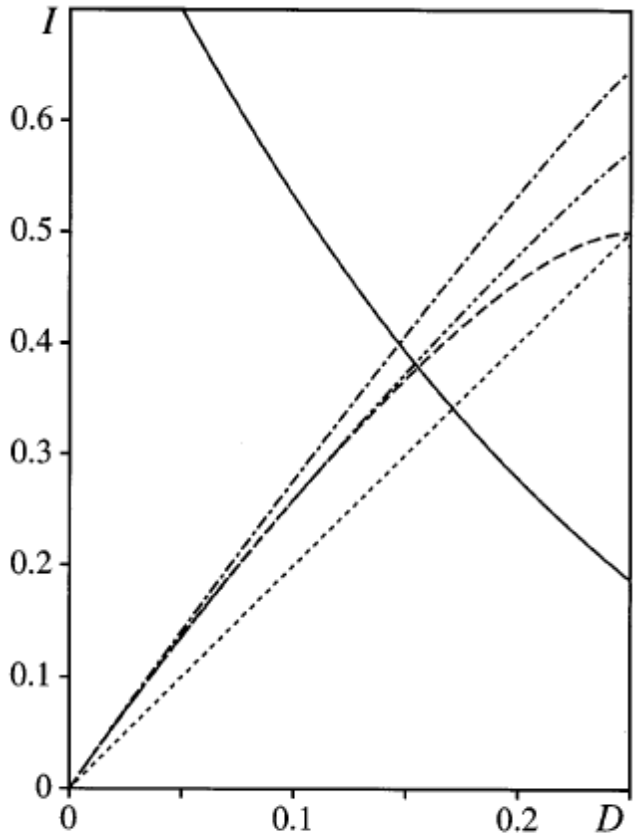

FIG. 2. Information vs disturbance for various eavesdropping methods.

Sprawy bieżące

Ankiety

http://usosweb.**fuw.edu.pl**

"Dla studentów">"Ankiety".


DO PRACY
ZGŁASZAJ SIĘ
TRZEŹWY i WYPOCZĘTY

Cel:

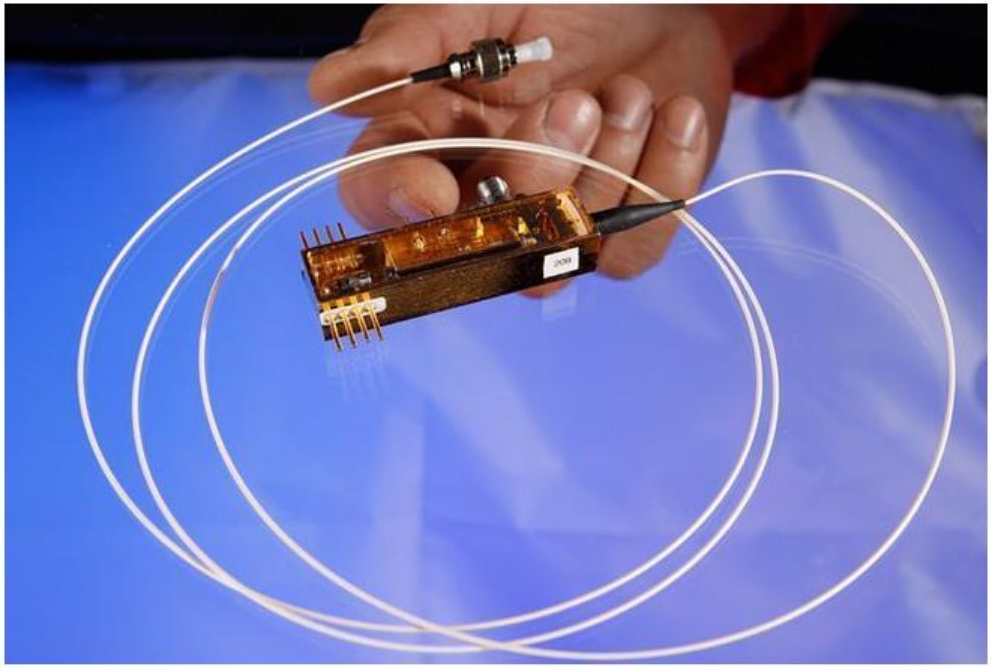

QUANTUM CRYPTOGRAPHY AT WORK

The miniature transmitter communicates with a trusted authority to generate random cryptographic keys to encode and decode information. In 2013, researchers used devices like this to send information securely over the electric grid.

Los Alamos National Laboratory

https://www.popsci.com/what-is-quantum-cryptography

Deterministic creation and electrical driving of quantum emitters in atomically thin semiconductor
Dhiren Kara, University of Cambridge, UK

ARTICLE

Received 24 Jan 2017 | Accepted 24 Feb 2017 | Published 22 May 2017

DOI: 10.1038/ncomms15093 OPEN

Large-scale quantum-emitter arrays in atomically thin semiconductors

Carmen Palacios-Berraquero[1,*], Dhiren M. Kara[1,*], Alejandro R.-P. Montblanch[1], Matteo Barbone[1,2], Pawel Latawiec[3], Duhee Yoon[2], Anna K. Ott[2], Marko Loncar[3], Andrea C. Ferrari[2] & Mete Atatüre[1]

Quantum light emitters have been observed in atomically thin layers of transition metal dichalcogenides. However, they are found at random locations within the host material and usually in low densities, hindering experiments aiming to investigate this new class of emitters. Here, we create deterministic arrays of hundreds of quantum emitters in tungsten diselenide and tungsten disulphide monolayers, emitting across a range of wavelengths in the visible spectrum (610–680 nm and 740–820 nm), with a greater spectral stability than their randomly occurring counterparts. This is achieved by depositing monolayers onto silica substrates nanopatterned with arrays of 150-nm-diameter pillars ranging from 60 to 190 nm in height. The nanopillars create localized deformations in the material resulting in the quantum confinement of excitons. Our method may enable the placement of emitters in photonic structures such as optical waveguides in a scalable way, where precise and accurate positioning is paramount.

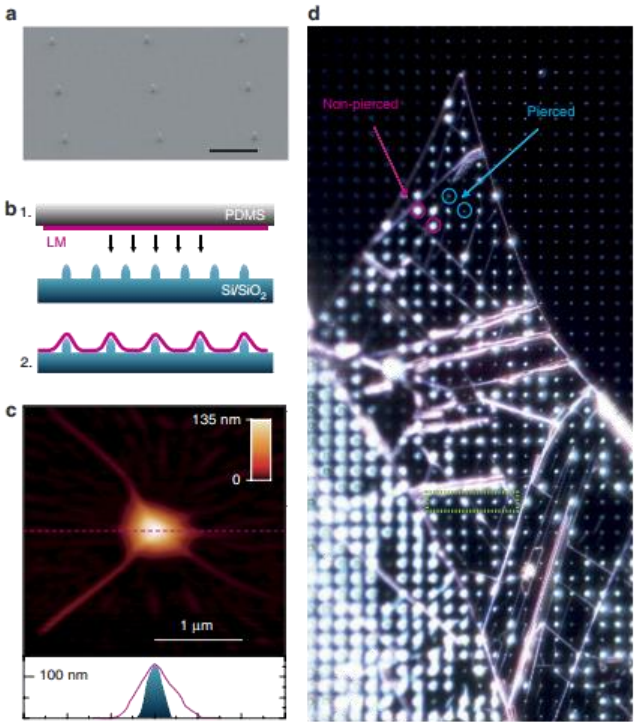

Figure 1 | Fabrication and characterization of scalable quantum confinement arrays. (**a**) SEM image of nanopillar substrate, fabricated by electron beam lithography. Black scale bar, 2 µm. (**b**) Illustration of the fabrication method: (1) mechanical exfoliation of LM on PDMS and all-dry viscoelastic deposition on patterned substrate; and (2) deposited LM on patterned substrate. (**c**, top) An AFM scan of 1L-WSe_2 on a nanopillar. (bottom) The AFM height profile of a bare nanopillar (blue-shaded region) and of the flake deposited over it (pink line), measured along the dashed pink line cut in the top panel. Colour-scale bar represents height in nm and white scale bar 1 µm. (**d**) Dark field optical microscopy image (real colour) of 1L-WSe_2 on nanopillar substrate (130 nm high, 4 µm separation). The full image corresponds to a 170 µm by 210 µm area. The green box highlights six adjacent nanopillars within the 1L-WSe_2 region, measured in Fig. 2. The blue circles indicate two pierced nanopillars, and the pink circles indicate two non-pierced nanopillars. PDMS, polydimethylsiloxane; SEM, scanning electron microscope.

Deterministic creation and electrical driving of quant

Dhiren Kara, University of Cambridge, UK

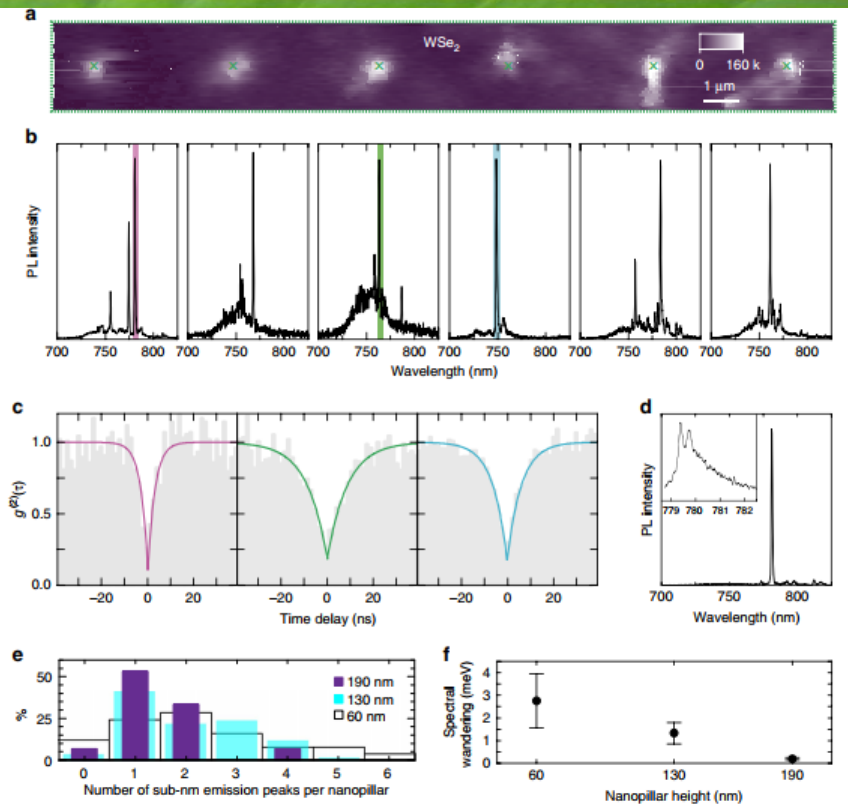

Figure 2 | Creation of quantum emitter arrays in 1L-WSe_2. (**a**) Integrated PL intensity raster scan of the region enclosed by the green rectangle in Fig. 1d, taken under 200 nW µm^{-2}, 532 nm laser excitation at 10 K. Green crosses mark the position of the six nanopillars beneath the 1L-WSe_2. Colour-scale bar maximum, 160 kcounts s^{-1}. (**b**) PL spectra taken at each of the corresponding green crosses in **a**, from left to right respectively, showing the presence of narrow lines at each nanopillar location. (**c**) Photon correlation measurements corresponding to the filtered spectral regions (10 nm wide) enclosed by the blue, green and pink rectangles, in **b**, with $g^{(2)}(0) = 0.087 \pm 0.065$, 0.17 ± 0.02 and 0.18 ± 0.03, and rise times of 8.81 ± 0.80 ns, 6.15 ± 0.36 ns and 3.08 ± 0.41 ns, respectively. (**d**) Spectrum taken from a 1L-WSe_2 on a 190 nm nanopillar, showing lower background and a single sub-nm emission peak. Higher-resolution spectrum in the inset reveals the fine-structure splitting of this QE peak. An asymmetry can be seen in the spectrum, which has been previously attributed to a phonon sideband in naturally occurring QEs[31]. (**e**) Probability distribution (in %) of the number of emission lines per nanopillar for samples using different nanopillar heights (60, 130 and 190 nm in white, blue and purple, respectively). A trend of higher probability of single QE emission peaks per nanopillar location with increasing height is evident, reaching 50% for 190 nm nanopillars. (**f**) Increasing nanopillar height also leads to a reduction of spectral wandering. Solid black circles represent the mean value of spectral wandering of several QEs for a given nanopillar height, while the error bars represent the standard deviation of each distribution, both extracted from time-resolved high-resolution spectral measurements (Supplementary Fig. 4). A total number of seven samples was used to collect the statistics necessary for Fig. 2e,f.

Deterministic creation and electrical driving of quantum emitters in atomically thin semiconductor
Dhiren Kara, University of Cambridge, UK

ARTICLE

Received 26 Jan 2017 | Accepted 24 Feb 2017 | Published 22 May 2017

DOI: 10.1038/ncomms15053 OPEN

Deterministic strain-induced arrays of quantum emitters in a two-dimensional semiconductor

Artur Branny[1], Santosh Kumar[1], Raphaël Proux[1] & Brian D. Gerardot[1]

An outstanding challenge in quantum photonics is scalability, which requires positioning of single quantum emitters in a deterministic fashion. Site positioning progress has been made in established platforms including defects in diamond and self-assembled quantum dots, albeit often with compromised coherence and optical quality. The emergence of single quantum emitters in layered transition metal dichalcogenide semiconductors offers new opportunities to construct a scalable quantum architecture. Here, using nanoscale strain engineering, we deterministically achieve a two-dimensional lattice of quantum emitters in an atomically thin semiconductor. We create point-like strain perturbations in mono- and bi-layer WSe_2 which locally modify the band-gap, leading to efficient funnelling of excitons towards isolated strain-tuned quantum emitters that exhibit high-purity single photon emission. We achieve near unity emitter creation probability and a mean positioning accuracy of 120 ± 32 nm, which may be improved with further optimization of the nanopillar dimensions.

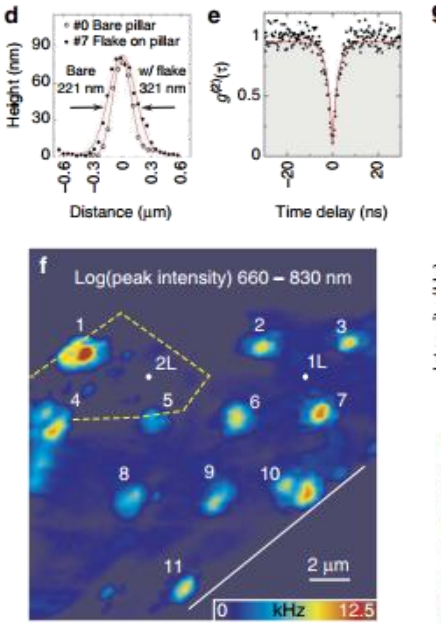

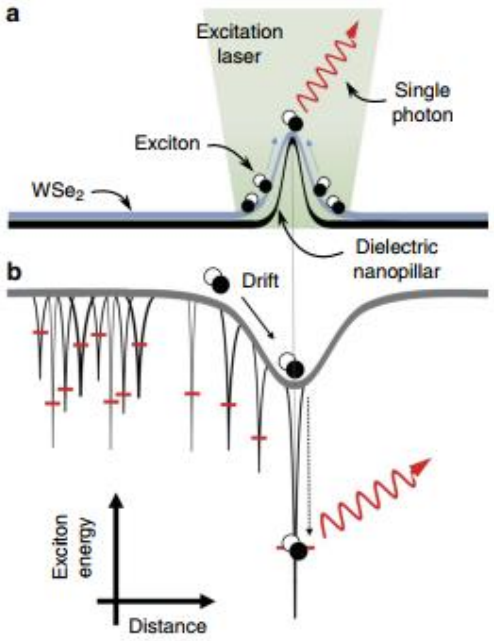

Figure 1 | A diagram of the scheme to obtain a strain-induced quantum emitter. (**a**) Atomically thin WSe_2 is deformed by a nanopillar to achieve a point-like elastic strain perturbation. (**b**) The strain locally modulates the WSe_2 band-gap. Superimposed on this artificial modulation of the exciton energy are randomly distributed localized excitons. Optically created excitons efficiently funnel to an individual strain tuned localized exciton trap at the nanopillar centre resulting in a single highly efficient quantum emitter.

Time-resolved magneto-optical spectroscopy of localized excitons in WSe_2
Santosh Kumar, Heriot-Watt University, UK

ARTICLE

Received 16 Jun 2016 | Accepted 30 Sep 2016 | Published 10 Nov 2016

DOI: 10.1038/ncomms13409 OPEN

Cascaded emission of single photons from the biexciton in monolayered WSe_2

Yu-Ming He[1,2], Oliver Iff[1], Nils Lundt[1], Vasilij Baumann[1], Marcelo Davanco[3], Kartik Srinivasan[3], Sven Höfling[1,4] & Christian Schneider[1]

Monolayers of transition metal dichalcogenide materials emerged as a new material class to study excitonic effects in solid state, as they benefit from enormous Coulomb correlations between electrons and holes. Especially in WSe_2, sharp emission features have been observed at cryogenic temperatures, which act as single photon sources. Tight exciton localization has been assumed to induce an anharmonic excitation spectrum; however, the evidence of the hypothesis, namely the demonstration of a localized biexciton, is elusive. Here we unambiguously demonstrate the existence of a localized biexciton in a monolayer of WSe_2, which triggers an emission cascade of single photons. The biexciton is identified by its time-resolved photoluminescence, superlinearity and distinct polarization in micro-photoluminescence experiments. We evidence the cascaded nature of the emission process in a cross-correlation experiment, which yields a strong bunching behaviour. Our work paves the way to a new generation of quantum optics experiments with two-dimensional semiconductors.

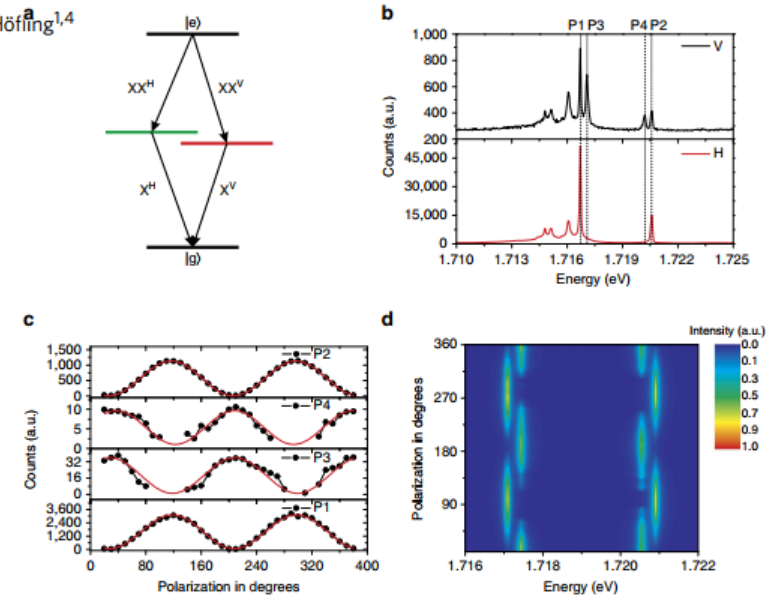

Figure 2 | Polarization-resolved photoluminescence. (**a**) Schematic representation of biexcitonic emission cascade. The fine-structure splitting is expected for the electron-hole exchange interaction in the presence of in-plane anisotropy. (**b**) Polarization-resolved spectrum at linear polarization H, V. Two pairs of spectral doublets are observed at 1.7167 (P1)-1.7171 eV (P3) and 1.7202 (P4)-1.7206 eV (P2). Four peaks are indicated by the dashed lines. (**c**) The integrated counts of the photon emission from P1, P2, P3, P4 as a function of the polarization detection angle. The red lines are the sinusoidal fits, showing two pairs of cross-linear-polarized doublets. (**d**) Contour representation of the four peaks, after normalizing to the maximum peak intensity, yielding a fine structure splitting ~0.4 meV.

(Invited) Beyond single photon emission with self-assembled quantum dots in a photonic wire: prospects for sensing
Mathieu Munsch, Basel University, Switzerland

ARTICLE

DOI: 10.1038/s41467-017-00097-3 OPEN

Resonant driving of a single photon emitter embedded in a mechanical oscillator

Mathieu Munsch[1], Andreas V. Kuhlmann[1], Davide Cadeddu[1], Jean-Michel Gérard[2], Julien Claudon[2], Martino Poggio[1] & Richard J. Warburton[1]

Coupling a microscopic mechanical resonator to a nanoscale quantum system enables control of the mechanical resonator via the quantum system and vice-versa. The coupling is usually achieved through functionalization of the mechanical resonator, but this results in additional mass and dissipation channels. An alternative is an intrinsic coupling based on strain. Here we employ a monolithic semiconductor system: the nanoscale quantum system is a semiconductor quantum dot (QD) located inside a nanowire. We demonstrate the resonant optical driving of the QD transition in such a structure. The noise spectrum of the resonance fluorescence signal, recorded in the single-photon counting regime, reveals a coupling to mechanical modes of different types. We measure a sensitivity to displacement of 65 fm/$\sqrt{\text{Hz}}$ limited by charge noise in the device. Finally, we use thermal excitation of the different modes to determine the location of the QD within the trumpet, and calculate the contribution of the Brownian motion to the dephasing of the emitter.

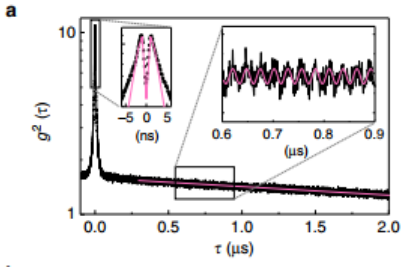

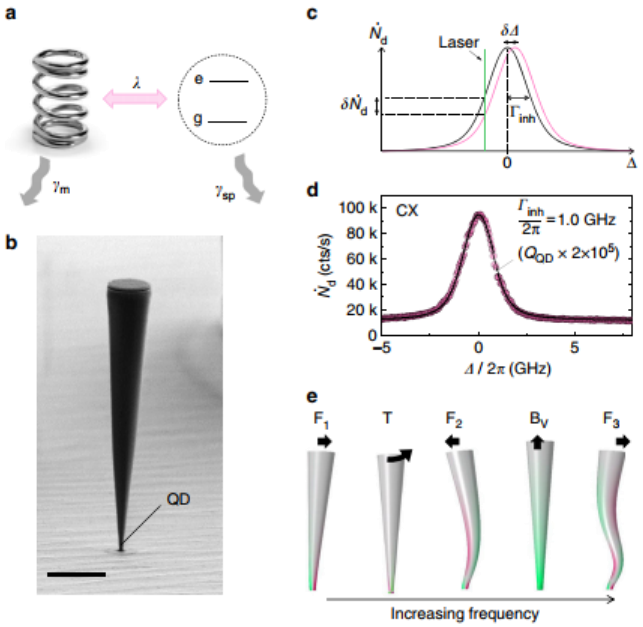

Fig. 1 Quantum dot coupling to a nanowire mechanical resonator. **a** Sketch of the hybrid system: a mechanical oscillator is coupled to a two-level quantum system. The coupling rate λ (*pink*) competes with the dissipation rates of both components (*grey*): the intrinsic phonon relaxation rate γ_m and the spontaneous emission rate of a photon γ_{sp}. **b** Practical realization: a quantum dot (QD) is embedded close to the bottom of a micrometre-sized mechanical resonator. The coupling originates from strain as the nanowire oscillates. The scale bar corresponds to 2 μm. **c** Effect of the coupling: a displacement u of the nanowire produces a shift $\delta\Delta$ in the QD frequency, modifying the detuning between the QD and the laser. Γ_{inh} is the linewidth of the QD, inhomogeneously broadened by spectral fluctuations. **d** Resonance fluorescence signal from the charged exciton (CX) as a function of laser detuning (fluorescence wavelength: 945.6 nm). $\Omega_R \simeq \gamma_{sp} = 1.1$ GHz. The fit uses a Voigt profile with a contribution to the linewidth of 0.45 GHz from the Lorentzian part, and 0.70 GHz from the Gaussian one. **e** The mechanical modes: F_1, F_2 and F_3 correspond to the first, second- and third-order flexural modes; T to a torsional mode and B_v to a vertical breathing mode. The *colour map* represents the strain along the vertical axis within the trumpet (*green*: tensile, *pink*: compressive). The *black arrows* represent the displacement of the nanowire's top facet

(Invited) Quantum dot devices for optical quantum technologies

Pascale Senellart, CNRS-LPN, Université Paris-Saclay, France

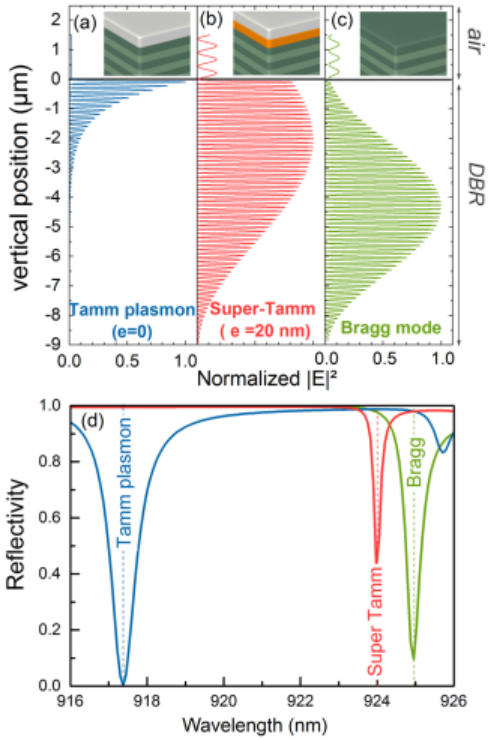

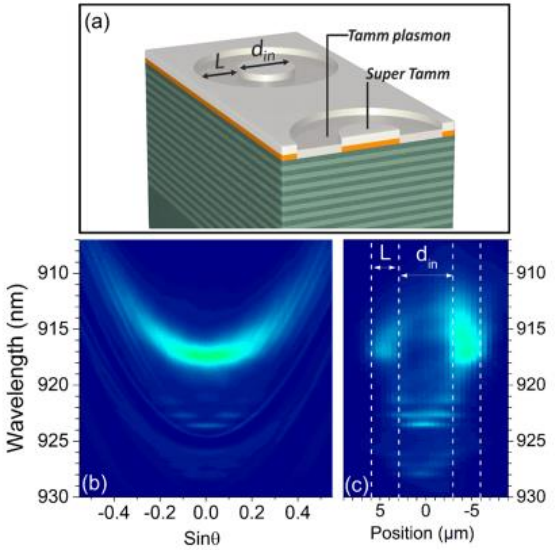

Figure 1. Spatial repartition of the normalized squared electric field calculated for the (**a**) Tamm plasmon mode (λ = 917.4 nm); (**b**) super Tamm mode (λ = 924 nm); (**c**) first Bragg mode (λ = 925 nm). (**d**) Calculated reflectivities of Tamm plasmon, super Tamm and bare DBR structures. The Tamm structures comprise a 45 nm thick silver layer deposited on the DBR, and a 20 nm low refractive index layer (n = 1.485) is inserted between the metal and the DBR to form the super Tamm mode.

SCIENTIFIC REPORTS

High quality factor confined Tamm modes

C. Symonds[1], S. Azzini[1], G. Lheureux[1], A. Piednoir[1], J. M. Benoit[1], A. Lemaitre[2], P. Senellart[2] & J. Bellessa[1]

We demonstrate that quality factors up to 5000 can be obtained in Tamm-like hybrid metal/semiconductor structures. To do this, a Bragg mirror is covered by a thin transparent layer and a metallic film. The reduced losses of these modes are related to an intermediate behavior between conventional Tamm plasmon and Bragg modes lying deeper in the semiconductor medium. One of the most striking features of this approach is that these super Tamm modes can still be spatially confined with the metal. Confinement on micrometric scale is experimentally demonstrated. The simplicity and versatility of high-Q mode control by metal structuration open perspectives for lasing and polaritonic applications.

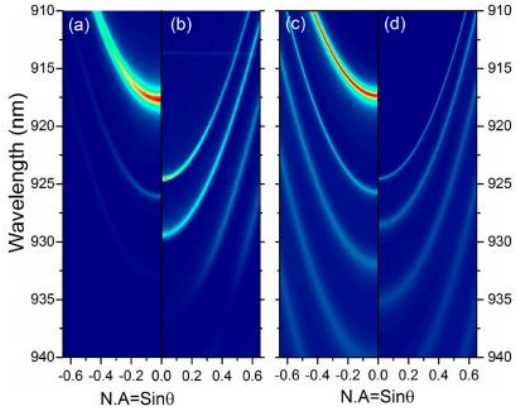

Figure 3. Experimental emission dispersion relations recorded on the (**a**) Tamm plasmon and (**b**) super Tamm plasmon (e = 35 nm) areas. (**c**) and (**d**) corresponds to reflectivities transfer matrix calculations on a Tamm and super Tamm structure, respectively.

(Invited) Quantum dot devices for optical quantum technologies

Pascale Senellart, CNRS-LPN, Université Paris-Saclay, France

SCIENTIFIC REPORTS

OPEN

Enhancement of spontaneous emission in Tamm plasmon structures

Received: 16 December 2016
Accepted: 25 July 2017
Published online: 21 August 2017

A. R. Gubaydullin[1,2], C. Symonds[2], J. Bellessa[2], K. A. Ivanov[1,3], E. D. Kolykhalova[1,4], M. E. Sasin[4], A. Lemaitre[5], P. Senellart[5], G. Pozina[6] & M. A. Kaliteevski[1,3,4]

It was theoretically and experimentally demonstrated that in metal/semiconductor Tamm plasmon structures the probability of spontaneous emission can be increased despite losses in metal, and theoretical analysis of experimental results suggested that the enhancement could be as high as one order of magnitude. Tamm plasmon structure with quantum dots has been fabricated and the emission pattern has been measured. Electromagnetic modes of the structure have been analyzed and modification of spontaneous emission rates has been calculated showing a good agreement with experimentally observed emission pattern.

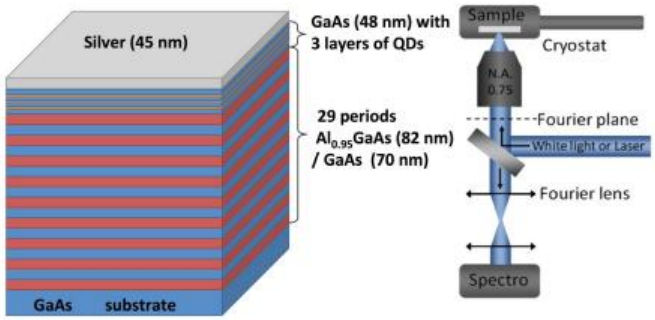

Figure 1. Scheme of the structure and experimental set-up.

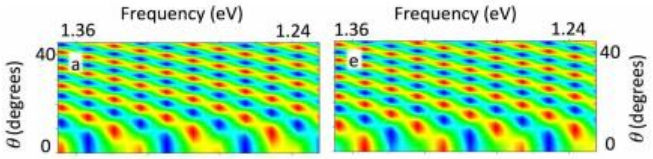

Figure 7. Dependence of the modal Purcell factor on frequency and direction of emission for a different position from the interface: (**a**) 17 nm; (**b**) 28 nm; (**c**) 35 nm; (**d**) 56 nm; (**e**) 71 nm; (**f**) 93 nm; (**g**) 142 nm; for the slab of GaAs of the thickness 28 μm surrounded by air. The Fig. 7 (**h**) demonstrates the pattern of modal Purcell factor averaged over the distance of the emitter from the interface on the interval corresponding to one wavelength.

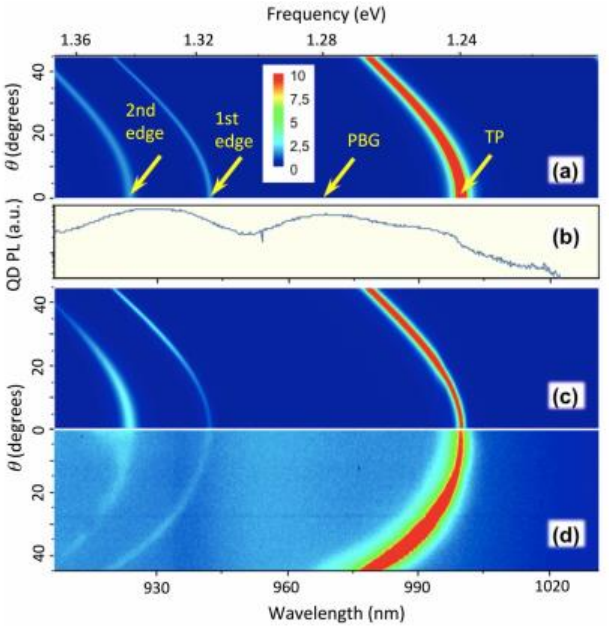

Figure 2. (**a**) Dependence of the calculated modal Purcell factor on frequency and angle of emission; (**b**) Emission spectrum of quantum dots; (**c**) Dependence of the product of the calculated modal Purcell factor and the emission spectra of quantum dots on frequency and angle of emission; (**d**) Experimentally measured photoemission spectra. Arrows mark the modes (TP –Tamm plasmon, PBG – photonic band gap, 1st edge – 1st edge state, 2nd edge – second edge state).

(Invited) Quantum dot devices for optical quantum technologies

Pascale Senellart, CNRS-LPN, Université Paris-Saclay, France

PRL **118,** 263901 (2017) PHYSICAL REVIEW LETTERS week ending 30 JUNE 2017

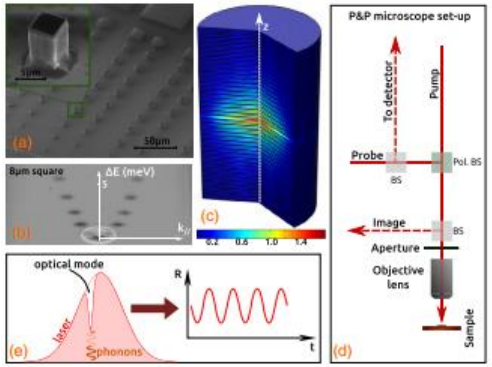

FIG. 1. (a) SEM images of an array of circular and square pillars with lateral sizes ranging from 50 to 1 μm. The inset presents a zoom on a 5 μm square pillar. (b) k-space image of the optical cavity modes for a square pillars of 8 μm lateral size. The shaded ellipse represents the profile (energy broadening and angular dispersion) of the pump and probe laser pulses. (c) Spatial distribution of $|dV/V|$ associated with a confined mechanical mode around 19 GHz, calculated using finite element methods. (d) Scheme of the ultrafast resonant laser microspectroscopy setup. (e) Scheme of the process leading to mechanical signals in reflectance difference time resolved spectroscopy.

Micropillar Resonators for Optomechanics in the Extremely High 19–95-GHz Frequency Range

S. Anguiano,[1] A. E. Bruchhausen,[1] B. Jusserand,[2] I. Favero,[3] F. R. Lamberti,[3,4] L. Lanco,[4] I. Sagnes,[4] A. Lemaître,[4] N. D. Lanzillotti-Kimura,[4] P. Senellart,[4,*] and A. Fainstein[1,†]

[1]*Centro Atómico Bariloche & Instituto Balseiro, C.N.E.A., CONICET, 8400 San Carlos de Bariloche, Río Negro, Argentina*
[2]*Institut des NanoSciences de Paris, UMR 7588 C.N.R.S.—Université Pierre et Marie Curie, 75015 Paris, France*
[3]*Matériaux et Phénomènes Quantiques, Université Paris Diderot, CNRS-UMR 7162, Sorbonne Paris Cité, 10 rue Alice Domon et Léonie Duquet, 75013 Paris, France*
[4]*Centre de Nanosciences et de Nanotechnologies, C.N.R.S., Université Paris-Sud, Université Paris-Saclay, C2N Marcoussis, 91460 Marcoussis, France*

(Received 21 December 2016; published 30 June 2017)

Strong confinement, in all dimensions, and high mechanical frequencies are highly desirable for quantum optomechanical applications. We show that GaAs/AlAs micropillar cavities fully confine not only photons but also extremely high frequency (19–95 GHz) acoustic phonons. A strong increase of the optomechanical coupling upon reducing the pillar size is observed, together with record room-temperature Q-frequency products of 10^{14}. These mechanical resonators can integrate quantum emitters or polariton condensates, opening exciting perspectives at the interface with nonlinear and quantum optics.

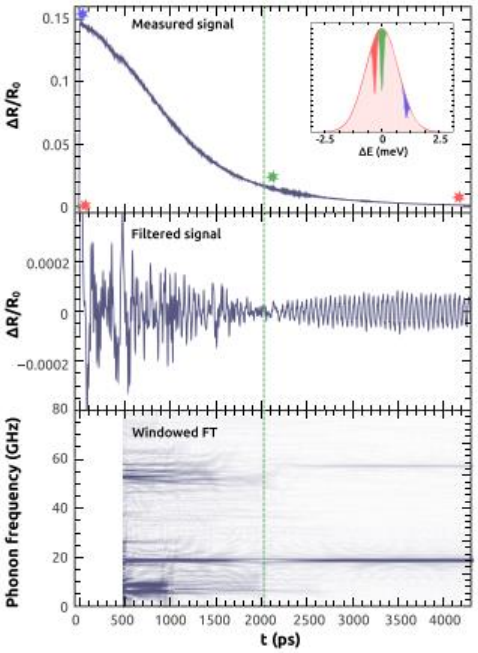

FIG. 2. Top: As-measured differential reflectance time trace for a 5 μm pillar, varying the delay t between the pump and probe pulses. The inset is a schematic representation of the laser pulse energy distribution, and the cavity mode (dip in the reflected probe) at different times after pump excitation. The time before (after) the arrival of the pump is indicated with the initial red(blue) star and dip. Excited carrier relaxation leads to the recovery of the cavity mode, which around 2000 ps passes through the central energy of the laser (vertical dashed line, green star, and dip). At longer times the equilibrium situation is recovered (final red star and dip). Middle: filtered time trace corresponding to frequencies between 5 and 100 GHz. Bottom: windowed Fourier transform (WFT) of the filtered trace, obtained with 1000 ps windows.

(Invited) Quantum dot devices for optical quantum technologies

Pascale Senellart, CNRS-LPN, Université Paris-Saclay, France

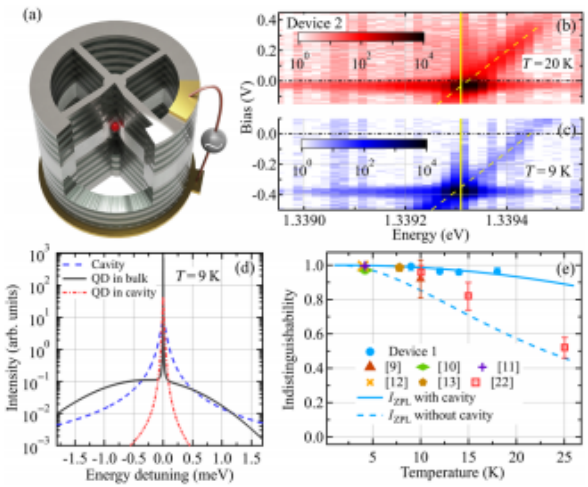

FIG. 1. (a) Schematic of the device. (b),(c) Resonant resonant fluorescence maps as a function of energy and bias voltage on device 2 at temperatures 20 and 9 K, respectively. The cavity and QD spectral positions as a function of the voltage are indicated with full and dashed yellow lines, respectively. (d) Comparison of the calculated emission spectra of a QD in a bulk photonic environment (the black solid line) and coupled resonantly to a cavity (the red dashed-dotted line) at 9 K. The cavity spectrum is also indicated (the blue dashed line). (e) Indistinguishability of the ZPL as a function of temperature. The measurements (device 1) are shown in blue circles. Calculations for the device 1 (the solid line) and without cavity-QED effects (the dashed line) are shown. We also indicate measurements reporting high indistinguishability of the ZPL, as well as the temperature dependence recently reported in Ref. [22] in the absence of the Purcell effect (the red squares).

PRL **118,** 253602 (2017) PHYSICAL REVIEW LETTERS week ending 23 JUNE 2017

Reducing Phonon-Induced Decoherence in Solid-State Single-Photon Sources with Cavity Quantum Electrodynamics

T. Grange,[1,2,*] N. Somaschi,[3,†] C. Antón,[3] L. De Santis,[3,4] G. Coppola,[3] V. Giesz,[3] A. Lemaître,[3] I. Sagnes,[3] A. Auffèves,[1,2,‡] and P. Senellart[3,§]

[1]*Université Grenoble Alpes, F-38000 Grenoble, France*

[2]*Centre National de la Recherche Scientifique, Institut Néel, Nanophysique et Semiconducteurs Group, F-38000 Grenoble, France*

[3]*Centre de Nanosciences et de Nanotechnologies, CNRS, Université Paris–Sud, UMR 9001, Université Paris–Saclay, C2N—Marcoussis, 91460 Marcoussis, France*

[4]*Université Paris–Sud, Université Paris–Saclay, F-91405 Orsay, France*

(Received 9 December 2016; published 23 June 2017)

Solid-state emitters are excellent candidates for developing integrated sources of single photons. Yet, phonons degrade the photon indistinguishability both through pure dephasing of the zero-phonon line and through phonon-assisted emission. Here, we study theoretically and experimentally the indistinguishability of photons emitted by a semiconductor quantum dot in a microcavity as a function of temperature. We show that a large coupling to a high quality factor cavity can simultaneously reduce the effect of both phonon-induced sources of decoherence. It first limits the effect of pure dephasing on the zero-phonon line with indistinguishabilities above 97% up to 18 K. Moreover, it efficiently redirects the phonon sidebands into the zero-phonon line and brings the indistinguishability of the full emission spectrum from 87% (24%) without cavity effect to more than 99% (76%) at 0K (20K). We provide guidelines for optimal cavity designs that further minimize the phonon-induced decoherence.

(Invited) Quantum dot devices for optical quantum technologies

Pascale Senellart, CNRS-LPN, Université Paris-Saclay, France

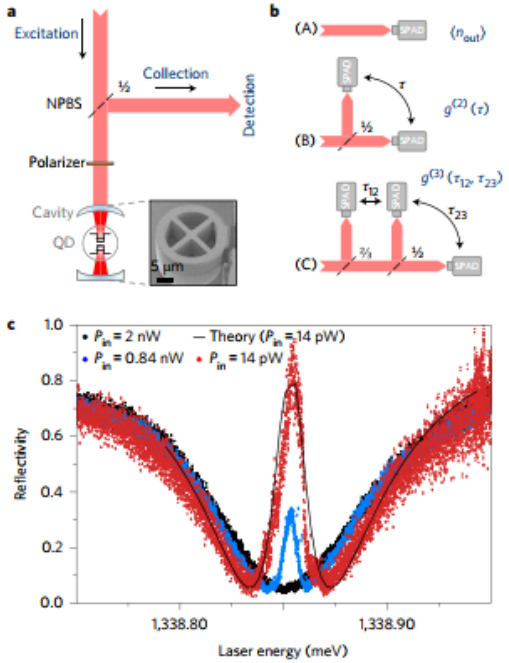

Figure 1 | Experimental design and characteristics of device 1. **a**, Experimental schematic: coherent photon wavepackets are sent to a quantum-dot cavity device. A non-polarizing beam splitter (NPBS) is used to separate the excitation from the collection. The insert shows a scanning electron microscopy image of the device. **b**, The light directly reflected is analysed using one of the three configurations labelled (A), (B) and (C) on the detection line. **c**, Reflectivity spectrum of device 1 obtained under continuous wave excitation for three excitation conditions. Black line: theoretical adjustment for the lowest excitation power.

nature nanotechnology

ARTICLES

PUBLISHED ONLINE: 15 MAY 2017 | DOI: 10.1038/NNANO.2017.85

A solid-state single-photon filter

Lorenzo De Santis[1], Carlos Antón[1], Bogdan Reznychenko[2,3], Niccolo Somaschi[1], Guillaume Coppola[1], Jean Senellart[4], Carmen Gómez[1], Aristide Lemaître[1], Isabelle Sagnes[1], Andrew G. White[5], Loïc Lanco[1,6], Alexia Auffèves[2,3]* and Pascale Senellart[1]*

A strong limitation of linear optical quantum computing is the probabilistic operation of two-quantum-bit gates based on the coalescence of indistinguishable photons. A route to deterministic operation is to exploit the single-photon nonlinearity of an atomic transition. Through engineering of the atom-photon interaction, phase shifters, photon filters and photon-photon gates have been demonstrated with natural atoms. Proofs of concept have been reported with semiconductor quantum dots, yet limited by inefficient atom-photon interfaces and dephasing. Here, we report a highly efficient single-photon filter based on a large optical nonlinearity at the single-photon level, in a near-optimal quantum-dot cavity interface. When probed with coherent light wavepackets, the device shows a record nonlinearity threshold around 0.3 ± 0.1 incident photons. We demonstrate that 80% of the directly reflected light intensity consists of a single-photon Fock state and that the two- and three-photon components are strongly suppressed compared with the single-photon one.

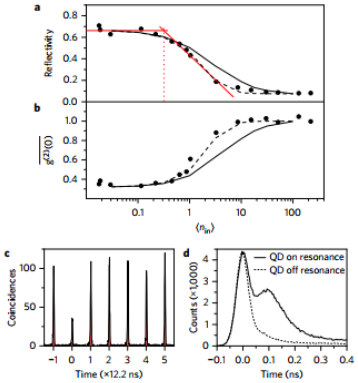

Figure 2 | Single photon nonlinearity and second-order correlation measurements. **a**, Measured (dots) and calculated (solid line) reflectivity of a 125 ps pulse resonant to the QD transition as function of the incident average photon-number $\langle n_{in} \rangle$. The red lines are linear fits to the low and intermediate $\langle n_{in} \rangle$ region. The intersection of the two lines defines the nonlinear threshold. **b**, Measured (black dots) and calculated (solid black line) time-integrated second-order correlation function, $g^{(2)}(0)$, as a function of $\langle n_{in} \rangle$. Dashed lines in **a**,**b** are the calculations assuming a power-dependent electron tunnelling out of the QD (see Supplementary Information). **c**, Measured two-photon coincidences for $\langle n_{in} \rangle$ = 0.1. **a**–**c** are measured on device 1. **d**, Time evolution of the intensity reflected by device 2 using high time resolution (<30 ps). The QD is brought off (dotted line) or on (solid line) resonance with the cavity mode by changing the applied bias.

Phonon limit to simultaneous near-unity indistinguishability and efficiency of solid-state single photon sources

Dara McCutcheon, University of Bristol, UK

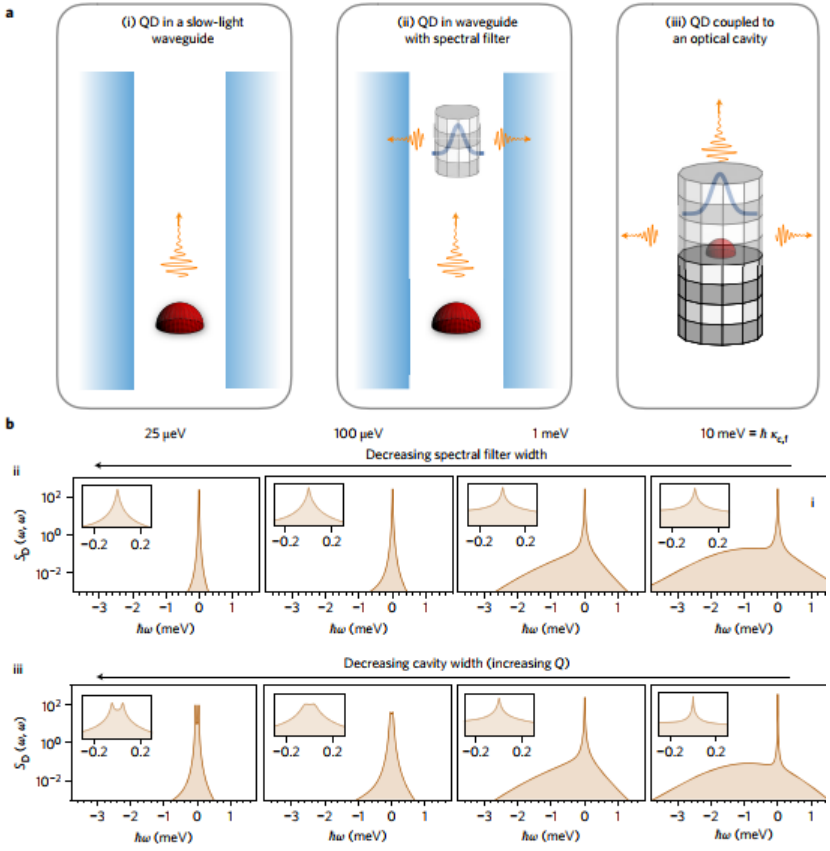

nature photonics

ARTICLES

PUBLISHED ONLINE: 3 JULY 2017 | DOI: 10.1038/NPHOTON.2017.101

Phonon scattering inhibits simultaneous near-unity efficiency and indistinguishability in semiconductor single-photon sources

Jake Iles-Smith[1*†], Dara P. S. McCutcheon[2†], Ahsan Nazir[3] and Jesper Mørk[1]

Semiconductor quantum dots (QDs) have recently emerged as a leading platform to generate highly indistinguishable photons efficiently, and this work addresses the timely question of how good these solid-state sources can ultimately be. We establish the crucial role of lattice relaxation in these systems in giving rise to trade-offs between indistinguishability and efficiency. We analyse the two source architectures most commonly employed: a QD embedded in a waveguide and a QD coupled to an optical cavity. For waveguides, we demonstrate that the broadband Purcell effect results in a simple inverse relationship, in which indistinguishability and efficiency cannot be simultaneously increased. For cavities, the frequency selectivity of the Purcell enhancement results in a more subtle trade-off, in which indistinguishability and efficiency can be increased simultaneously, although not arbitrarily, which limits a source with near-unity indistinguishability (>99%) to an efficiency of approximately 96% for realistic parameters.

Figure 2 | Single-photon source architectures and emission spectra. a, The architectures we analyse: a QD emitting into a slow-light waveguide without (i) and with (ii) a spectral filter, and a QD in an optical cavity (iii). **b**, Corresponding emission spectra as the filter (ii) or cavity (iii) is reduced in spectral width, which demonstrates the filtering property of a cavity. The insets show a magnification of the ZPL features and highlight the ZPL broadening (Purcell enhancement) in the cavity case, which ultimately gives rise to vacuum Rabi splitting. The unfiltered spectrum for case i closely resembles the broad filter $\hbar\kappa_f = 10$ meV case (ii), as indicated. Parameters: $T = 4$ K, $\alpha = 0.03$ ps^2, $\hbar\xi = 1.45$ meV, $\hbar\Gamma = 1$ μeV; the waveguides in cases i and ii have the Purcell factor $\Gamma_D/\Gamma = 10$, whereas the cavity in case iii has $\hbar g = 50$ μeV, giving $\Gamma_{cav}/\Gamma = 10$ when $\hbar\kappa_c = 1$ meV.

A fiber coupled source of identical single photons
Henk Snijders, Universiteit Leiden, Netherlands

https://arxiv.org/pdf/1703.10536.pdf

A stand-alone fiber-coupled single-photon source

Alexander Schlehahn[1], Sarah Fischbach[1], Ronny Schmidt[1], Arsenty Kaganskiy[1], André Strittmatter[1,2], Sven Rodt[1], Tobias Heindel[1,*], and Stephan Reitzenstein[1]

[1]Institut für Festkörperphysik, Technische Universität Berlin, 10623 Berlin, Germany
[2]Present address: Abteilung für Halbleiterepitaxie, Otto-von-Guericke Universität, 39106 Magdeburg, Germany
*tobias.heindel@tu-berlin.de

ABSTRACT

In this work, we present a stand-alone and fiber-coupled quantum-light source. The plug-and-play device is based on an optically driven quantum dot delivering single photons via an optical fiber. The quantum dot is deterministically integrated in a monolithic microlens which is precisely coupled to the core of an optical fiber via active optical alignment and epoxide adhesive bonding. The rigidly coupled fiber-emitter assembly is integrated in a compact Stirling cryocooler with a base temperature of 35 K. We benchmark our practical quantum device via photon auto-correlation measurements revealing $g^{(2)}(0) = 0.10^{+0.16}_{-0.10}$ under continuous-wave excitation and we demonstrate triggered non-classical light at a repetition rate of 80 MHz. The long-term stability of our quantum light source is evaluated by endurance tests showing that the fiber-coupled quantum dot emission is stable within ±3% over several successive cool-down/warm-up cycles. Additionally, non-classical photon emission is [illegible]led for a user-intervention-free 100-hour test run, showing stable single-photon count rates with a standard deviation

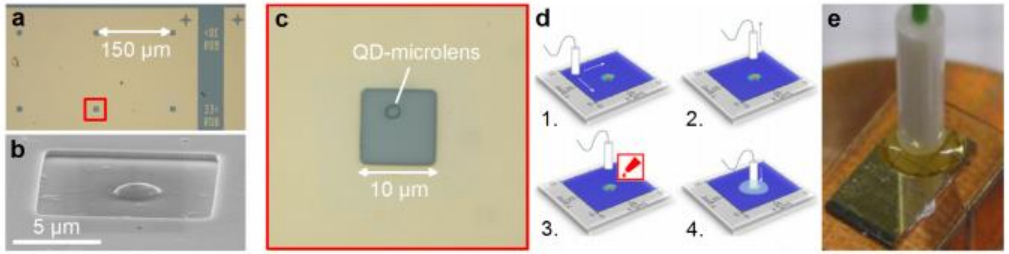

Figure 1. Fabrication of fiber-coupled QD microlenses. (a) Microscope image of the sample surface before fiber-coupling. A gold-mask contains arrays of apertures with a pitch of 150 μm. Each target aperture contains a single deterministically fabricated QD-microlens. Marker structures allow for unambiguous identification of target apertures and microlenses. (b) SEM image of a deterministic single-QD microlens fabricated via 3D in-situ electron-beam lithography and reactive ion etching. (c) Microscope image of a single aperture (dimensions: 10μm × 10μm) containing a microlens deterministically fabricated above a pre-selected QD. Suitable QD-microlenses are pre-characterized using standard micro-photoluminescence spectroscopy at 10 K. (d) Illustration of the room-temperature fiber-coupling process: 1. Fiber-scan across sample surface and monitoring of GaAs-bandgap emission within the gold apertures excited by 651 nm laser. Emission of the bandgap is only visible above apertures and markers. 2. Precise alignment of the fiber above a precharacterized target aperture and lifting of the fiber by about 5 mm. 3. Attaching a small drop of epoxide adhesive to the fiber-ferrule. 4. Lowering of the fiber to its previous position and monitoring of GaAs emission during hardening (≈ 2 hours). (e) Photograph of a fiber-coupled QD sample after the process illustrated in (d) showing the fiber ferrule glued to the sample.

A fiber coupled source of identical single photons
Henk Snijders, Universiteit Leiden, Netherlands

https://arxiv.org/pdf/1705.05876.pdf

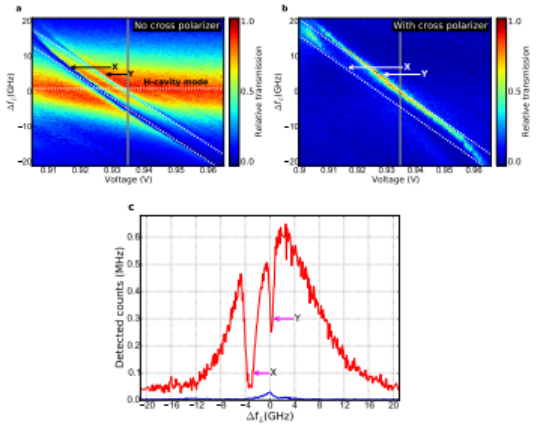

Figure 2. a, b: False color plots of resonant transmission as a function of laser frequency and gate voltage. In panel a, the incident laser light is polarized along the H cavity axis, and the transmitted light is detected without polarization selection. In b, the remnant laser light is filtered out using a crossed polarizer oriented along the V-polarized cavity mode, to select the photons coherently scattered from the Y-transition of the QD. Panel **c** shows cross sectional plots (red line: without polarization selection, blue line: with crossed polarizer, scan time 1 s) at a gate voltage of 0.935 V (grey line in a and b). Indicated are the X and Y QD transitions and the H-polarized cavity mode.

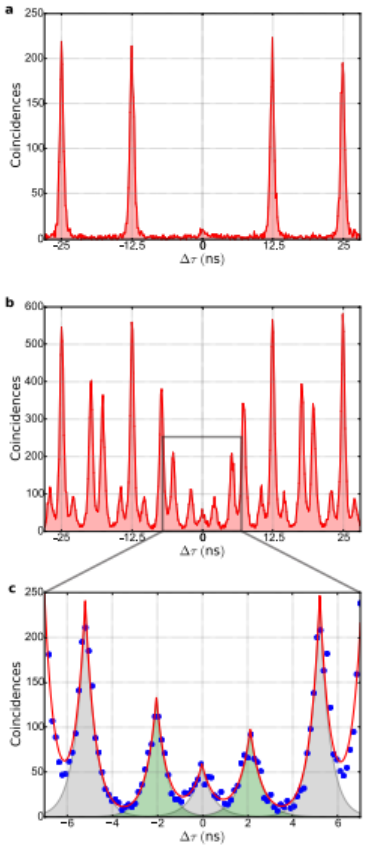

A fiber coupled cavity QED source of identical single photons

H. Snijders,[1] J. A. Frey,[2] J. Norman,[3] V. P. Post,[1] A. C. Gossard,[3] J. E. Bowers,[3] M. P. van Exter,[1] W. Löffler,[1,*] and D. Bouwmeester[1,2]

[1] *Huygens-Kamerlingh Onnes Laboratory, Leiden University, P.O. Box 9504, 2300 RA Leiden, The Netherlands*

[2] *Department of Physics, University of California, Santa Barbara, California 93106, USA*

[3] *Department of Electrical & Computer Engineering, University of California, Santa Barbara, California 93106, USA*

A high-fidelity source of identical single photons is essential for numerous quantum technologies such as quantum repeaters and optical quantum information processing [1, 2]. Hallmarks thereof are a near-unity single-photon purity, near-unity indistinguishability of consecutively emitted photons, and high brightness through a near-unity number of photons per time bin [3–5]. In order to embed such sources in quantum networks, optical fiber integration is essential but complicated by cryogenic compatability and noise. Here we demonstrate a resonantly pumped, quantum dot (QD) based, transmission operated, single-mode fiber coupled single photon source with a purity of 97%, indistinguishability of 90%, and a brightness of 17%. This is achieved by deploying a unique micropillar cavity design in a closed-cycle cryostat, which is operated using a through-fiber cross-polarization technique to remove the pump laser light from the resonantly scattered single photons. These results pave the way for fully fiber integrated photonic quantum networks, as our technology is equally applicable for cavity-QED based photonic quantum gates [6, 7].

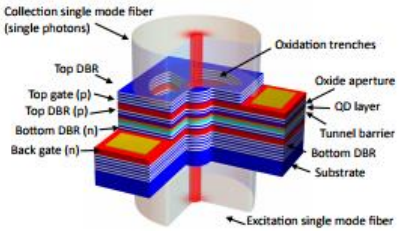

Figure 1. Sketch of the micro-cavity quantum dot device with attached fibers from bottom (excitation fiber) and top (single photon collection fiber). The trenches are used for wet-chemical oxidation of a sacrificial AlAs layer to form an intra-cavity lens or aperture that leads to transverse confinement of the optical cavity mode.

A fiber coupled source of identical single photons
Henk Snijders, Universiteit Leiden, Netherlands

nature COMMUNICATIONS

ARTICLE

Received 1 Apr 2016 | Accepted 15 Jul 2016 | Published 30 Aug 2016

DOI: 10.1038/ncomms12578 OPEN

Purification of a single-photon nonlinearity

H. Snijders[1], J.A. Frey[2], J. Norman[3], M.P. Bakker[1], E.C. Langman[2], A. Gossard[3], J.E. Bowers[3], M.P. van Exter[1], D. Bouwmeester[1,2] & W. Löffler[1]

Single photon nonlinearities based on a semiconductor quantum dot in an optical microcavity are a promising candidate for integrated optical quantum information processing nodes. In practice, however, the finite quantum dot lifetime and cavity-quantum dot coupling lead to reduced fidelity. Here we show that, with a nearly polarization degenerate microcavity in the weak coupling regime, polarization pre- and postselection can be used to restore high fidelity. The two orthogonally polarized transmission amplitudes interfere at the output polarizer; for special polarization angles, which depend only on the device cooperativity, this enables cancellation of light that did not interact with the quantum dot. With this, we can transform incident coherent light into a stream of strongly correlated photons with a second-order correlation value up to 40, larger than previous experimental results, even in the strong-coupling regime. This purification technique might also be useful to improve the fidelity of quantum dot based logic gates.

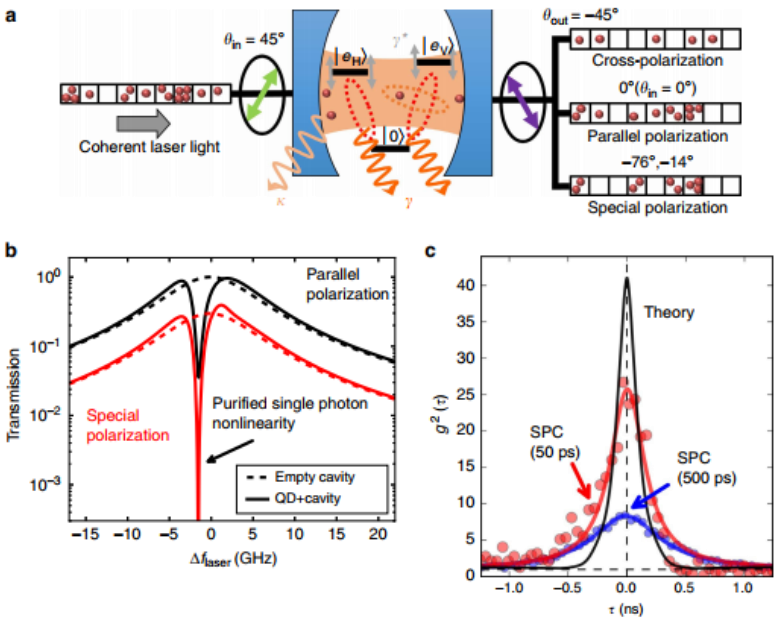

Figure 1 | The purification technique. **(a)** Cartoon of the experiment: polarization pre- and postselection in a resonant transmission CQED experiment enables tuning of the photon statistics from antibunched to bunched. **(b)** Theoretical resonant transmission spectra for coherent light with mean photon number $<<1$, with and without the QD, comparing the conventional case (parallel polarizers) with the case of special polarization postselection along θ^*_{out}: close to one of the QD resonances, single-photon transmission is perfectly suppressed, despite the finite lifetime and cavity coupling of the QD transition. **(c)** Second-order correlation function for the special polarization angle case, comparing theory and experiment using two different sets of single photon counters (SPCs) with different timing jitter, 50 ps and 500 ps.

The role of phonon interaction in the photon indistinguishability of resonantly driven semiconductor quantum dots

Antoine Reigue, INSP-UPMC, France

PHYSICAL REVIEW B **90**, 041303(R) (2014)

Indistinguishable single photons generated by a quantum dot under resonant excitation observable without postselection

Léonard Monniello,[1,2] Antoine Reigue,[1,2] Richard Hostein,[1,2] Aristide Lemaitre,[3] Anthony Martinez,[3] Roger Grousson,[1,2] and Valia Voliotis[1,2,*]

[1]*UPMC Univ Paris 06, UMR 7588, Institut des NanoSciences de Paris, 4 Place Jussieu, F-75005 Paris, France*
[2]*CNRS, UMR 7588, Institut des NanoSciences de Paris, 4 Place Jussieu, F-75005 Paris, France*
[3]*CNRS, UPR 20, Laboratoire de Photonique et Nanostructures, Route de Nozay, F-91460 Marcoussis, France*

(Received 31 March 2014; revised manuscript received 20 June 2014; published 21 July 2014)

We report on two-photon interference of highly indistinguishable single photons emitted by a quantum dot. Strictly resonant excitation with picosecond laser pulses has been used to prepare coherent states with a significantly increased coherence time ($T_2 \sim 1$ ns) and reduced lifetime ($T_1 \sim 650$ ps), as compared to a nonresonant excitation scheme. Indistinguishable photons, with visibilities greater than 70%, have been observed by measuring the Hong-Ou-Mandel dip without postselection of the interfering photons. Near-unity indistinguishable photons should be achievable by preventing fluctuations in the electrostatic environment in the vicinity of the dots, considered as an important source of decoherence.

DOI: 10.1103/PhysRevB.90.041303 PACS number(s): 78.67.Hc, 71.35.−y, 78.47.D−, 78.55.Cr

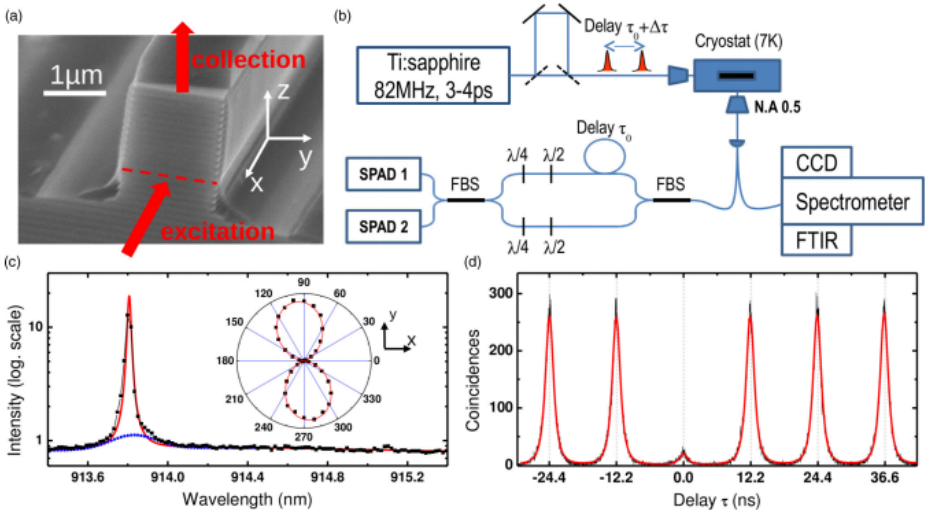

FIG. 1. (Color online) (a) Scanning electron microscope (SEM) image of one ridge. One can see the Bragg mirrors above and under the QD layer, whose position is marked by a red dashed line. Red arrows show the excitation and the collection paths. (b) Schematic drawing of the experimental setup. A pulsed ps Ti:sapphire laser comes through a first delay line, resulting in two pulses separated by $\tau_0 \pm \Delta\tau$ with $\tau_0 = 3$ ns every 12.2 ns. The luminescence is collected by a large numerical aperture (NA) microscope objective, coupled into an optical fiber and sent either into a spectrometer, or a fibered Mach-Zender interferometer with two fibered BSs with a fixed τ_0 delay for photon correlation studies. A fibered polarization setup equivalent to one $\lambda/2$ and $\lambda/4$ plates compensates the birefringence induced by the optical fibers. (c) Resonant spectrum in a semilogarithmic scale of the studied QD at 7 K: Experimental data (black dots) are fitted with a Lorentzian line (red line) and a wide Gaussian (blue dotted line) corresponding to the scattered laser. The inset shows the polar diagram of the QD resonant emission. (d) Second-order correlation function $g^2(\tau)$. At zero delay $g^2(0) = 0.07$ is obtained by normalizing the central peak integrated intensity by the average area of the five adjacent peaks. The fitting function for each peak is an exponential decay with the exciton radiative lifetime.

The role of phonon interaction in the photon indistinguishability of resonantly driven semiconductor quantum dots

Antoine Reigue, INSP-UPMC, France

PRL **118,** 233602 (2017) PHYSICAL REVIEW LETTERS week ending 9 JUNE 2017

Probing Electron-Phonon Interaction through Two-Photon Interference in Resonantly Driven Semiconductor Quantum Dots

Antoine Reigue,[1] Jake Iles-Smith,[2,*] Fabian Lux,[1] Léonard Monniello,[1] Mathieu Bernard,[1] Florent Margaillan,[1] Aristide Lemaitre,[3] Anthony Martinez,[3] Dara P. S. McCutcheon,[4] Jesper Mørk,[2] Richard Hostein,[1] and Valia Voliotis[1,†]

[1]*Sorbonne Universités, UPMC Université Paris 06, CNRS UMR 7588, Institut des NanoSciences de Paris, F-75005 Paris, France*

[2]*Department of Photonics Engineering, DTU Fotonik, Ørsteds Plads, 2800 Kongens Lyngby, Denmark*

[3]*Centre de Nanosciences et de Nanotechnologies, CNRS, Université Paris-Sud, Université Paris-Saclay, 91460 Marcoussis, France*

[4]*Quantum Engineering Technology Labs, H. H. Wills Physics Laboratory and Department of Electrical and Electronic Engineering, University of Bristol, Merchant Venturers Building, Woodland Road, Bristol BS8 1FD, United Kingdom*

(Received 21 December 2016; published 6 June 2017)

We investigate the temperature dependence of photon coherence properties through two-photon interference (TPI) measurements from a single quantum dot (QD) under resonant excitation. We show that the loss of indistinguishability is related only to the electron-phonon coupling and is not affected by spectral diffusion. Through these measurements and a complementary microscopic theory, we identify two independent separate decoherence processes, both of which are associated with phonons. Below 10 K, we find that the relaxation of the vibrational lattice is the dominant contribution to the loss of TPI visibility. This process is non-Markovian in nature and corresponds to real phonon transitions resulting in a broad phonon sideband in the QD emission spectra. Above 10 K, virtual phonon transitions to higher lying excited states in the QD become the dominant dephasing mechanism, this leads to a broadening of the zero phonon line, and a corresponding rapid decay in the visibility. The microscopic theory we develop provides analytic expressions for the dephasing rates for both virtual phonon scattering and non-Markovian lattice relaxation.

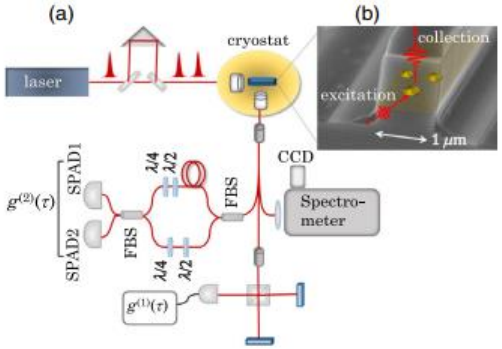

FIG. 1. (a) Scheme of the experimental setup. A tunable Ti: sapphire (82-MHz) laser delivers 3-ps pulses and, for HOM experiments, pairs of pulses separated by 3 ns. The laser is focused by a microscope objective on the cleaved edge of one ridge, and the RF is collected from the top surface by a second microscope objective. The sample and the two objectives are inside a closed-cycle He temperature-variable cryostat. The signal is coupled to a fibered setup (FBS denotes the fibered beam splitters) for either standard spectroscopy or Michelson interferometry ($g^{(1)}$) or TPI experiments ($g^{(2)}$) using a 3-ns unbalanced Mach-Zehnder interferometer. Single-photon avalanche diodes (SPAD1 and SPAD2) collect the signal. (b) Scanning electron microscopy image of one ridge, with the dots schematically drawn in the layer.

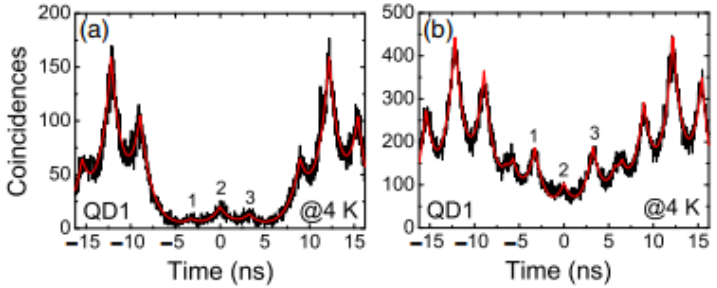

FIG. 2. Second-order correlation measurements for QD1 at 4 K for a 1-hr acquisition time. (a) Coincidences histogram for the HBT experiment. We extract $g^{(2)}_{\mathrm{HBT}} = 0.12 \pm 0.02$. (b) Coincidences histogram for the TPI experiment. After correction by the remaining laser background, we obtain $V_{\mathrm{TPI}} = 0.79 \pm 0.03$.

Phonon-assisted two-photon interference from remote quantum emitters
Marcus Reindl, Johannes Kepler University, Austria

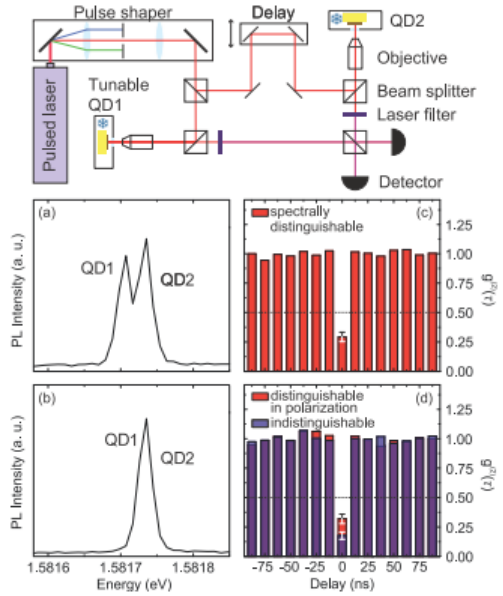

FIG. 1. (Top) Schematic of the experimental setup to measure two-photon interference between two remote quantum dots. QD 1 is mounted on a piezoelectric actuator inside the cryostat (snowflake) to allow for strain-tuning of its emission energy. (a) Photoluminescence spectrum of the neutral exciton transitions from two remote QDs. The photons stemming from these transitions do not spectrally overlap and are fully distinguishable. (b) Spectrum of the same transitions when the exciton transition of QD 1 is strain-tuned in resonance with the exciton transition of QD 2. (c) Normalized second-order intensity correlation measurement between spectrally distinguishable photons emitted from the transitions shown in (a). (d) Same as in (c) when the two transitions are tuned in energetic resonance. The blue data is taken when both photons have the same polarization, i.e., the photons are indistinguishable. The red data is taken when the photons have perpendicular polarization, i.e., the photons are fully distinguishable. The dashed line represents the theoretically expected value of 0.5 of the center peak for fully distinguishable photons.

PHYSICAL REVIEW B **96**, 075430 (2017)

Two-photon interference from two blinking quantum emitters

Klaus D. Jöns,[1,*] Katarina Stensson,[1] Marcus Reindl,[2] Marcin Swillo,[1] Yongheng Huo,[3,2,4] Val Zwiller,[1] Armando Rastelli,[2] Rinaldo Trotta,[2,†] and Gunnar Björk[1,‡]

[1]*Department of Applied Physics, Royal Institute of Technology (KTH), AlbaNova University Center, SE - 106 91 Stockholm, Sweden*
[2]*Institute of Semiconductor and Solid State Physics, Johannes Kepler University Linz, 4040, Austria*
[3]*Institute for Integrative Nanosciences, IFW Dresden, 01069, Germany*
[4]*Hefei National Laboratory for Physical Sciences at Microscale, University of Science and Technology Shanghai, 201315, China*

(Received 20 April 2017; revised manuscript received 16 July 2017; published 21 August 2017)

We investigate the effect of blinking on the two-photon interference measurement from two independent quantum emitters. We find that blinking significantly alters the statistics in the Hong-Ou-Mandel second-order intensity correlation function $g^{(2)}(\tau)$ and the outcome of two-photon interference measurements performed with independent quantum emitters. We theoretically demonstrate that the presence of blinking can be experimentally recognized by a deviation from the $g_D^{(2)}(0) = 0.5$ value when distinguishable photons from two emitters impinge on a beam splitter. Our findings explain the significant differences between linear losses and blinking for correlation measurements between independent sources and are experimentally verified using a parametric down-conversion photon-pair source. We show that blinking imposes a mandatory cross-check measurement to correctly estimate the degree of indistinguishability of photons emitted by independent quantum emitters.

2 separate cryostats!

(Invited) Exciton-polaritons in atomically thin crystals on sub-wavelength thick photonic resonators

Hui Deng, University of Michigan, USA

APPLIED PHYSICS LETTERS **107**, 191105 (2015)

Elliptical quantum dots as on-demand single photons sources with deterministic polarization states

Chu-Hsiang Teng,[1] Lei Zhang,[2] Tyler A. Hill,[2] Brandon Demory,[1] Hui Deng,[2] and Pei-Cheng Ku[1,a)]

[1]*Department of Electrical Engineering and Computer Science, University of Michigan, 1301 Beal Ave., Ann Arbor, Michigan 48105, USA*

[2]*Department of Mechanical Engineering, University of Michigan, 2350 Hayward St., Ann Arbor, Michigan 48105, USA*

(Received 28 July 2015; accepted 29 October 2015; published online 9 November 2015)

In quantum information, control of the single photon's polarization is essential. Here, we demonstrate single photon generation in a pre-programmed and deterministic polarization state, on a chip-scale platform, utilizing site-controlled elliptical quantum dots (QDs) synthesized by a top-down approach. The polarization from the QD emission is found to be linear with a high degree of linear polarization and parallel to the long axis of the ellipse. Single photon emission with orthogonal polarizations is achieved, and the dependence of the degree of linear polarization on the QD geometry is analyzed. © *2015 AIP Publishing LLC*. [http://dx.doi.org/10.1063/1.4935463]

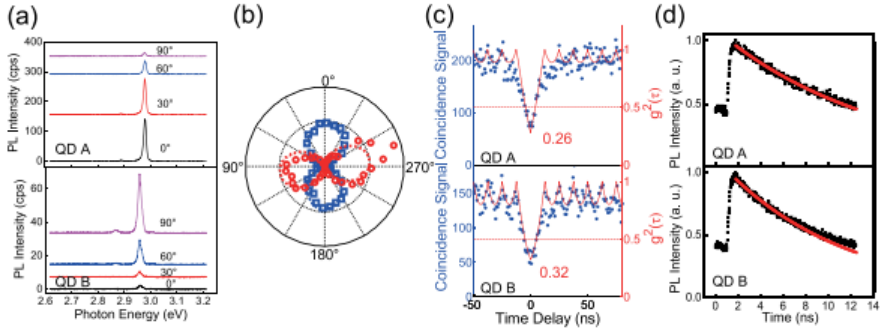

FIG. 2. (a) Polarized PL spectra from QD A and QD B at various polarization angles. (b) Polar plots of normalized PL intensity of QD A (blue) and QD B (red) and the corresponding fitting curves (dotted lines) using $I_{min} + (I_{max} - I_{min})\cos^2(\theta - \theta_{ref})$, where θ_{ref} was the fitted polarization angle. The degree of linear polarization (DLP) was calculated based on $(I_{max} - I_{min})/(I_{max} + I_{min})$ from the fitting curves. (c) $g^{(2)}(\tau)$ of QD A and QD B subjected to 102 W/cm^2 of excitation intensity. (d) Time-resolved PL and exponential fitting (red curves). The $g^{(2)}$ fitting rendered lifetime values were 13.7 ± 3.45 ns and 9.3 ± 1.25 ns for QD A and QD B, respectively, and the fitting of time-resolved PL resulted in 14.6 ± 0.46 ns and 11.1 ± 0.42 ns lifetime. The deviation of QD B from a single exponential fitting after 8 ns is attributed to the background emission from the substrate.

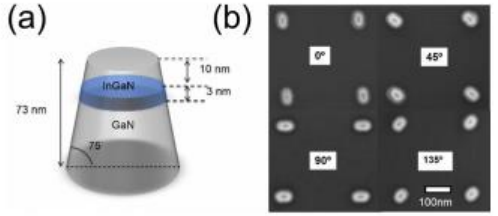

FIG. 1. (a) The schematic of the elliptical QD synthesized by a top-down process. The disk-shaped InGaN QD is sandwiched by GaN barrier materials. (b) The top-view scanning electron micrographs of four different QD orientations: 0°, 45°, 90°, and 135°.

Electrically tunable artificial gauge potential for exciton polaritons
Emre Togan, ETH, Switzerland

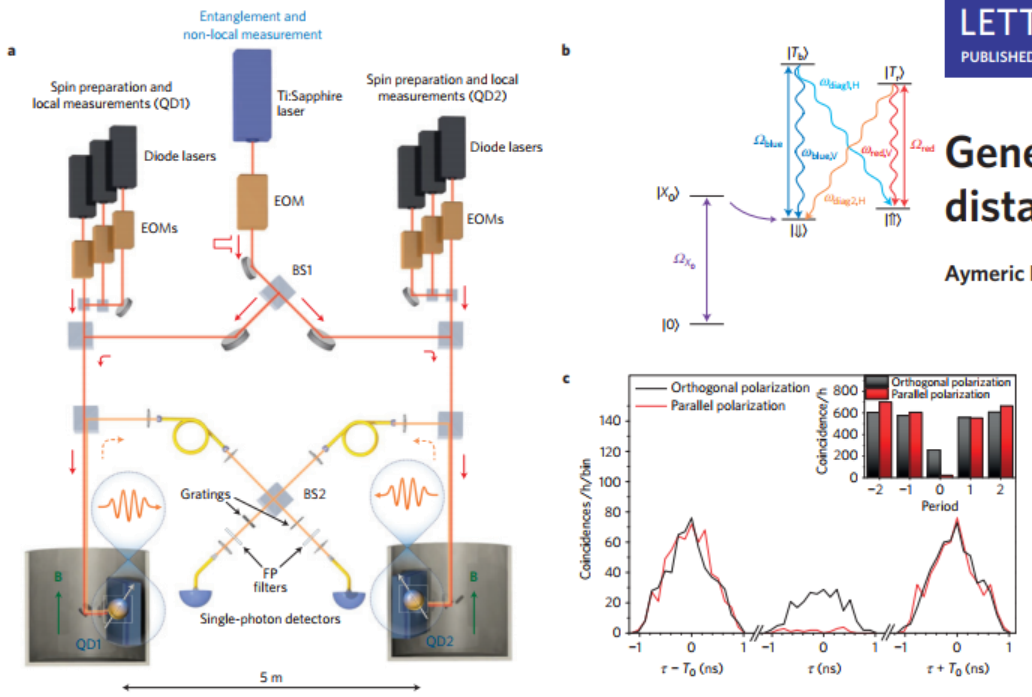

Figure 1 | Experimental set-up. a, Two bath cryostats separated by 5 m host quantum-dot samples in Voigt geometry. The quantum dots can be addressed by diode lasers (in black) for local state preparation and readout, and by a Ti:Sapphire laser (in blue) for entanglement generation and non-local measurement. EOM stands for electro-optic modulator. **b**, Energy-level diagram of a single quantum dot. On excitation of the neutral exciton ($|X^0\rangle$) state, the electron can tunnel out, leaving behind a single hole. Application of a finite magnetic field gives rise to spin-dependent optical selection rules with four allowed transitions of identical oscillator strength. **c**, Characterization of the indistinguishability of the Raman photons from the two dots with a Hong-Ou-Mandel experiment: coincidence counts on the two output arms of BS2 are plotted as a function of the delay between the recorded photon arrival times under pulsed excitation. T_0 is the repetition period of 52 ns. When the input modes have parallel polarizations (red curve), the coincidence counts within the time window (−1 ns, 1 ns) are 11 times smaller than for the case of the input modes having orthogonal polarization.

LETTERS
PUBLISHED ONLINE: 21 DECEMBER 2015 | DOI: 10.1038/NPHYS3605
nature physics

Generation of heralded entanglement between distant hole spins

Aymeric Delteil[1†], Zhe Sun[1†], Wei-bo Gao[1,2†], Emre Togan[1], Stefan Faelt[1] and Ataç Imamoğlu[1*]

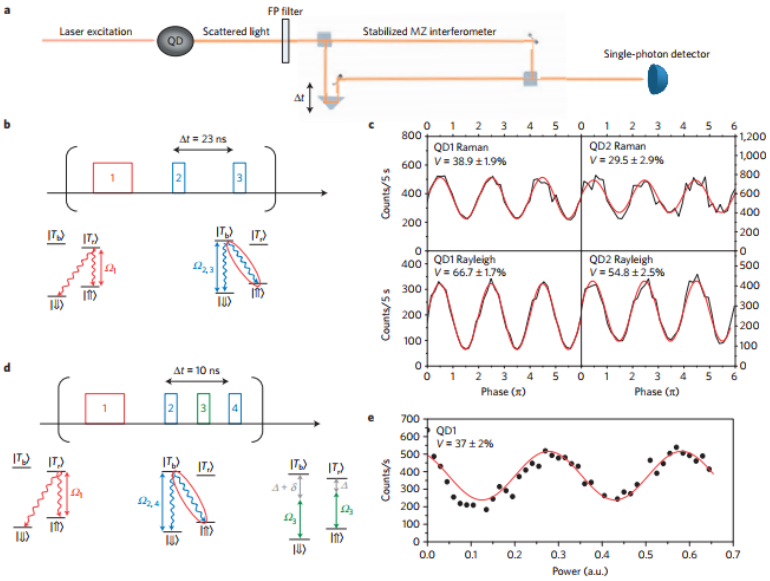

Electrically tunable artificial gauge potential for exciton polaritons
Emre Togan, ETH, Switzerland

nature COMMUNICATIONS

ARTICLE

Received 28 Nov 2016 | Accepted 6 Jan 2017 | Published 23 Feb 2017

DOI: 10.1038/ncomms14540 OPEN

Electrically tunable artificial gauge potential for polaritons

Hyang-Tag Lim[1,*], Emre Togan[1,*], Martin Kroner[1], Javier Miguel-Sanchez[1] & Atac Imamoğlu[1]

Neutral particles subject to artificial gauge potentials can behave as charged particles in magnetic fields. This fascinating premise has led to demonstrations of one-way waveguides, topologically protected edge states and Landau levels for photons. In ultracold neutral atoms, effective gauge fields have allowed the emulation of matter under strong magnetic fields leading to realization of Harper-Hofstadter and Haldane models. Here we show that application of perpendicular electric and magnetic fields effects a tunable artificial gauge potential for two-dimensional microcavity exciton polaritons. For verification, we perform interferometric measurements of the associated phase accumulated during coherent polariton transport. Since the gauge potential originates from the magnetoelectric Stark effect, it can be realized for photons strongly coupled to excitations in any polarizable medium. Together with strong polariton–polariton interactions and engineered polariton lattices, artificial gauge fields could play a key role in investigation of non-equilibrium dynamics of strongly correlated photons.